Journal of Science and Sustainable Development (JSSD)

Volume 14 Number 2
2026

ISSN: 2304-2702 (Print)
: 2414-4479 (online)

The International Journal of Ambo University

Journal of Science and Sustainable Development

National and International Advisory Board Members

Journal of Science and Sustainable Development (JSSD)

The International Journal of Ambo University

Journal of Science and Sustainable Development is a semiannual publication of Ambo University, P. O. Box 19, Ambo, Ethiopia.

Journal of Science and Sustainable Development (JSSD)

Ambo University

Ambo University which was founded in 1939 is one of the oldest higher learning institutions in Ethiopia. The primary objective of the University is to promote and advance academics and research in all aspects of sciences to contribute to the sustainable development of the country. Among the various ways of promoting academics and disseminating research outputs are publishing the **JSSD**, **Ambo University Newsletter, various books** and **proceedings**. Ambo University is known for frequently organizing international conferences, workshops and public speeches as means of promoting academics and research ultimately contributing to better understanding of new and available technologies at local, regional and international level. Financial support for various researches being conducted by the University staff is provided by the ministry of education and other external funding agencies such as Ethiopian Institute of Agricultural Research (EIAR), Ministry of Science and Technology (MoST), Institute of Biodiversity Conservation (IBC), International Livestock Research Institute (ILRI), private agencies such as Agri-share Ethiopia. Ambo University, therefore, would appreciate and acknowledge all article contributors, financial assistance providers, and reviewers showing willingness to contribute for the sustainable publication of this imperative journal.

The current, biannual journal and the quarterly newsletter exist to advance scholarly discourse about scientific research, academic knowledge and extracurricular activities taking place in the University as well as in other scientific institutions. The journal considers articles from a wide variety of interest areas and from a wide spectrum of disciplines. Manuscripts are usually reviewed within one-to two months of submission. It is not possible to promise automatic acceptance of the manuscript. Based on the reviewers’ comments, the Editorial Board deserves the right to reject manuscripts that are not up to standard. Authors are advised to strictly follow the *instructions for authors* as a mere deviation from the basics of the Journal format can lead to automatic rejection of the manuscript without going in depth into it.

JSSD: Journal of Science and Sustainable Development

JSSD is an international, a bi-annual Journal of Ambo University, Ethiopia. The Journal was launched in 2012. The journal is designed for an international readership both within Africa and Overseas. The JSSD will accept for publication original research articles, review articles, short communications and features articles in both basic and applied sciences. The journal covers all disciplines which are highly relevant to Ethiopia and other countries sustainable developments through the development of academic aspects. Therefore, the Ambo University is open to invite all suitably qualified individuals and organizations to contribute in all areas of your interest based on the guidelines of the publications. Research manuscripts in Science, Academy, Technology and other related disciplines will be considered for the publication in the JSSD.

Objectives:

- To produce a publication that is credible and informative which will serve as a medium for professionals in science and related fields to interact and share information and knowledge for the purpose of the advancement of the scientific community and sustainable development.

- To promote the effective teaching of science, technology and management; identifying problems and developing solutions through dissemination of new information from researches align in the direction of solving the basic need of the country.

- To contribute to the pool of scientific information by providing (creating) more access for researchers to have their original scientific work relevant to the need of the country and the world at large.

Instructions for Authors

The **Ambo University Journal of Science & Sustainable Development (JSSD)** is an open access journal that provides rapid publication (bi-annually) of articles in all areas of the subject such as natural, social and health sciences, agriculture, technology, art and etc. The Journal welcomes the submission of manuscripts that meet the general criteria of significance and scientific excellence. Papers will be published shortly after acceptance.

Electronic submission of manuscripts is strongly encouraged, provided that the text, tables, and figures are included in a single Microsoft Word file.

Submit manuscripts as e-mail attachment to the Editorial Office at: aujssd@ambou.edu.et / aujssd2024@gmail.com. A manuscript number will be mailed to the corresponding author shortly after submission. The **cover letter** should include the corresponding author's full address (e-mail and P.O. Box). The whole manuscript with tables and figures embedded in the text in word document should be sent to the editors as an attachment.

The Journal of Science & Sustainable Development will only accept manuscripts submitted as e-mail attachments.

Article Types

Three types of manuscripts may be submitted:

Original Articles: These should describe new and carefully confirmed findings, and experimental procedures should be given in sufficient detail for others to verify the work. The length of a full paper should be the minimum required to describe and interpret the work clearly. The original articles submitted to JSSD should not have been previously published and not being considered for publication elsewhere. Papers should be in English and be prepared in A4 (8.27" X 11.69") page size, using standard fonts with font size of 12, with double-spacing, and margins of at least 1" (2.5cm) all around. Times New Roman fonts must be used and remain uniform throughout the text. Authors are required to strictly follow the Journal's formatting guidelines in all sections of the manuscript. Original research articles should not exceed 8,000 words and may include up to six Tables and/or Figures, with a maximum of 45 references in the reference list.

Reviews: Submissions of reviews covering topics of current interest are welcome and encouraged. Reviews should be concise and no longer than 10000 words with a maximum of 10 Figures/Tables and 100 references. The submitted review papers are also subjected to peer-review. It is expected that review articles would be written by authors with years of experience and have done substantial work on the subject area being reviewed. Please note that systematic reviews should be submitted as Reviews paper, whereas meta-analysis should be submitted as Original article.

Short Communications: A Short Communication is suitable for recording the results of completed small investigations or giving details of new models or hypotheses, innovative methods, techniques or apparatus. The items of standard manuscript preparation as listed are applicable, though the style of main sections need not conform to that of full-length papers. Abstracts are limited to between 100 and 150 words, results and discussion should be combined into a single section. Short Communications are limited to a maximum of two figures and one table with a total of 3000 words without including Figures and Tables. Results and Discussion should be combined into a single section. It should be noted that short communication may not be used for preliminary publications of the data; therefore, the same material cannot be published elsewhere as an original paper after it has been published in JSSD.

Review Process

All submitted manuscripts are initially screened by the Editorial Board to assess their alignment with the journal's scope, compliance with formatting requirements, overall quality, similarity index, and scientific merit. Articles that pass the initial screening will be evaluated by qualified reviewers selected from the journal's database or invited externally by the Editorial Board. Authors cannot nominate reviewers. Only reviewers randomly selected from our database or external reviewers with specialization in the subject area will be contacted to evaluate the manuscript. The process will be double blind review. Decisions will be made as rapidly as possible based on reviewer's recommendation, editorial board decision. The Journal strives to return reviewers' comments to authors as soon as possible. The editorial board will re-review manuscripts that are accepted pending revision. It is the goal of the JSSD to publish manuscripts shortly after submission.

Original Articles

All portions of the manuscript must be typed **double-spaced** and all pages numbered starting from the title page.

The **Title** should be short and brief phrase describing the contents of the paper. Abbreviations are not permitted in the title, except for those that are widely recognized and commonly accepted. The Title Page should include the authors' full names and affiliations, the name of the corresponding author along with current phone, fax and E-mail information

The A**bstract** should be informative and completely self-explanatory, briefly present the topic, state the scope of the experiments, indicate significant data, and point out major findings and conclusions. The abstract should be 250 to 300 words in length. Complete sentences, active verbs, and the third person written in past tense should be used. Standard nomenclature should be used and abbreviations should be avoided. No literature should be cited. Following the abstract, about 3 to 5 key words that will provide indexing references should be listed. A list of non-standard Abbreviations should be added only when the full term is very long and used often. Each abbreviation should be spelt out and introduced in parentheses the first time it is used in the text. Only recommended SI units should be used. Standard abbreviations (such as ATP and DNA) need not be defined.

Following the abstract, about 3 to 5 **key words** that will provide indexing references should be listed.

The **Introduction** should provide a clear statement of the problem, the relevant literature on the subject, and the proposed approach or solution. It should be understandable to colleagues from a broad range of scientific disciplines.

Materials and Methods should be complete enough based on laid down standard procedures for science, arts, and social research that allow trials/surveys/experiments to be reproduced. Detailed information should be provided on design, sampling population/techniques and data analysis procedure. However, only truly new procedures should be described in detail; previously published procedures should be cited, and important modifications of published procedures should be mentioned briefly. Capitalize trade names and include the manufacturer's name and address. Subheadings should be used. Methods in general use need not be described in detail.

Results should be presented with clarity and precision. The results should be written in the past tense when describing findings in the author(s)' experiments. Previously published findings should be written in the present tense. Results should be explained, but largely without referring to the literature. Discussion, speculation and detailed interpretation of data should not be included in the results but should be put into the discussion section.

The **Discussion** should interpret the findings in view of the results obtained in this and in past studies on this topic. State the conclusions in a few sentences at the end of the paper. The Results and Discussion sections can include subheadings, and when appropriate, both sections can be combined.

The **conclusion** section of a manuscript submitted to JSSD should be clear, concise, and directly linked to the study objectives and findings. A conclusion should leave readers with a clear understanding of the study's importance, reliability, and contribution to sustainable development research. If recommendations are included, they should be evidence-based and derived directly from the study findings. Please avoid repeating detailed data, statistics, or discussions already presented in the results and discussion section.

The **Acknowledgments** of people, grants, funds, etc. should be brief.

Tables should be kept to a minimum and be designed to be as simple as possible. Tables are to be typed double-spaced throughout, the captions. Each table should be numbered consecutively in Arabic numerals. Tables should be self-explanatory without reference to the text. The same data should not be presented in both table and graph forms or repeated in the text.

Figure: Figure captions should be typed in numerical order. Graphics should be prepared using applications capable of generating high resolution GIF, TIFF, JPEG or PowerPoint before pasting in the Microsoft Word manuscript file. Use Arabic numerals to designate figures and lower case letters for their parts e.g. (Figure 1).

References: In the text, a reference identified by means of an author's name should be followed by the date of the reference in parentheses. For articles with two authors, cite both authors' last names connected by "and" followed by comma and the year of publication. When there are more than two authors, only the first author's name should be mentioned, followed by 'et al'. In the event that an author cited has two or more works published during the same year, the reference, both in the text and in the reference list, should be identified by a lower case letter 'a' and 'b' after the date to distinguish the works.
Examples:

Abayomi (2000), Agindotan *et al*. (2003), (Kelebeni, 1983), (Kumasi *et al*., 2001), (Usman and Smith, 1992), (Chege, 1998; Chukwura, 1987a,b; Tijani, 1993,1995)

References should be listed at the end of the paper in alphabetical order. Articles in preparation or articles submitted for publication, unpublished observations, personal communications, etc. should not be included in the reference list but should only be mentioned in the article text (e.g., A. Kingori, University of Nairobi, Kenya, personal communication). Journal names are abbreviated according to American Psychological Association (APA). Authors are entirely responsible for ensuring the accuracy of their references and must carefully follow the APA referencing style.

Examples:

Journal articles

Chikere, C. B., Omoni, V. T. & Chikere, B. O. (2008). Distribution of potential nosocomial pathogens in a hospital environment. *African Journal of Biotechnology*, 7, 3535-3539.

Books

Pelczar, J. R., Harley, J. P. & Klein, D. A. (1993). *Microbiology: Concepts and Applications*. McGraw-Hill Inc., New York, USA.

Edited Book chapters

Davis, P. K. & Rehfeldt, R. A. (2007). Functional skills training for people with intellectual and developmental disabilities. In J. K. Luiselli, J. A. Matson & F. R. Volkmar (Eds.), *Handbook of intellectual and developmental disabilities* (pp. 581–599), Springer.

Thesis/ Dissertations

Gezahegn, Y. B. (2007). *Barriers to teaching and learning mathematics in grade four. Masters Thesis*, University of Oslo, Norway.Weldeab, C. T. (2006). *Family, school, and community: Challenges in raising and educating children with intellectual disability: A case study among parents, teachers, and social workers in Ethiopia*. Doctoral dissertation, University of Oslo, Norway.

Proofs and Reprints: Electronic proofs will be sent (e-mail attachment) to the corresponding author as a portable document format (PDF) file. Page proofs are considered to be the final version of the manuscript. With the exception of typographical or minor clerical errors, no major changes will be allowed on the manuscript at proof stage. Because Ambo University JSSD will be published freely online to attract a wide audience, authors will have free electronic access to the full text (in PDF) of the article. Authors can freely download the PDF file from which they can print copies of their articles.

Change to authorship: Before an accepted manuscript is published, requests to add or remove an author, or to rearrange the author names, must be sent to the Editor in Chief from the corresponding author of the accepted manuscript and must include: (a) why the name should be added or removed, or the authors names rearranged and (b) written confirmation from all authors showing that they agree with the addition, removal or rearrangement. In the case of addition or removal of an author; this includes confirmation from the author being added or removed. Requests that are not sent by the corresponding author will be forwarded by the Editor in Chief to the corresponding author, who must follow the procedure as described above. The publication of such manuscript on the journal issue shall be suspended until authorship has been agreed.

Copyright: Submission of a manuscript implies; that the work described has not been published before (except in the form of an abstract, proceeding or thesis) that it is not under consideration for publication elsewhere; that if and when the manuscript is accepted for publication, the authors agree to automatic transfer of the copyright to the publisher.

Fees and Charges: Authors are not required to pay any fee for publishing on JSSD.

Journal of Science and Sustainable Development (JSSD), 2026, 14(2), 1-13

ISSN: 2304-2702 (print); 2414-4479 (online)
DOI: 10.20372/au.jssd.14.2.2026.0749

RESEARCH PAPER

Assessing Community-Based Watershed Management: Technical Quality of Soil Conservation Structures and Their Impacts on Soil Properties in Belo-Chikle Micro-Watershed, Elfeta District, Oromia, Ethiopia

Birhanu Kebede Kuris* and Melkamu Alemu

College of Natural and Computational Sciences; Department of Biology, Ambo University, Ambo, Ethiopia

***Corresponding Author:** Email: taddeebirruu@gmail.com*

Abstract

Soil erosion is one of the major causes of food insecurity and environmental degradation in Ethiopia. In recent years, a community-based watershed management program has been introduced in Ethiopia. In Elfeta District, there is a lack of tangible scientific information on the performance of soil conservation practices implemented through this program. The aim of this study was to assess the technical fitness of physical soil conservation structures implemented via a community-based watershed management program, its effect on soil physicochemical properties, and the extent of farmers' participation in the program. Field observation and physical structure component measurements were used to assess the technical fitness. Whereas, composite soil samples were collected from steep, moderate, and gentle slope classes to evaluate the effects of conservation practices on soil properties. A structured questionnaire was used to assess farmers' participation in soil conservation. As compared to the nationally established specification of graded soil bund for areas similar to Elfeta District, technical errors were found in bund spacing and vertical interval. The soil moisture content, bulk density, clay content, pH, electrical conductivity, organic matter, total nitrogen, and cation exchange capacity were significantly ($p < 0.05$) affected by slope gradient. These properties become better as the slope gradient decreases. To ensure the sustainability of watershed management practices and minimize observed technical faults on conservation structures, continued technical support, trainings, and follow-ups are required from the districts' experts and extension services in the study area.

Keywords: Watershed management, physical structure, soil erosion, soil and water conservation

Introduction

Land degradation remains one of the biggest environmental problems worldwide, threatening both developed and developing countries, and it has been a major global agenda because of its adverse impact on the environment, food security, and quality of life (Slegers, 2008). Land degradation includes all processes that diminish the capacity of land resources to perform essential functions and services in ecosystems (Hurni *et al*., 2010). Principal processes of land degradation include erosion by water and wind, chemical degradation (comprising acidification, salinization, fertility depletion, and decrease in cation retention capacity), physical degradation (comprising crusting, compaction, hard-setting, etc.), and biological degradation (reduction in total and biomass carbon and decline in land biodiversity) (UNCCD, 2024; Reddy *et al*., 2018). Erosion affects soil physical conditions (e.g., reduction of soil thickness and capacity to hold water) and chemical properties (e.g., loss of nutrients), impacting agricultural production (Hurni *et al.*, 2010). Therefore, soil erosion has a negative impact on the environment, agricultural productivity, food safety, and overall quality of life (Atnafe *et al.*, 2015). Nearly all Sub-Saharan Africa (SSA) lands are vulnerable to soil depletion, and Ethiopia is one of the countries most affected by land degradation problems (Bekele and Drake, 2003).

According to Pimentel (2006) and Mekonen and Tesfahunegn (2011), approximately 10 million hectares of cropland are abandoned worldwide each year and 6.5 million hectares in Africa. Mulugeta and Stahr (2010) also indicate that every year, around 12 tons/(ha/year) of soil is lost in Ethiopia due to erosion, and the economic impact of this loss is estimated at around $139 million, which significantly affects the country's domestic agricultural product (GDP) growth.

The major reasons why land degradation remains a problem all over the world are lack of appropriate identification and evaluation of the degradation processes and of the cause-and-effect relations of soil degradation for each specific situation and the generalized use of empirical approaches to select and apply soil and water conservation (SWC) practices. Sometimes, wrong selection and implementation of soil and water conservation practices and structures may increase land degradation processes and derived environmental impacts (Pla Sentís, 2002). Gizaw *et al.* (2019) also stated that the problems of land degradation are increasing throughout the world due to the generalized use of empirical approaches to select and apply soil and water conservation (SWC) practices. Yericho and Belay (2015) also pointed out that poor community participation, lack of structural alignment with standards, inappropriate time of implementation, lack of diversified SWC measurements, and absence of regular maintenance and management of the structures were some of the major limitations of the intervention. Therefore, the design of SWC structures considers the extent of erosion, cause of erosion, and suitability of land (Gizaw *et al.*, 2019). The same finding discovered that lack of training, extension service, lack of farm tools, and skilled manpower are the major problems during SWC structure implementation.

The soil and water conservation system in Ethiopia was launched in the 1970s with the aid of international organizations. The focus of the launched conservation system was to reduce soil degradation, improve agricultural production, enhance food security, and reduce poverty. Twenty years ago, national soil and water conservation initiatives (community-based programs) were promoted to ensure sustainable development of the environment, food security, and socio-economic development (Yericho and Belay, 2015). Some conservation practices implemented through this project can minimize soil erosion in Ethiopia's highlands, improve basic soil conditions such as pH, cation exchange capacity (CEC), electrical conductivity (EC), organic content (OC), etc., and increase crop yields (Adimassu *et al.*, 2013; Bekele and Drake, 2003).

Soil and water conservation technology in many parts of Ethiopia has not been equally successful or effective, and farmers' participation remains below expectations. Constraints such as technical skill gaps, inadequate field guidance, weak extension support, and insufficient post-implementation follow-up have been identified as significant barriers to sustained participation and maintenance (Hassen *et al.*, 2021; Kedir *et al.*, 2025; Kebede and Mesele, 2014; Lemike *et al.*, 2026). Even though successful stories from northern Ethiopia are reported, there is limited scientific evidence that justifies the success of soil conservation technology in central Ethiopia, including Elfeta District.

In recent years, national soil and water conservation campaigns (mass community programs) have been introduced in Ethiopia to guarantee sustainable development of the watershed, food safety, and socio-economic growth (Yericho and Belay, 2015). However, successful stories from northern Ethiopia are reported; mass mobilization approaches lead to the implementation of soil and water conservation structures with inappropriate design, and consequently, soil conservation activities have had a lesser impact than expected and resulted in gully formation in many parts of the country. Such a problem may be due to a technical gap and lack of trained manpower (Gizaw *et al*., 2019). The technical gap causes failure of implemented SWC technologies, which in turn causes serious land degradation. The failure of implemented structures was observed and reported repeatedly in most parts of the country due to wrong SWC structure design specification (Gizaw *et al*., 2019; Yericho and Belay, 2019). Now a days millions of hectares of land are covered with procedures for soil and water conservation nationally, including the study area. Similarly, Tamiru and Gemechu (2016) indicated that that soil and water conservation structures implemented via mass-community mobilization programs and individual farmer initiatives are becoming popular solutions to minimize the impacts of land degradation in the study area.

In spite of having the aforementioned efforts on watershed management development, the effectiveness of the intervention was not often evaluated in many parts of the country. The experience in Ethiopia showed that the practice of evaluation of the effectiveness of the project is overlooked for three main reasons, such as lack of political administrative commitment, insufficiency of budget allocated for monitoring and evaluation, and inadequacy of the institutional arrangements that underlie monitoring and evaluation (Wassie, 2000). Therefore, the objective was to assess the community-based watershed management practices: focus on the technical fitness of the physical structure and its effect on selected soil physicochemical properties in the Belo-Chikle micro-watershed, as the watershed is very important for natural resource conservation and agricultural production.

Materials and methods

Description of Study Areas

The study area-Elfeta District is located in West Shoa Zone, Oromia National Regional State, Ethiopia with a central geographical position of 9°7′0″N37°58′0″E. The district is located 126 km South-West of Addis Ababa the capital of Ethiopia and as wall as the capital of the National Regional State Oromia and at 68 km North of Ambo town the administrative center of West Shoa zone (Fig. 1). The district is delineated by Chobi and Jeldu to North, Dandi to East and Ambo District in South and West Direction. Elfeta District has total land area of 39,342 hectares out of which 66% of the area is used for farming, 19.57% of the area is used for grazing, 9.3 % of the area is covered by forest, 2.5% of the area is covered by river and water bodies and 2.78% hectares are unusable land (EDADO, 2018).

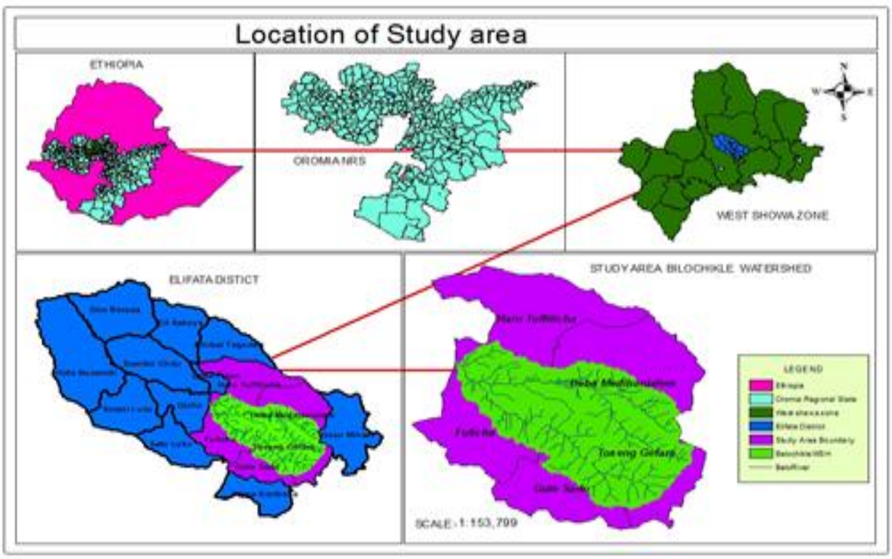

Figure 1. Map of the study area

The Belo-Chikle micro watershed is found in the highland of the district, covers total land area of 540 ha and encompass Toseng-gefere Kebele entirely and partial part of other four kebeles (Deba-medhanelem, Haro-Tufticha, Fallicha and Gute-sado). It is the largest watershed of the district and it was the area where the community-based watershed management practice adopted (EDADO, 2018). The total households of the watershed were 1719m^2. Amanuel (2018) and Yericho (2019) the study area has been categorized in to 1–7% gentle slope, 7–15% moderate slope, and 15–30% steep slope. The mean annual rainfall ranges from 900 - 1400 mm whereas the minimum and maximum temperatures are 13 and 23°C, respectively and average mean 16°C (EDADO, 2018).

The geology of central high land of the country is characterized by late tertiary that covers the Pre-Cambrian rocks that underlie all other rocks in Ethiopia (Mohr, 1971). Throughout the Blue Nile basin in Ethiopia the soils are generally Vertisols or Laptosols. The Upper basin is mainly formed from clay and clay-loam soil type, but the riverbed has a loam and sandy loam type of soil. The dominate soil types of the area (Belo-Chikle micro-watershed) is Nitisols (EDADO, 2018) which are among the most extensive agricultural soil in the Ethiopian highlands but soil degradation threatens their productive capacity.

Tamiru (2016) indicated that, contour plowing, traditional ditches, cut off drain and Water ways, soil bund and stone bund are the most common conservation methods practiced in the district including the study micro watershed to reduce soil erosion. Fallowing was rarely implemented due to lack of inadequate land.

Methods of Data Collection

Direct field observations and measurements of physical soil and water conservation structures (graded soil bonds) implemented through mass-community mobilization campaigns were used to evaluate the technical fitness of the study area conservation practices. The observations and measurements were carried out on six separate fields located on gentle, moderate, and steep slope classes. Using a tape meter, water level, string (rope), and graduated poles, field measurements of soil bunds, embankment height, embankment top width, embankment bottom width, ditch depth, ditch size, berm length, vertical interval, and space between bunds were performed.

The composite soil samples were collected from croplands situated at moderate, steep, and gentle slopes treated with soil bund through a mass-community mobilization program in the delineated micro watershed. The soil samples were collected from 1, 2, and 4 m away from soil bunds using an auger at 0–15 cm sampling depth. A total of 27 composite samples were collected for laboratory analysis. In addition, undisturbed core samples were taken to determine soil bulk density and moisture content.

The sample size of HHs for the study is 117 HHs, which was determined by using the formula developed by Kothari (2004) at a confidence level of 95% and an expected error of 0.05. A proportional sampling technique was employed to decide the numbers of respondent households from each slope class. Accordingly, 48, 40, and 29 HHs were sampled from gentle, moderate, and steep slope classes, respectively, based on their total population (i.e., 699, 427, and 593). Lists of household heads recorded at the village (locally called "kebele") administrative office were used as a sample frame for random selection of the households for the questionnaire and face-to-face interview. Besides, focused group discussions (FGD) and key informant (KI) interviews were used to triangulate and supplement the information acquired from the household survey.

Soil Laboratory Analysis

Selected soil physicochemical parameters were analyzed at the Soil Laboratory of Ambo University. The samples were air-dried, ground, and passed through 2 mm soil sieve mesh for soil texture, pH, electrical conductivity, organic carbon, total nitrogen, available phosphorous, and cation exchange capacity of the soil. Soil particle size distribution was determined by using the hydrometer method (Waling *et al.*, 1989), in which hydrogen peroxide (H_2O_2) was used to destroy organic matter, whereas sodium hexametaphosphate ($(NaPO_3)_6$) and sodium carbonate (Na_2CO_3) were used as dispersing agents. Bulk density was determined by the core method, the ratio of solid mass to total volume of the core sample after the soil was dried in an oven at 105°C for 24 hrs.

The soil reaction (pH-H_2O) was measured using the pH meter method. The pH meter glass electrode was inserted in the suspension of 1:2.5 (soil: water on a mass-to-volume basis) after calibrating the pH meter with buffer solutions of pH 4 and 7. Similarly, soil EC was measured using the glass electrode method within the suspension of a 1:2.5 (soil: water on a mass-to-volume basis) using an EC meter. Total nitrogen was determined using Kjeldahl digestion, distillation, and titration procedures (Bremmer, 1996). Soil organic carbon was determined following the wet digestion and titration method of Walkley and Black (1934), whereas soil organic matter content was computed from OC. The available soil phosphorous was extracted using the Bray-II method (Van Reeuwijk, 1992), and P in the extract was measured via spectrophotometer at a wavelength of 882 nm. Soil cation exchange capacity (CEC) was determined after leaching the soil sample with the ammonium acetate method (1N NH_4OAc) at pH 7.0 (Waling *et al.*, 1989).

Data Analysis

The two-way factorial analysis of variance (ANOVA) was used to test the effects of slope and sample distance on basic soil properties. The ANOVA was performed following the General Linear Model (GLM) procedure at a probability (P) of .05 and a confidence interval (CI) of 95%. After checking the assumptions of ANOVA, the main and interaction effects of the independent variables (soil parameters) were analyzed using SPSS version 20 software. Normal distribution and confidence interval of the soil dataset were tested using the Shapiro–Wilk test. The chi-square test was used to assess the effect of socio-economic and demographic factors on farmers' participation in soil conservation practices. In addition, the binary logistic regression model was used to analyze the relationship between the dichotomous dependent variable and the independent variables (Park, 2013). It enables determining the impact of multiple independent variables on the dependent variable.

Table 1. Nationally recommended specifications of graded soil bunds for areas similar to the study area

Bund components	Embankment height	Embankment top width	Embankment bottom width	Berm length	Ditch Depth)	Ditch width	Length
Average Recommended/Specification standards (m)	0.50	0.45	1.30	0.25	0.50	0.40	70

Source: FEPA (2004) and Gizaw *et al*. (2019)

Results and Discussion

Technical Fitness of Physical Soil and Water Conservation Structures

Graded soil bund was the common soil and water conservation structure built at croplands situated in different slope classes (steep, moderate, and gentle). As proposed, six separate crop fields were identified, and important soil bund dimensions, including embankment and spacing, as well as soil bund channel dimensions, were measured and computed with national standard values.

The observed and measured field results indicated the structure components (embankment top width, embankment bottom width, berm length, ditch width, and ditch depth) of bunds constructed at the study area were compatible with the national specifications (Table 1). Similarly, the constructed soil bund channel dimensions at the study area were matched with standard and calculated specifications. But the space between successive bunds deviated with -1m, vertical interval deviated with -0.8 m bottom width deviated with -0.05m and bund length deviated with -10m (at field number 5), vertical intervals deviated with -0.8m, spacing deviated with -1m, embankment height deviated with +0.05 m, embankment top width deviated with +0.01 m, bottom width deviated with -0.05 m bund length deviated with -10 m(at field number 6), embankment bottom width deviated -0.05 m (at field number 1), embankment height deviated with -0.05 m and bottom width deviated with -0.05 m (at field number 2), and the ditch width (at field number 5) deviated with -0.05 m of the components built through mass-community mobilization program on croplands of the study area were incompatible with the national specifications.

Table 2. Comparison of implemented and standard soil bund embankment and spacing

Field No.	Slope (%)	Dimension	Soil Bund Embankment and Spacing		Deviation
			Implemented (m)	Standard (m)	
1	6	Spacing	20.00	20.00	0.00
		Vertical Interval	1.20	1.20	0.00
		Height	0.50	0.50	0.00
		Top width	0.45	0.45	0.00
		Bottom Width	1.25	1.30	-0.05
		Length	70.00	70.00	0.00
		Berm Length	0.25	0.25	0.00
2	6	Spacing	20.00	20.00	0.00
		Vertical Interval	1.20	1.20	0.00
		Height	0.45	0.50	-0.05
		Top width	0.45	0.45	0.00
		Bottom Width	1.25	1.30	-0.05
		Length	70.00	70.00	0.00
		Berm Length	0.25	0.25	0.00
3	12	Spacing	15.00	15.00	0.00
		Vertical Interval	1.80	1.80	0.00
		Height	0.50	0.50	0.00
		Top width	0.45	0.45	0.00
		Bottom Width	1.30	1.30	0.00
		Length	70.00	70.00	0.00
		Berm Length	0.25	0.25	0.00
4	15	Spacing	14.00	140	0.00
		Vertical Interval	2.10	2.10	0.00
		Height	0.50	0.50	0.00
		Top width	0.45	0.45	0.00
		Bottom Width	1.30	1.30	0.00
		Length	70.00	70.00	0.00
		Berm Length	0.25	0.25	0.00
5	20	Spacing	14.00	13.00	-1.00
		Vertical Interval	2.60	1.80	-0.80
		Height	0.55	0.55	0.00
		Top width	0.51	0.51	0.00
		Bottom Width	1.45	1.40	-0.05
		Length	70.00	60.00	-10.00
		Berm Length	0.25	0.25	0.00
6	20	Spacing	14.00	13.00	-1.00
		Vertical Interval	2.60	1.80	-0.80

Height	0.50	0.55	0.05
Top width	0.50	0.51	0.01
Bottom Width	1.45	1.40	-0.05
Length	70.00	60.00	-10.00
Berm Length	0.25	0.25	0.00

The space between successive bunds of the components built on croplands at the steep slope class through the mass-community mobilization program was meaningfully wider than the recommended standards or calculated specification (Table 2). The results of key informant and focused group discussions revealed that the area where the community was continually assisted by extension services and situated on the gentle and moderate slope better performed the entire bund structure dimension computed to the given standards. The farmers situated in the steep slope area feel more about the size of the farmland occupied by the conservation structure than the quality of the work. The farmers focused on the quantity (area coverage with bund) rather than the quality of the activities.

The key informant and focused group discussion revealed that the reason why the problems observed related to the physical fitness of the conservation structure were due to lack of sufficient training and technical support during the construction and misunderstanding of the farmers on the importance of space between bunds and the vertical interval. The wider spaces between bunds were preferred by farmers to minimize possession of cultivable areas with physical structures. Unlikely, wider space between bunds may cause the formation of erosion in cropland and needs more labor for maintenance of bunds.

The work of Yericho (2015) revealed the imperfect physical structure is ineffective in controlling erosion and requires immediate repairs. Inadequate technical support for farmers is reported as a cause for ineffective soil and water conservation practices (Kebede, 2015). When the space between soil and water conservation structures is wider than the required space, the risk of soil erosion on cropland could increase (Amanuel *et al*., 2018; Tegenge and Biniam, 2017; Yericho, 2019).

Table 3. Comparison of implemented and standard soil bund channel dimensions

Field No.	**Slope (%)**	**Dimension**	**Soil Bund Channel Dimension**		
			Implemented (m)	**Standard (m)**	**Deviation**
1	6	Depth	0.48	0.50	-0.02
		Width	0.30	0.30	0.00
2	6	Depth	0.48	0.50	-0.02
		Width	0.30	0.30	0.00
3	12	Depth	0.50	0.50	0.00
		Width	0.40	0.40	0.00
4	15	Depth	0.50	0.50	0.00
		Width	0.40	0.40	0.00
5	20	Depth	0.50	0.50	0.00
		Width	0.35	0.40	-0.05
6	20	Depth	0.50	0.50	0.00
		Width	0.40	0.40	0.00

On top of this, the vertical interval of bunds constructed at the steep slope of the study area was lower than the national standard; this could facilitate surface runoff and destruction of bunds as well as croplands via allowing accumulation of water in the bunds. As rainwater accumulated inside the structures, soil erosion and runoff damaged the constructed structures (Table 3). This agrees with Tegenge and Biniam (2017), who reported that when the vertical interval of a graded soil bund is lower than the required standard, a huge amount of runoff can be generated and cause damage to the bund embankment and croplands.

Effects of Soil Bund on Soil Properties

The slope position was significantly ($p < 0.05$) affected soil clay content in the study area but soil-sampling distance from bunds was non-significantly ($p > 0.05$) affected the studied soil properties. A high clay proportion was observed at gentle slope and low at steep slope, as the slope gradient increases clay content declined. The distribution of clay content of the soil sample was different among slope classes. Thus, the clay contents of the soil increase as the slope gradient (degree of elevation) decrease. A high clay proportion was observed at gentle slope (23.72%) and low at steep slope (12.58), this indicated as the slope gradient of the sample increases the clay content (%) declined). Supporting this, the estimated marginal means of clay (%) contents of the soil sample revealed the clay (%) contents of the soil sample increases as the slope of the sample gradient decreases. The difference in clay proportion among slope positions could be due to the influence of topography (slope) and past erosion events that removed clay from steep slope and deposited at gentle slope area. Study by Muche and Molla (2024), reported that a slope position has meaningful effect on soil texture through its influence on soil formation and erosion processes. Soil and water conservation structures influence the processes of soil erosion and deposition at different slope position (Adimassu *et al.*, 2013).

Similar to clay contents, the moisture contents of the soil vary among slope classes, and high moisture content was observed at gentle slopes (7.11%) and low at steep slopes (4.4%), indicating that as the slope gradient of the sample decreases, the moisture content of the soil increases (Table). The estimated marginal means of moisture (% content in the soil sample increase as the slope of the sample gradient decreases. Amanuel *et al.* (2018) also found that the soil moisture increases along the slope gradient; this is due to the nature of water movement, low bulk density, clay content, and soil organic matter content. Similarly, Abay *et al.* (2016) reported that the soil moisture increased at low bulk density and high soil organic matter content.

The soil bulk density was different along slope classes, and the bulk density (g/cm^3) of the soil increases as the slope elevation goes up (Table 3). The lowest bulk density was recorded at a gentle slope (0.60 g/cm^3) and the highest at a steep slope (1.07 g/cm^3). The estimated marginal means of bulk density (g/cm^3) of the soil sample increases as the slope of the sample gradient decreases. Similarly, Amanuel *et al.* (2018) found that the change in soil bulk density along slope position was attributed to soil organic carbon and clay fraction. Hailu *et al.* (2012) also reported that the bulk density rises with organic carbon and accumulation of crop residues. Moreover, soil bulk density is directly related to slope position, and as the slope gradient increases, bulk density also increases and vice versa (Bezabih *et al.*, 2016).

The pH value of the soil varies between different slope classes, and the value was decreasing as the slope elevation degree increases (Table). Accordingly, a high pH value (5.82) was observed at the gentle slope and the lowest (3.98) at the steep slope. The estimated marginal means of the pH (H_2O) value of the soil sample increases as the slope of the sample gradient decreases. The presence of the highest soil pH at a gentle slope was associated with high soil OC, CEC, and clay fraction moved with runoff and erosion from steep slope positions (Amanuel *et al.*, 2018). Fantaw *et al.* (2006) also stated that the surface runoff in steep slopes decreases soluble basic cations, increases $H+$ activity, and reduces soil pH value.

The electrical conductivity of the soil was affected by slope position (Table). The electrical conductivity of the soil has an inverse relation with the slope gradient. Thus, a relatively higher

EC (0.80 dS/m) was recorded at a gentle slope and a lower one (0.045 dS/m) at a steep slope. The estimated marginal means of the electrical conductivity (dS/m) of the soil sample increases as the slope of the sample gradient decreases. Similarly, Amanuel *et al*. (2018) stated Electrical conductivity inversely related with slope gradient this occurs due to removal of basic cations with erosion from steep slope and accumulation at gentle slope areas associated with high rainfall of the area. Also, Bezabih *et al*. (2016) found that EC differs along slope position due to runoff and soil erosion processes that affect soil basic cations.

The soil organic matter was differing in terms of slope classes. The result indicated that as one goes through slope classes from steep slope to gentle, the content of organic matter increases, and the highest amount (14.02%) was recorded at gentle slope and the lowest (11.04%) at steep slope. The estimated marginal means of organic matter of the soil sample increase as the slope of the sample gradient decreases. Likewise, Amanuel *et al*. (2018) explained that in the rain area, a high amount of organic carbon exists at the lower watershed area (gentle slope). This could be due to the removal of organic matter through erosion and surface runoff from steep slopes and deposition in gentle slopes, and the presence of better soil moisture at gentle slopes. Higher clay fractions are typically found at lower slope positions due to deposition from upper slopes (Hailu *et al*., 2012).

The distribution of total nitrogen was affected by slope position; thus, the highest amount of total nitrogen content was recorded at a gentle slope (1.93%) and the lowest at a steep slope (0.86%). The estimated marginal means of total nitrogen of the soil sample increase as the slope of the sample gradient decreases. This could be due to the removal of nitrogen with organic matter through erosion and surface runoff from steep slopes and deposition in gentle slopes, and the presence of better soil moisture at gentle slopes. But in the case of the sample distance of the bund, there were no meaningful differences among the contents of nitrogen. The soil nitrogen content decreases with increasing slope; the content was low at steep slopes and high at gentle slope positions (Mulugeta, 2015). The removal of nitrogen with organic matter through erosion and surface runoff from steep slopes and deposition in gentle slopes, and the presence of better soil moisture at gentle slopes (Amanuel *et al*., 2018).

The distribution of cation exchange capacity of the soil was varied along slope gradients; thus, the soil cation exchange capacity has an inverse relation with degree of elevation. The highest amount was recorded at a gentle slope (43.09 meq/100 g) and the lowest at a steep slope (27 meq/100 g) (Table). The estimated marginal means of cation exchange capacity of the soil sample increases as the slope of the sample gradient decreases.

Factors Affect Farmers Participation in Soil and Water Conservation Practices

The binary logit model was used to identify determinant factors that influence the level of farmers’ participation in SWC practices (materials and methods). The result revealed that HH's gender (GEND), extension contact (EDAC), slope of plot (LSLOP), number of livestock of the household (LIVSTK), land holding or farm size (FRMSIZE), land use type (LANDUS), perceived profitability of the structure (PPRF), perception of SWC structure (PRCST), and average distance of HHs from farm plot (AVD) variables were found to significantly affect the level of farmers' participation in SWC practices (Table 4). Other variables like farmer age (FARMAGE), HHs educational level (EDULEVEL), HH family size (FS), availability of training (TRAN), land security (LANDSECU), labor availability (LABOAVA), and soil fertility status of the plot (SOFR) had no significant relation to the level of farmers’ participation in SWC practices (Table 4).

Table 4. Binary Logit Model Output of Determinant Factor

Variables	***B***	***S.E.***	***Wald***	***Df***	***Sig.***	***Exp(B)***
HH AGE	-15.319	2413.814	1.806	1	0.179	0.000

HH EDU.	0.168	2039.577	0.246	1	0.620	1.183
HH FS	-16.140	1516.137	0.230	1	0.632	0.000
GEND	18.931	17992.637	4.770	1	0.029	6.011
LANDSECU	31.293	3040.084	1.119	1	0.290	7.336
TRAN	-0.848	3795.866	0.413	1	0.520	0.428
EDAC	33.355	3887.637	6.042	1	0.014	8.500
FRMSIZE	-39.471	5832.303	69.625	1	0.000	0.000
LSLOP	17.431	5539.184	33.843	1	0.000	0.000
SOFR	11.051	3096.539	2.287	1	0.130	2.213
LABOAVA	2.420	7552.469	0.092	1	0.761	11.244
LIVSTK	-5.838	3873.455	35.228	1	0.000	0.003
PRCST	1.383	6104.891	6.964	1	0.008	3.988
PPRF	17.047	2602.091	42.274	1	0.000	7.450
AVD	-30.493	0.576	4.758	1	0.000	5.375
LANDUS	-0.29	0.823	47.703	1	0.029	1.749
Constant	-87.523	41381.622	1.806	1	0.000	0.000

Chi-square=139.202
-2log likelihood= 6.165a
Cox and Snell R Square =0.679
Nagelkerke R Square= 0.976
No. of observation:117
HH=Household, AGE=Age, EDU=Education, FS= family size, GEND=Gender, SCUL= Land security, TRAN= Available of training, EDAC=Extension contact, FRMSIZE=Farm size, SLP=Slope of plot, SOFR=Soil fertility status of the plot, LABA= Labour availability, PRCST=Perception on structure, PRRF=Perceived profitability of the structure, LANDUS=Land use type, AVD= average distance of a plot from homestead

Conclusion and Recommendations

Conclusion

Community-based watershed management practices are one of the most important approaches used to address soil erosion and land degradation problems. Most of the physical soil and water structures built through this program in the Belo-Chikile micro-watershed were technically fit with the national standard of similar to the study area. But at the steep slope area, the space between consecutive bunds was meaningfully wider than the national standard, and the vertical interval is below the calculated value. These limitations are potential causes for soil conservation structure malfunction and sometimes aggravate erosion problems through facilitating conditions for further erosion. Soil reaction (pH), clay content, bulk density, moisture content, electrical conductivity, organic carbon, total nitrogen, and cation exchange capacity are changed with slope gradient, and all the above soil properties become better at gentle slopes than steep ones. The contribution of graded soil bund for soil property improvement is relatively uniform among slope classes (steep, moderate, and gentle). The observed difference in soil properties between slope classes is due to the effects of topography and past erosion events. Most participate in soil conservation activities. The extension contacts, slope of plot, perceived profitability of the structure, perception of SWC structure, and average distance of the farm plot have positive and significant influence on the decision to participate in the community-based watershed management practices of the household heads. The amount of livestock on the household, landholding or farm size, and land use type have a negative and significant influence on the adoption of soil and water conservation measures.

Recommendations

Most of the farmers actively participated in the program; by providing quality extension services and training on soil and water conservation practices, it is possible to enhance farmer participation and correct the technical limitations observed on bund spacing and vertical interval. This implies that the regional and local administrations should provide extension and training services on the introduced SWC practices for the farmers and agricultural extension service workers. The District Agricultural Offices should take into account these determining factors to supplement the farmers' participation in the program. These measures encourage farmers to take soil and water conservation practices on their farmlands and at the level of watershed.

Conflict of Interest

The authors declare no conflict of interest.

Funding

No financial support was provided to carry out this research. We did from our pocket.

Availability of Data and Material

The data will be made available upon request.

Authors contribution

Birhanu Kebede Kuris provided conceptualization, validation, supervision, writing – review & editing; Melkamu Alemu did conceptualization, investigation, formal analysis, validation and, writing – original draft

References

Abay, C., Abdelkadir, A. & Mengistu, T. (2016). Effects of graded stone bunds on selected soil properties in the Central Highlands of Ethiopia. *International Journal of Natural Resources Ecology and Management*, 1(2), 42–50.

Adimassu, Z., Gorfu, B., Nigussie, D., Mowo, J., & Hilemichael, K. (2013). Farmers' preference for soil and water conservation practices in central highlands of Ethiopia. African Crop Science Journal, 21(3), 781–790.

Amanuel, B., Abebayehu, A. & Endalkachew, K. (2018). Assessment of community-based watershed management practices: Emphasis on technical fitness of physical structures and its effect on soil properties in Lemo District, Southern Ethiopia. *Environmental Systems Research, 7,* 20. Article 20

Atnafe D., Ahmed, M. & Adane, M. (2015). Determinants of adopting techniques of soil and water conservation in Goromti Watershed, Western Ethiopia. *Journal of Soil Science and Environmental Management*, 6(6), 168–177.

Bekele, W. & Drake, L. (2003). Soil and water conservation decision behavior of subsistence farmers in the Eastern Highlands of Ethiopia: A case study of the Hunde-Lafto area. *Ecological Economics*, 46(3), 437–451.

Bezabih, B., Aticho, A., Mossisa, T. & Dume, B. (2016). The effect of land management practices on soil physical and chemical properties in Gojeb Sub-river Basin of Dedo District, Southwest Ethiopia. *Journal of Soil Science and Environmental Management*, 7(10), 154–165.

Bremmer, J. (1996). Total nitrogen. In D. L. Sparks (Ed.), *Methods of soil analysis: Part 3. Chemical methods* (pp. 1085-1121). American Society of Agronomy; Soil Science Society of America.

Elfeta District Agriculture and Development Office (EDADO) (2018). *Annual report* (Unpublished report).

Federal Environmental Protection Authority (FEPA) (2004). *Guidelines on soil and water conservation on cultivated land*. Addis Ababa, Ethiopia.

Fantaw, Y., Ledin, S & Abdelkadir, A. (2006). Soil property variations in relation to topographic aspect and vegetation community in the south-eastern highlands of Ethiopia. *Forest Ecology and Management*, 232(1), 90–99.

Food and Agriculture Organization (FAO) and Intergovernmental Technical Panel on Soils (ITPS) (2015). *Status of the world's soil resources (SWSR): Main report*. FAO.

Gizaw, T., Kalkidan, F., Yalemtsehay, D. & Leta, H. (2019). Evaluating technical standards of implemented soil and water conservation technologies in Jimma Zone, Southwestern Ethiopia. *Agricultural Research and Technology: Open Access Journal*, 19(4). Article 556100

Hassen, G., Bantider, A., Legesse, A., Maimbo, M., & Yildiz, F. (2021). Assessment of design and constraints of physical soil and water conservation structures in respect to the standard in the case of Gidabo sub-basin, Ethiopia. Cogent Food & Agriculture, 7(1), 1855818.

Hailu, W., Moges, A., & Yimer, F. (2012). The effects of 'Fanya juu' soil conservation structure on selected soil physical & chemical properties: The case of Goromti Watershed, Western Ethiopia. Resources and Environment, 2(4), 132–140.

Hurni, H., Abate, S., Bantider, A., Debele, B., Ludi, E., Portner, B. & Birru, Y. (2010). Land degradation and sustainable land management in the highlands of Ethiopia. In: Hurni, H. & Wiesmann, U. (Eds.), *Global change and sustainable development: A synthesis of regional experiences from research partnerships*, (Vol. 5, pp. 187–207). Geographica Bernensia.

Kebede, W. & Mesele, N. (2014). Farmers' adoption of soil and water conservation technology: A case study of the Bokole and Toni sub-watersheds, southern Ethiopia. *Journal of Science & Development*, 2(1), 35–48.

Kedir, J. B., Tadesse, T. B., Umer, S., Kufa, A. & Erango, S. T. (2025). Beyond implementation: Assessing farmers' perception of the sustainability of soil and water conservation measures in central Ethiopia. *Discover Sustainability*, 6, Article 02464.

Kothari, C. R. (2004). *Research methodology*. New Age International Publishers.

Lemike, S., Sinore, T., Wang, F., Zhao, Y., Girma, F., Getnet, G. T. & Kabato, W. S. (2026). Managing land degradation under changing climate in Ethiopia: A review of soil and water conservation practices, gaps, and pathways toward sustainable landscape. *Environmental Sciences Europe,* 38, Article 01474.

Mekonen, K. & Tesfahunegn, G. (2011). Impact assessment of soil and water conservation measures at Medego watershed in Tigray, Northern Ethiopia. *Maejo International Journal of Science and Technology*, 5(3), 312–330

Mohr, P. A. (1971). *The Geology of Ethiopia.* Haile Selassie I University Press.

Muche, K. & Molla, E. (2024). Assessing the impacts of soil water conservation activities and slope position on the soil properties of the Gelda watershed, Northwest Ethiopia. *Applied and Environmental Soil Science*, 2024, 6858460.

Mulugeta, D. & Stahr, K. (2010). Assessment of integrated soil and water conservation measures on key soil properties in South Gonder, north-western highlands of Ethiopia. *Soil Science and Environmental Management*, 1(7), 164-176.

Park, H. (2013). An introduction to logistic regression: From basic concepts to interpretation with particular attention to nursing domain. *Journal of Korean Academy of Nursing*, 43(2), 154–164.

Pimentel, D. (2006). Soil erosion: A food and environmental threat. *Environment, Development and Sustainability*, *8*(1), 119–137.

Pla Sentís, I. (2002). Assessment of Environmental Impacts Derived of Soil and Water Conservation Practices. In: *Proceedings of the 12th ISCO Conference 282–290*. Tsinghua University Press.

Reddy, G. P. O., Kumar, N., & Singh, S. K. (2018). Remote sensing and GIS in mapping and monitoring of land degradation. In: *Geotechnologies and the Environment*, (pp. 401–424), Springer.

Slegers, M. F. W. (2008). If only it would rain: Farmers' perceptions of rainfall and drought in semi-arid central Tanzania. *Journal of Arid Environments,* 72, 2106–2123.

Tamiru, C. G. & Gemechu, S. O. (2016). Towards integrated soil erosion management in Elfeta District, West Shoa Zone, Oromia Regional State, Ethiopia. *Journal of Environment and Earth Science,* 6(9), 166–173.

Tegenge, M. & Biniam, S. (2017). *Estimating soil erosion risk and evaluating erosion control measures for soil conservation planning at Koga watershed in the highlands of Ethiopia*.

United Nations Convention to Combat Desertification, (2024). *Global land outlook thematic report on rangelands and pastoralists*. UNCCD.

Van Reeuwijk, L. P. (1992). *Procedures for soil analysis* (3rd ed.). International Soil Reference and Information Centre.

Waling, I., Van Vark, W., Houba, V. J. G. & Van der Lee, J. J. (1989). *Soil and plant analysis: A series of syllabi, Part 7: Plant analysis procedures.* Wageningen Agricultural University.

Walkley, A. & Black, I. A. (1934). An examination of the Degtjareff method for determining soil organic matter and a proposed modification of the chromic acid titration method. *Soil Science,* 37(1), 29-38.

Wassie, B. (2000). *Project planning, implementation and evaluation*. United Nations Centre for Regional Development, Africa Office.

Yericho, B. & Belay, S. (2015). Assessment of the effectiveness of watershed management intervention in Chena District, Kaffa Zone, Southwestern Ethiopia. *Journal of Water Resource and Protection,* 7(15), 1257–1269.

Yericho B. (2019). Technical viability of physical soil and water conservation structures implemented in Lake Hawassa watershed, southern Ethiopia. *Journal of Soil Science and Environmental Management,* 10(4), 68–74.

Journal of Science and Sustainable Development (JSSD), 2026, 14(2), 14-30
Copyright © Ambo University
ISSN: 2304-2702 (print); 2414-4479 (online)
DOI: 10.20372/au.jssd.14.2.2026.0750

RESEARCH PAPER

Historical and Future Land Use and Land Cover Dynamics in the Erer Sub-Basin Wabi-Shebelle River Basin, Ethiopia

Birhanu Legesse Wakjiraa[1*], Asfaw Kebede Kassa[2], Awdenegest Moges[3], and Olkeba Tolessa Leta[4]

[1]*Ph.D. candidate, Department of Natural Resources Management, Ambo University, Ethiopia. +251 0920901147, birelegesse2000@gmail.com, https://orcid.org/0009-0008-7237-4315*

[2]*Hydraulics and Water Resource Engineering, Haramaya Institute of Technology, Ethiopia. asfaw649@gmail.com, https://orcid.org/0000-0002-6496-7216*

[3]*Department of Agricultural Engineering, Hawassa University, Ethiopia. awde_moges@yahoo.co.uk https://orcid.org/0000-0001-6084-8327.*

[4]*St. Johns River Water Management District, Palatka, FL, United States. olkebat2005@gmail.com, https://orcid.org/0000-0003-3479-901X*

** The corresponding author: birelegesse2000@gmail.com*

Abstract

Rapid land use and land cover (LULC) change threatens ecosystem sustainability, yet its future patterns and dynamics remain insufficiently understood in developing countries like Ethiopia. The study aimed to evaluate the historical LULC changes and predict its future changes in the northeast of the Wabi-Shebelle River Basin (WSRB), Ethiopia. We used the Support Vector Machine (SVM) algorithms in ArcGIS Pro to classify LULC classes from multi-sensor Landsat imagery (MSS, ETM+, OLI). The Cellular Automata (CA)-Markov model and Land Change Modeler (LCM) in TerrSet with Idrisi software were used to predict future LULC changes. Between 1985 and 2022, water bodies, forests, and shrub lands decreased by 84.1%, 47.4%, and 22.6%, respectively, whereas built-up, agricultural, and barren lands increased by 2862.4%, 44.6%, and 75.5%, respectively. By 2062, under the business-as-usual scenario, water bodies, forests, and shrub lands are projected to decline by 80.1%, 40.1%, and 19.8%, respectively, while developed, agricultural, and barren lands are expected to increase by 566.3%, 18.5%, and 4.9%, respectively. The SVM and CA–Markov models effectively classified historical LULC and simulated future changes. Although LULC conversion is projected to continue, its rate is expected to slow as much of the highly suitable land, particularly in the upper region, has already been converted. Sustainable land management and targeted conservation measures should be prioritized to limit further LULC conversion and protect the remaining natural ecosystems, particularly in the upper region.

Keywords: LULC; SVM; CA-Markov; Wabi-Shebelle River Basin

Introduction

Land use and land cover (LULC) dynamics refer to the spatial and temporal changes in land use (the management and utilization of land for specific purposes) and land cover (the physical and biological features covering the Earth's surface) (Cumani and Latham, 2015; Kutter *et al*., 2016). These changes are driven by both natural processes and human activities, resulting in continuous landscape transformation over time (Demissie *et al*., 2017; Horamo *et al*., 2021). The LULC transformations have profound impacts on ecosystem services (Zhao *et al*., 2020), biodiversity (Yohannes *et al*., 2017), hydrological processes (Balha *et al*., 2023), soil quality (Bekele, 2019), climate regulation, and socioeconomic development (Roy *et al.*, 2022). Sustainable land management, environmental preservation, and well-informed decision-making all depend on an understanding of these shifts.

Advances in satellite remote sensing have made it possible to obtain accurate and consistent Earth observation data, while GIS enables the storage, integration, analysis, and visualization of spatial data, enabling detection of historical LULC changes. Landsat imagery is one of the most popular remotely captured datasets for LULC mapping due to its free accessibility, moderate spatial resolution, and long-term archive (Goward *et al*., 2006). These satellite data can be analyzed, categorized, and combined with supplementary geographical data in a GIS system to produce trustworthy LULC maps.

Several techniques for classifying satellite images have been developed for LULC mapping, including supervised methods such as Maximum Likelihood Classification (MLC), Minimum Distance, Decision Tree (DT), Random Forest (RF), Artificial Neural Networks (ANN), and Support Vector Machine (SVM), as well as unsupervised approaches such as ISODATA and K-means clustering (Debnath *et al*., 2023). Among these methods, SVM has become well-known because of its capacity to handle non-linear class boundaries and spectrally comparable land cover types while reliably classifying multispectral satellite imagery with few training samples (Saigal, 2021). Compared with other machine learning algorithms such as artificial neural networks (ANN) and deep learning models, SVM requires fewer training samples, lower computational resources, and less parameter tuning while maintaining competitive classification accuracy over a larger area (Jozdani *et al*., 2019). Because of these benefits, SVM is a suitable and reliable classifier for creating precise historical LULC datasets from Landsat imagery.

Similarly, numerous future LULC dynamics simulation models have been developed, including Markov Chain (Bell, 1974), Cellular Automata (CA) (White and Engelen, 1993), CA-Markov (Eastman, 2020), CLUE-S (Conversion of Land Use and its Effects at Small Regional Extent) (Verburg *et al*., 2002), Artificial Neural Network (ANN)-based models (Pijanowski *et al*., 2002), and the more recent Patch-generating Land Use Simulation (PLUS) model (Liang *et al*., 2021). Even though these models have proven to be highly predictive, many of them need large datasets relating to socioeconomics, the environment, and policy, as well as complex calibration techniques and a lot of processing power. Each model differs in how it reflects temporal transitions, allots space, and integrates environmental and socioeconomic driving forces.

In this study, we employed a CA–Markov model, which provides a practical balance between model simplicity, spatial realism, and prediction accuracy by combining the strengths of Markov chain analysis and CA. Markov chains model class transitions, and cellular automata spatially allocate them via neighborhood rules (Eastman, 2020). The Kappa indices of agreements are used to statistically evaluate the agreement between the simulated and actual LULC maps, a crucial process in LULC map prediction (van Vliet *et al*., 2011).

In Ethiopia, especially in the northeastern region of the WSRB, where high population density, persistent food insecurity (Assede *et al*., 2023), and climate changes (Toni et al., 2022) put growing pressure on land resources, rapid LULC change is a significant environmental challenge for sustainable development. Although LULC dynamics have been investigated in some watersheds within the basin (Hailu, 2024), the northeast WSRB remains poorly studied, and its future LULC trajectories have not been assessed, which limits evidence-based land management and sustainable planning in the region.

This study aims to (i) assess the historical LULC dynamics of the northeast WSRB using SVM-based classification and (ii) predict future LULC changes by integrating the CA–Markov model, thereby providing insights to support sustainable land-use planning and resource management.

Materials and Methods

Study Area

This study was carried out in one of the biggest sub-basins in the northeast WSRB. It is situated geographically between latitudes 7° 33′ N and 9° 30′ N and longitudes 41° 37′ E and 42° 26′ E with elevation ranging from 481 to 3383 m above sea level. The study area has three major watersheds, namely Gobele, Erer, and Erer-guda (Fig. 1).

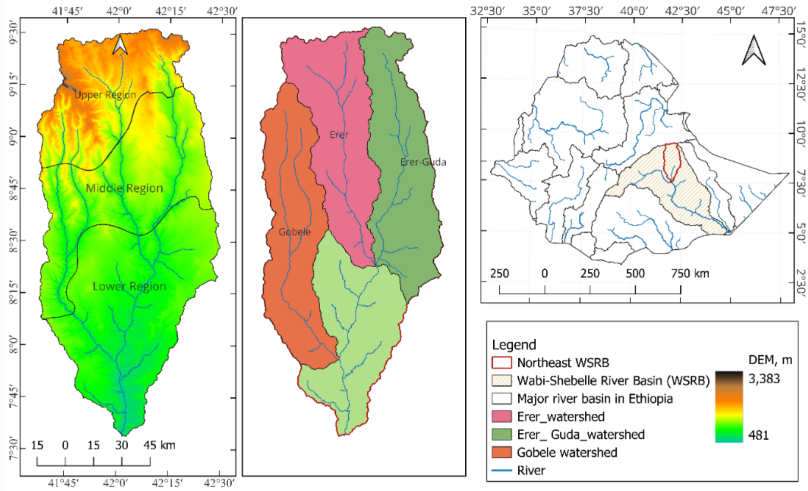

Figure 1. Location and geographical characteristics of the northeast Wabi-Shebelle River Basin: the subdivision of the sub-basin (upper, middle, and lower regions); the Digital Elevation Model (DEM); and the major watersheds (Erer, Erer-Guda, and Gobele watersheds).

In order to account for the variations in surface reflectance of satellite images, the study area was divided into three regions—upper (24.32%), middle (33.62%), and lower (42.06%)—based on the agro-ecology (Table 1). In the upper region, the ranges of annual precipitation and temperature are 600–1,260 mm and 16–28°C, respectively. The lower region receives annual precipitation ranging between 250 and 500 mm and a mean temperature between 20 and 35°C.

Table 1. Upper, middle, and lower regions of the study area based on agroecology.

Regions	Agro-ecological zones	Area (Km²)
Upper	Tepid to cool sub-moist mid-highlands (SM2) Tepid to cool moist mid-highlands (M2) Tepid to cool sub-humid mid-highlands (SH2) Tepid to cool humid mid-highlands (H2)	3605.61 (24.32%)
Model	Hot to warm sub-moist lowlands (SM1) Hot to warm, moist lowlands (M1) Hot to warm subhumid lowlands (SH1)	4984.63 (33.62%)
Lower	Hot to warm arid lowland plains (A1). Hot to warm semi-arid lowlands (SA1)	6236.28 (42.06%)

Source: Ministry of Water and Energy of Ethiopia.

The hot lowland area is lightly populated and practices a pastoral farming system, herding drought-resistant livestock, mainly camels, goats, sheep, and cattle. On the other hand, the upper region is heavily populated and uses a mixed agricultural system with intensive, integrated crop-livestock mixed farming systems with key crops like khat, sorghum, maize, potatoes, and other vegetables.

From field observation, the major LULC includes agricultural land, shrub land, barren land, waterbodies, forests, and built-up areas. In the upper region of the study area, due to the small average landholding size, less than 0.85, of households, they opt for farming cash crops (khat, coffee) and cattle fattening (Tadesse *et al*., 2014). There is hardly any communal grassland, and the main sources of cattle feed are crop wastes and the leaves of fodder bushes and trees (Tadesse *et al*., 2014). Thus, grassland and swampy areas are not considered in the LULC classification because they cover insignificant areas of land.

The major geological formation is sedimentary formations, with Precambrian rocks and metamorphic rocks outcropping (Kebede, 2015NWRC, 1973). The dominant soil types include Calcaric regosols, Eutric nitisols, Eutric regosols, Dystric cambisols, and Humic cambisols. The available hydrological data is sparse, with most stations not properly installed, resulting in low flow series with zero value (Awass, 2009).

Image Acquisition, Pre-processing, and Classification

Landsat imagery (Table 2) for 1985, 2000, and 2022 was acquired from the U.S. Geological Survey (USGS) Earth Explorer (https://glovis.usgs.gov). Landsat images were chosen due to their accessibility and long-term availability (Zhang et al., 2022). The images from December to February were selected for their cloud-free and similar vegetation status.

Table 2. Landsat images and their characteristics. Where MSS (Multispectral Scanner), ETM+ (Enhanced Thematic Mapper Plus), OLI (Operational Land Imager), and TIRS (the Thermal Infrared Sensor).

Product	Sensor	Acquisition Date (yyyy/mm/dd)	Path/Row	Resolution (m)	Day/night
Landsat 3	MSS	1985/01/20 1985/01/20	166/54,55	30	Day
Landsat 7	ETM+	2000/12/23 2000/12/07	166/54,55	30	Day
Landsat 8	OLI/TIRS	2022/01/26	166/54,55	30	Day

Source: (https://glovis.usgs.gov)

Images were subjected to pre-processing to execute radiometric and atmospheric rectifications and to augment the quality of Landsat imagery utilizing the Semi-Automatic Classification Plugin (SCP) of QGIS (Congedo, 2021). Ground control points were used to conduct geometric correction, which eradicates geometric distortions present in satellite imagery.

The LULC classifications were performed using a Support Vector Machine (SVM) model in ArcGIS Pro. The study employed a supervised object-based classification method with a minimum of two segments, considering the spatial resolution of Landsat imagery and the study area's size. The SVM was selected because it has a record of accomplishment of achieving a higher level of overall classification accuracy than the other machine learning algorithms (Basheer *et al*., 2022; Woldemariam *et al*., 2022).

Table 3. LULC descriptions

LULC class	Description
Water (Wa)	Surface water bodies like rivers, lakes, wetlands, and ponds.
Barren (Ba)	Bare lands, sediment deposits at the bank of rivers, degraded hill land, construction areas, and rocky areas.
Agriculture (Ag)	Land designated for the cultivation of crops, intercropping (crops + khat), and irrigated area.
Developed (De)	Residential, commercial areas, industrial establishments, roads, and other uncategorized surface pavements.
Shrub (Sh)	Areas covered with shrubs, bushes, and acacia mixed with herbs and grasses.
Forest (Fo)	Areas covered with either dense natural trees, plantations, or parks.

Source: Author.

Post-processing

Accuracy assessment

We collected 678 ground reference points using a global positioning system (GPS) for 2022, while the reference points created in ArcGIS Pro were obtained from a Google Earth Pro image with an acquisition date like the Landsat imagery for 1985 and 2000. A stratified random sampling method was employed to ensure enough samples across all LULC classes (FAO, 2016). We estimated the number of reference points (N) using Equation (1) (Olofsson *et al.*, 2014).

$$N = \left(\frac{\sum W_i * S_i}{SE}\right)^2$$

Where SE is the standard error of estimated overall accuracy (OA) that we would like to achieve, W_i is the mapped proportion of the area of class i, and S_i is the standard deviation of stratum i.

The overall accuracy (OA) was calculated from the error matrix to assess the classification accuracy across the LULC classes (Congalton and Green, 2019; FAO, 2016). Cohen's Kappa coefficient (K), which is a vigorous nonparametric statistical measure, was employed to consider the land use classification by chance (Rwanga and Ndambuki, 2017). The value of K ranges from -1 to 1, where a kappa of -1, 0, and 1 indicate disagreement, agreement by chance, and perfect agreement, respectively (Viera and Garrett, 2005) (Table 4).

Table 4. Over all accuracy (OA), Producer's accuracy (PA), user's accuracy (UA), and Kappa coefficient (K) of Land use/Land cover (LULC) classification for a) 1985, b) 2000, and c) 2022. Google Earth Pro Image was used as references in the 1985 and 2000, whereas, ground reference points (collected using GPS) were used for reference in 2022.

a)	**Reference from Google Earth Pro, 1985**								
	LULCC	Wa	De	Fo	Ba	Sh	Ag	Total	UA
Classified Landsat image (10 and 11 February, 1985)	Wa	72	0	3	0	0	1	76	0.95
	De	0	80	0	4	0	1	85	0.94
	Fo	7	0	79	1	6	2	95	0.83
	Ba	1	2	0	76	3	6	88	0.86
	Sh	1	2	12	11	202	4	232	0.87
	Ag	1	0	4	3	6	123	137	0.90
	Total	82	84	98	95	217	137	713	713
	PA	0.88	0.95	0.81	0.8	0.93	0.9		
Kappa coefficient = 0.86 and Overall accuracy = 0.89									
b)	**Reference from Google Earth Pro, 2000**								
	LULCC	Wa	De	Fo	Ba	Sh	Ag	Total	UA
	Wa	64	0	1	3	0	1	69	0.93

Classified Landsat image (date:07 and 23 December 2000)	De	1	80	0	12	1	1	95	0.84
	Fo	2	0	98	0	0	3	103	0.95
	Ba	1	2	2	121	8	7	141	0.86
	Sh	0	0	1	2	120	4	127	0.94
	Ag	2	2	0	0	6	107	117	0.91
	Total	70	84	102	138	135	123	652	652
	PA	0.91	0.95	0.96	0.88	0.89	0.87		
	Kappa coefficient = 0.88 and Overall accuracy = 0.90								

c)	Reference from Ground Truth, collected using GPS								
	LULC	Wa	De	Fo	Ba	Sh	Ag	Total	UA
Classified Landsat image (date:26 February 2022)	Wa	76	0	3	1	3	1	84	0.9
	De	0	80	1	8	1	6	96	0.83
	Fo	2	0	90	1	6	1	100	0.90
	Ba	0	2	0	109	4	2	117	0.93
	Sh	2	0	6	7	144	2	161	0.89
	Ag	0	0	0	4	12	104	120	0.87
	Total	80	82	100	130	170	116	678	
	PA	0.95	0.98	0.90	0.84	0.85	0.90		
	Kappa coefficient = 0.87 and Overall accuracy = 0.89								

LULC change analysis

The annual rates (r) of change for different LULC classes were determined by employing the formula based on compound interest law as suggested by Puyravaud (2003) (Equation 2). The comprehensive dynamic degree (c) of LULC gives the degree of intensity of LULC change during the study period. It was determined using Equation (3) (Wang *et al.*, 2020).

$$r = \frac{1}{(t_2 - t_1)} \ln(\frac{A_2}{A_1}) \qquad \textbf{(1)}$$

Where A_1 and A_2 are areas of LULC class at the time t_1 and t_2, respectively.

$$c = \left(\frac{\sum_{i=1}^{n} \Delta S_{i=j}}{2 \sum_{i=1}^{n} S_i} \right) / t \ * 100 \qquad \textbf{(2)}$$

where S_i is the area of classified land-use type at the initial time of the study; $\Delta S_{i=j}$ the absolute value of the area in which class i converted to class j in the research period, i ≠ j; n is the number of land-use types in the area, and t is the length of the monitoring period.

LULC Change Prediction and Validation

The AC-Markov model within Land Change Modeler (LCM) in TerrSet was used to predict the LULC of 2042 and 2062. The AC-Markov, which utilizes the transitional probability matrix, was used due to its capability of forecasting the states of LULC based on historical conditions. The CA-Markov model is used most frequently because it integrates the advantages of cellular automata and Markov chain analysis to predict future land use trends based on its change history (Eastman, 2020; Gebresellase *et al.*, 2023).

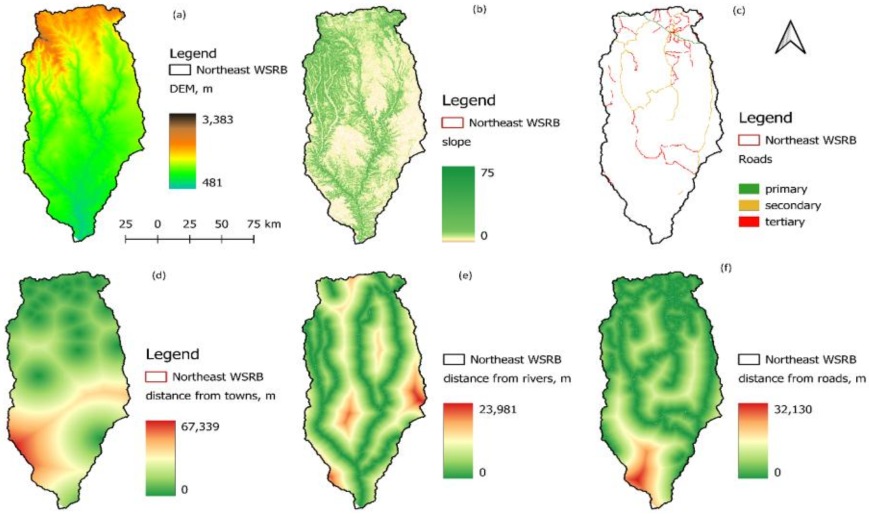

Figure 2. Driving variables for LULC transition in LCM: (a) Digital Elevation Model (DEM), (b) slope in degrees, (c) basic road networks, (d) distance from city center, (e) distance from river, and (f) distance from roads.

Historical LULC maps and spatial driver variables like stream network, land slope, road network, DEM, and city center were utilized for predicting LULC change. A DEM with a spatial resolution of 30 m was obtained from the Advanced Spaceborne Thermal Emission and Reflection Radiometer (ASTER) (https://search.earthdata.nasa.gov/). Road networks were extracted from the Open Street Map (https://www.openstreetmap.org/). The developed areas were extracted from the classified LULC map of 2022. The Euclidean distance method in the ArcGIS Pro platform was used to develop the distance from streams, road networks, and the city center (Fig. 2).

LULC maps of 1985 and 2000 were used to simulate the LULC map of 2022, which was used to evaluate the model's prediction capability. The study used LULC maps from 2000 and 2022 to predict potential transitions between LULC classes, and a transition matrix was estimated to predict future LULC changes for 2042 and 2062.

The Kappa indices of agreement were used to evaluate the agreement between the classified and simulated LULC map in 2022. Kappa indices of agreements—Kappa for location ($K_{location}$), Kappa standard ($K_{standard}$), and Kappa for no information (K_{no})–were employed to compare the classified and the simulated LULC in 2022 (van Vliet *et al*., 2011). Kappa indices of agreement range from 0 to 1. Where Kappa < 0.5 indicates a rare agreement, 0.5 < Kappa < 0.75 indicates a moderate level of agreement, 0.75 < Kappa < 1 indicates a high degree of agreement, and Kappa = 1 indicates complete agreement (Munthali *et al*., 2020).

Results

Historical LULC Maps

Table 5 and Fig. 3 show LULC classes in the upper, middle, and lower regions of the northeast WSRB between 1985 and 2022. For users, producers, overall accuracy, and the Kappa coefficient shown in Appendix Table 1, higher classification accuracies, more than 80%, were achieved.

Table 5. LULC classes (in km² and %), classification overall accuracy, and Kappa coefficient in the Upper, Middle, and Lower regions of NEWSRB for the years 1985, 2000, and 2022.

Year	ID	Upper Region		Middle Region		Lower Region		Total	
		Area, km²	**%**	**Area, km²**	**%**	**Area, km²**	**%**	**Area, km²**	**%**
1985	Water	17.40	0.48	6.43	0.13	18.53	0.30	42.40	0.29
	Developed	2.60	0.07	1.70	0.03	0.38	0.01	4.70	0.03
	Forest	249.80	6.9	182.20	3.70	195.10	3.20	627.10	4.23
	Barren	225.80	6.3	663.50	13.3	736.80	11.90	1626.10	10.97
	Shrubs	1140.50	31.6	3501.30	70.40	5199.00	83.90	9840.70	66.37
	Agriculture	1969.60	54.6	629.20	12.70	88.00	1.40	2686.70	18.12
Overall Accuracy		0.89		0.87		0.87			
Kappa Coefficient		0.90		0.87		0.84			
2000	Water	9.50	0.26	0.70	0.01	14.09	0.23	24.30	0.16
	Developed	25.00	0.69	6.22	0.12	0.46	0.01	31.60	0.21
	Forest	193.30	5.40	92.30	1.90	314.70	5.50	630.40	4.25
	Barren	398.80	11.10	1033.00	20.70	1473.90	23.20	2875.60	19.39
	Shrubs	949.90	26.40	2909.30	58.40	4289.00	68.80	8148.20	54.95
	Agriculture	2029.10	56.30	942.80	18.90	145.60	2.30	3117.50	21.02
Overall Accuracy		0.92		0.90		0.87			
Kappa Coefficient		0.90		0.87		0.84			
2022	Water	1.00	0.03	0.54	0.01	5.19	0.08	6.80	0.05
	Developed	103.20	2.86	29.00	0.58	5.55	0.09	137.80	0.93
	Forest	109.80	3.00	97.20	2.00	122.80	2.00	329.80	2.22
	Barren	247.50	6.90	1106.60	22.20	1499.40	24.00	2853.50	19.25
	Shrubs	721.00	20.00	2411.00	48.40	4484.00	71.90	7615.90	51.37
	Agriculture	2423.10	67.20	1340.30	26.90	119.30	1.90	3882.80	26.19
Overall Accuracy		0.89		0.89		0.89			
Kappa Coefficient		0.86		0.86		0.85			

The results indicate that agriculture has become the dominant land use in the upper region, covering 54.6% of the area. Moreover, the agricultural coverage has increased from 2686.70 km² (18.12%) in 1985 to 3882.80 km² (26.19%) in 2022 in the entire study area (Fig. 3).

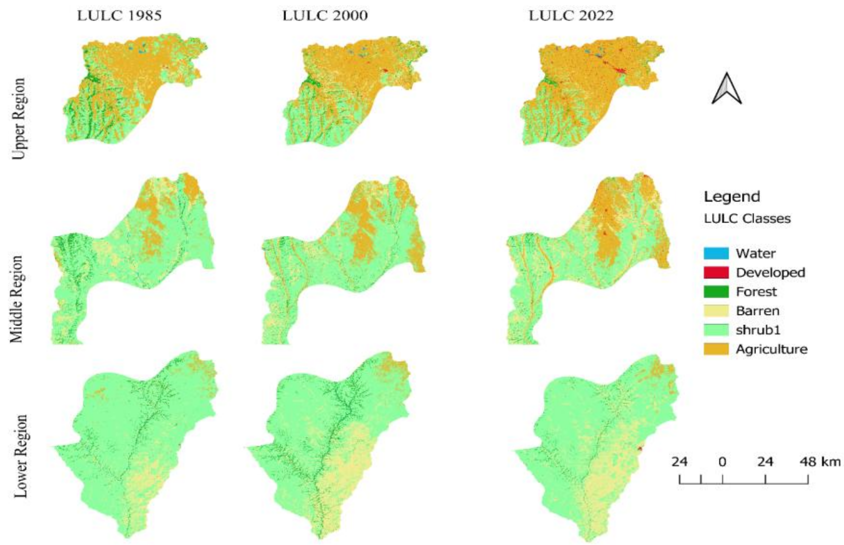

Figure 3. LULC class map during 1985, 2000, and 2022 in the upper, middle, and lower regions of the study area (Note: The map directions, legends, and scales are for all maps).

The developed area has also expanded during the study period, particularly in the upper region. In 1985, the built-up area in the upper region covered less than 0.10% (2.60 km²); by 2022, it accounted for 2.86% (103.20 km²). On the other hand, barren land covered 11.9% of the lower region in 1985 and 1499.40 km² (24%) in 2022.

Change in LULC

Table 6 shows the Northeast WSRB experienced substantial LULC changes between 1985 and 2022. Water bodies, forests, and shrub lands decreased by 84.1%, 47.4%, and 22.6%, respectively, whereas built-up, agricultural, and barren lands increased by 2862.4%, 44.6%, and 75.5%, respectively. These changes indicate intensive conversion of natural land covers to human-dominated land uses, primarily driven by agricultural expansion, urbanization, and land degradation.

Table 6. LULC changed during 1985–2000, 2000–2022, and 1985–2022 (in km² and %).

LULC	Area (Km²)			Change in %		
	1985	2000	2022	2042-2022	2062-2042	2062-2022
Water	42.40	24.30	6.80	-42.70	-72.20	-84.10
Developed	4.70	31.60	137.80	580.30	335.50	2831.90
Forest	627.10	600.40	329.80	-4.30	-45.10	-47.40
Barren	1626.10	2905.60	2853.50	78.70	-1.80	75.50
Shrubs	9840.70	8148.20	7615.90	-17.20	-6.50	-22.60
Agriculture	2686.70	3117.50	3883.80	16.00	24.60	44.60

Additionally, the intensity of land-use change during the study period was analyzed using the comprehensive dynamic degree of land-use classes. The comprehensive dynamic degree of land-use change obtained in the upper, middle, and lower regions from 1985 to 2022 were 0.31%, 0.24%, and 0.10%, respectively. The highest and lowest dynamic degrees of land use were observed in the upper and lower regions, respectively.

Transition Among LULC Classes

Table 7 shows the LULC transition area matrix between 1985–2000 and 2000–2022, in which parts of the classes exchanged to other class and some part was gained from the other classes. For instance, most shrub land was converted to barren land (1,517.1 km²) and agricultural land (969.4 km²), indicating substantial land degradation and agricultural expansion. On the other hand, shrub land gained 315.8 and 381.5 km² from forest and barren land, respectively. Developed land also gained significant area during the study period at the expense of agricultural land (12.2 km^2) and shrub lands (10.2 km^2) which might indicate urbanization has been a major factor in the LULC dynamics due to rapid population growth.

Table 7. Transition area matrix (km^2), gains and losses of LULC classes between 1985 and 2000, and 2000 and 2022.

	LULC classes	2000							
		Wa	De	Fo	Ba	Sh	Ag	Total	Loss
1985	Water (Wa)	**23.80**	0.10	1.80	2.90	1.90	12.00	42.40	18.60
	Developed (De)	0.00	**4.50**	0.10	0.10	0.10	0.00	4.70	0.20
	Forest (Fo)	0.10	0.60	**223.10**	34.30	315.80	53.30	627.20	404.10
	Barren (Ba)	0.10	4.20	35.60	**1103.10**	381.50	101.90	1626.20	523.10
	Shrubs (Sh)	0.10	10.20	315.30	1517.10	**7028.60**	969.40	9840.80	2812.20
	Agriculture (Ag)	0.20	12.20	24.60	248.10	420.40	**1980.90**	2686.30	705.40
Total		24.30	31.70	600.40	2905.60	8148.20	1136.50	14827.50	
Gain		0.50	27.20	377.30	1802.50	1119.60	1136.50		
	LULC classes	**2022**							
		Wa	**De**	**Fo**	**Ba**	**Sh**	**Ag**	**Total**	**Loss**
2000	Water	**6.80**	0.00	0.20	4.80	5.00	8.40	24.20	18.40
	Developed	0.00	**30.00**	0.40	0.20	0.60	0.60	31.70	1.70
	Forest	0.10	3.00	**218.50**	11.30	275.80	91.70	600.40	381.90
	Barren	0.10	5.70	2.30	**1737.20**	904.00	256.30	2905.60	1168.40
	Shrubs	0.10	13.30	81.90	934.00	**6257.80**	861.20	8148.20	1890.40
	Agriculture	0.70	85.80	26.60	166.00	172.90	**2665.60**	3117.40	451.80
Total		6.80	137.80	329.80	2853.50	7615.90	3883.80	14827.50	
Gain		0.90	107.80	111.30	1116.30	1358.10	1218.20		

Predicted LULC map for 2042 and 2062

Table 8 reveals that the projected and change in 2022–2062, slower than that of the historical change rate. Water bodies, forests, and shrub lands are projected to decline by 80.1%, 40.1%, and 19.8%, respectively, while built-up, agricultural, and barren lands are expected to increase by 566.3%, 18.5%, and 4.9%, respectively. The lower rates of change relative to the historical period suggest a gradual stabilization as well as the degradation of the landscape.

Table 8. Present and predicted LULC of the northeast WSRB. LULC 2022 is based on Landsat 8 image classification using a Support Vector Machine (SVM).

LULC	Area (Km^2)			Change in %		
	2022	2042	2062	2042-2022	2062-2042	2062-2022
Water	6.80	5.31	4.06	-21.90	-23.50	-40.25
Developed	137.80	406.93	918.18	195.31	125.63	566.31
Forest	329.80	228.83	197.44	-30.62	-13.72	-40.13
Barren	2853.50	2898.71	2992.33	1.58	3.23	4.87
Shrubs	7615.90	7079.92	6111.63	-7.04	-13.68	-19.75
Agriculture	3883.80	4208.20	4603.70	8.35	9.40	18.54

The LULC maps for 2042 and 2062 were predicted using the CA-Markov model in Idrisi software after obtaining satisfactory Kappa indices of agreement between actual and predicted LULC maps in 2022. Kappa indices of agreement—$K_{location}$ (0.82), $K_{standard}$ (0.75), and K_{no} (0.80)–were attained in the evaluation of the model's LULC change prediction capability. Fig. 4 illustrates the projected LULC changes from the base year 2022 to 2042 and 2062 (Fig. 4).

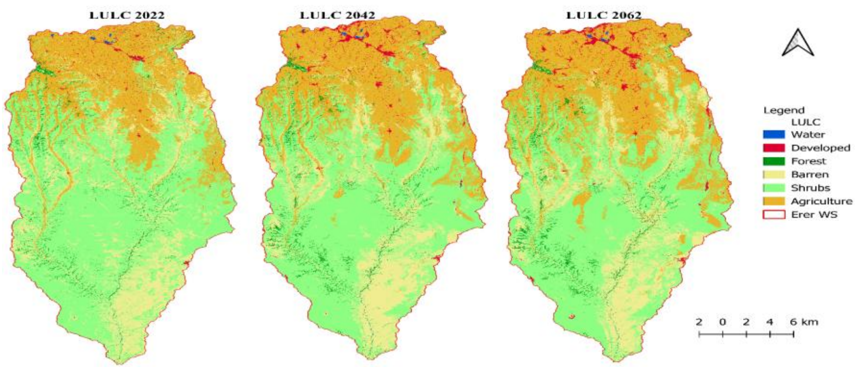

Figure 4. LULC maps in 2022, 2042 and 2062

Discussions

Historical LULC Changes

Figure 4 shows the base LULC map (2022) and predicted LULC maps for 2042 and 2062. The transition probability matrix is given in Table 9. The LULC projection reveals a significant landscape transformation by 2062, dominated by rapid urban expansion, which is projected to increase by 92.8% (2042) and 122.8% (2062) relative to the 2022 baseline. Agricultural land is also projected to slightly expand. This growth in developed and agricultural areas occurs at the direct expense of natural landscapes, with forest, shrub land, and barren land all showing a consistent decline over the projection period.

Table 9. Transition Probability matrix of change between LULC classes in 2042 and 2062

2042						
LULC	Wa	De	Fo	Ba	Sh	Ag
Wa	0.65	0.01	0.02	0.13	0.13	0.06
De	0	0.62	0.01	0.10	0.09	0.19
Fo	0	0.00	0.62	0.03	0.27	0.07
Ba	0	0.01	0.00	0.77	0.15	0.07
Sh	0	0.00	0.01	0.08	0.87	0.05
Ag	0	0.01	0.00	0.03	0.04	0.91
2062						
LULC	Wa	De	Fo	Ba	Sh	Ag
Wa	0.39	0.02	0.03	0.22	0.24	0.11
De	0.00	0.35	0.01	0.16	0.16	0.33
Fo	0.00	0.00	0.35	0.07	0.46	0.12
Ba	0.00	0.01	0.00	0.6	0.26	0.13
Sh	0.00	0.00	0.01	0.13	0.77	0.09
Ag	0.00	0.02	0.01	0.05	0.09	0.83

The results of the analysis of historical LULC dynamics showed substantial changes have been undergone in the northeast WSRB from 1985 to 2022. The region's population growth (ESS, 2023) and urbanization have led to the expansion of built-up areas, while the demand for food has led to an increase in agricultural coverage. The expansion of agricultural land at the expense of forest, on the other hand, could aggravate soil erosion and reduce water resources (Wolde *et al*., 2023; Woldemariam and Harka, 2020), particularly in the upper region. The developed and agricultural land decreases toward the sub-outlet, which might be associated with low population density. On the other hand, the barren and shrub land area increases toward the lower end of the sub-basin, which could be due to climatic changes such as drought and rising temperatures and mismanagement of land resulting in land degradation (Grover and Musick, 1990).

Moreover, the analysis also showed that the area coverage of water bodies, forests, and shrub land continuously declined over the study period. A decrease in water bodies could negatively affect freshwater availability for aquatic ecosystems, agricultural production, and domestic consumption. This finding is consistent with the review of Regasa *et al*. (2021) on LULC analyses in Ethiopia, where natural land has widely transitioned to developed uses, agriculture, and commercial infrastructure. Between 2000 and 2022, developed areas in Africa increased by 68% due to urbanization in Ethiopia, Kenya, Rwanda, Nigeria, and Ghana (Potapov *et al*., 2022).

The study area is already experiencing shocks from climate change and suffering from food insecurity (Mulugeta *et al*., 2018; Tofu *et al*., 2023). The changes in LULC could exacerbate these problems by reducing the availability of natural resources and increasing the vulnerability of the local population unless sustainable land use practices that balance economic development with environmental conservation are implemented.

The results of our analysis are consistent with the findings of the previous works (Entahabu *et al*., 2023; Woldemariam *et al*., 2022; Wudineh, 2023) which concluded that agricultural land and developed areas are expanding, whereas forest land, water bodies, and shrub land are shrinking. Furthermore, with the exception of the claim on an increase in water bodies linked to the growth of Lake Abaya's surface area, the results are consistent with the findings of the study carried out in the Gidabo River Basin, Ethiopia (Girma *et al*., 2022). Toma *et al*. (2023) also found that cultivated land, built-up area, and bare land expanded while shrub land and forest shrank annually between 1990 and 2020 in the Ajora-Woybo Watershed, Southern Ethiopia.

LULC change prediction

The findings of the predicted LULC changes showed a similar pattern to the historical LULC changes but with a slower rate. The future LULC change could have significant implications for the environment and the people living in the area. The decrease in waterbodies, forests, and shrubs could lead to a loss of biodiversity and ecosystem services, such as water regulation and carbon sequestration. The increase in development and agriculture could lead to habitat fragmentation, soil degradation, and increased greenhouse gas emissions. Promoting sustainable agricultural expansion policy and implementing natural resource management practices like soil and water conservation, re-afforestation, and afforestation of degraded land can help curb water resource reduction and expand barren land, thereby reducing the effects of agricultural land increase.

These results correspond to the works of Beshir *et al*. (2023) who simulated the LULC changes for 2037 and 2052 in the Upper WSRB. They discovered that the largest increases (23.80%) and decreases (7.84%) were in the areas of settlement and water bodies, respectively.

Conclusions and Recommendations

This study shows that during the past 40 years, the northeast WSRB has seen significant LULC alteration, mostly due to rapid urbanization and agricultural expansion. Significant increases in built-up, agricultural, and barren lands coincided with notable decreases in water bodies, forests, and shrub lands between 1985 and 2022, suggesting ongoing stress on natural ecosystems. These trends are predicted to continue through 2062, according to future simulations under the business-as-usual scenario, while the rate of change is anticipated to decline as the availability of highly appropriate land for conversion becomes scarcer. The successful implementation of the CA-Markov model and the Support Vector Machine (SVM) classifier validates its efficacy for both future land change prediction in the basin and historical LULC mapping. Overall, the results show that ongoing conversion of natural landscapes will progressively diminish ecosystem services, biodiversity, and water resources in the absence of effective intervention, endangering the basin's long-term environmental viability.

Strengthening integrated land management policies that strike a balance between urbanization, agricultural growth, and ecosystem preservation should be the top goal in order to promote sustainable land use in the northeast of the Wabi-Shebelle River Basin. The surviving forests, shrub lands, and bodies of water should be the main focus of conservation and restoration efforts, especially in the upper portion of the basin where natural ecosystems are still mostly intact. In order to direct future development toward appropriate locations and prevent further incursion into environmentally sensitive landscapes, land use planning should take the anticipated LULC changes into account. In order to facilitate prompt policy interventions and evidence-based decision-making, it is also necessary to institutionalize ongoing monitoring of land use patterns utilizing remote sensing and GIS technology. Lastly, lowering the strain on natural resources and guaranteeing the basin's long-term ecological resilience would require encouraging sustainable farming methods and involving nearby people in conservation efforts.

Declarations

Competing interests

The authors have no competing interests to declare that are relevant to the content of this article

Funding

The study was funded by Ministry of Education of Ethiopia and Haramaya University.

Data Availability Statement

The datasets generated during and/or analyzed during the current study are available from the corresponding author on reasonable request.

Author contributions

All the authors contributed to the conceptualization and design of the study. The corresponding author, Birhanu Legesse Wakjira, acquired and analyzed the data and wrote the manuscript. The other authors, Asfaw Kebede Kassa, Awdenegest Moges, and Olkeba Tolessa Leta, critically revised and strengthened the overall manuscript.

Acknowledgments

I would like to express gratitude to Ethiopian ministry of Education and Haramaya University for funding this research work. The majority of the materials and information utilized were gathered from the Ministry of Water and Energy and the National Meteorological Agency of Ethiopia and are gratefully acknowledged for granting access to the data.

References

Assede, E. S. P., Orou, H., Biaou, S. S. H., Geldenhuys, C. J., Ahononga, F. C. & Chirwa, P. W. (2023). Understanding Drivers of Land Use and Land Cover Change in Africa: A Review. *Current Landscape Ecology Reports*, 8(2), 62–72. https://doi.org/10.1007/s40823-023-00087-w

Awass, A. A. (2009). *Hydrological Drought Analysis-occurrence, severity, risks: the case of Wabi-Shebele River Basin, Ethiopia*. MSc. Thesis, University Siegen, Germany.

Balha, A., Singh, A., Pandey, S., Kumar, R., Mallick, J. & Singh, C. K. (2023). Assessing the Impact of Land-Use Dynamics to Predict the Changes in Hydrological Variables Using Effective Impervious Area (EIA). *Water Resources Management*, 37(10), 3999–4014. https://doi.org/10.1007/s11269-023-03536-7

Basheer, S., Wang, X., Farooque, A. A., Nawaz, R. A., Liu, K., Adekanmbi, T. & Liu, S. (2022). Comparison of Land Use Land Cover Classifiers Using Different Satellite Imagery and Machine Learning Techniques. *Remote Sensing*, 14(19). https://doi.org/10.3390/rs14194978

Bekele, T. (2019). Effect of Land Use and Land Cover Changes on Soil Erosion in Ethiopia. *International Journal of Agricultural Science and Food Technology*, 026–034. https://doi.org/10.17352/2455-815x.000038

Bell, E. J. (1974). Markov Analysis of Land Use Change-An Application of Stochastic Processes to Remotely Sensed Data. *Socio-Economic Planning Sciences*, 8(6), 311–316.

Beshir, S., Moges, A. & Dananto, M. (2023). Trend analysis, past dynamics and future prediction of land use and land cover change in upper Wabe-Shebele river basin. *Heliyon*, 9(9). https://doi.org/10.1016/j.heliyon.2023.e19128

Congalton, R. G. & Green, K. (2019). *Assessing the Accuracy of Remotely Sensed Data: Principles and Practices*. 3rd edition. CRC Press, Taylor & Francis Group, LLC. http://www.taylorandfrancis.com

Congedo, L. (2021). Semi-Automatic Classification Plugin: A Python tool for the download and processing of remote sensing images in QGIS. *Journal of Open Source Software*, 6(64), 3172. https://doi.org/10.21105/joss.03172

Cumani, R. & Latham, J. (2015). *FAO Land Cover Mapping methodology, tools and standards & GLC–SHARE database*. FAO meeting document, Rome, Italy.

Debnath, M., Islam, N., Gayen, S. K., Roy, P. B., Sarkar, B. & Ray, S. (2023). Prediction of spatio-temporal (2030 and 2050) land-use and land-cover changes in Koch Bihar urban agglomeration (West Bengal), India, using artificial neural network-based Markov chain model. *Modeling Earth Systems and Environment*, 2023, https://doi.org/10.1007/s40808-023-01713-6

Demissie, F., Yeshitila, K., Kindu, M. & Schneider, T. (2017). Land use/Land cover changes and their causes in Libokemkem District of South Gonder, Ethiopia. *Remote Sensing Applications: Society and Environment*, 8, 224–230. https://doi.org/10.1016/j.rsase.2017.10.001

Eastman, J. R. (2020). TerrSet Geospatial Monitoring and Modeling System, Tutorial Version 2020.v.19.0.0. *Angewandte Chemie International Edition*, 6(11), 449.

Entahabu, H. H., Minale, A. S. & Birhane, E. (2023). Modeling and Predicting Land Use/Land Cover Change Using the Land Change Modeler in the Suluh River Basin, Northern Highlands of Ethiopia. *Sustainability*, 15(10). https://doi.org/10.3390/su15108202

ESS, (Ethiopian Statistical Service) (2023). *Population Size by Sex, Region, Zone and Wereda*. July 2023. http://www.statsethiopia.gov.et/wp-content/uploads/2023/08/Population-of-Zones-and-Weredas-Projected-as-of-July-2023.pdf

FAO (Food and Agricultural Organization) (2016). *Map Accuracy Assessment and Area Estimation Map Accuracy Assessment and Area Estimation: A Practical Guide (46).* Rome, Italy, www.fao.org/publications.

Gebresellase, S. H., Wu, Z., Xu, H. & Muhammad, W. I. (2023). Scenario-Based LULC Dynamics Projection Using the CA–Markov Model on Upper Awash Basin (UAB), Ethiopia. *Sustainability*, 15(2), 1683. https://doi.org/10.3390/su15021683

Girma, R., Fürst, C. & Moges, A. (2022). Land use land cover change modeling by integrating artificial neural network with cellular Automata-Markov chain model in Gidabo river basin, main Ethiopian rift. *Environmental Challenges*, 6. https://doi.org/10.1016/j.envc.2021.100419

Goward, S., Arvidson, T., Williams, D., Faundeen, J., Irons, J. & Franks, S. (2006). Historical Record of Landsat Global Coverage: Mission Operations, NSLRSDA, and International Cooperator Stations. *Photogrammetric Engineering & Remote Sensing*, 72(10), 1155–1169. https://doi.org/https://doi.org/10.14358/PERS.72.10.1155.

Grover, H. D. & Musick, H. B. (1990). Shrubland encroachment in southern New Mexico, U.S.A.: An analysis of desertification processes in the American southwest. *Climatic Change*, 17(2–3), 305–330. https://doi.org/10.1007/BF00138373

Hailu, S. E. (2024). *Spatiotemporal Analysis of Land Use/Land Cover Change, and Their Implication on Climate Variability: The Case of Gobele Watershed of Wabi Shebelle Basin, Eastern Ethiopia*. MSc. Thesis, Haramaya University, Ethiopia.

Horamo, Y., Ayele, F. & Atiso, H. (2021). Land use and Land Cover Change Analysis, Causes and Effects on Agricultural Productivity, Case of Anlemo District in Hadiya zone, Ethiopia. *Himalayan Journal of Social Sciences and Humanities*, 16(1). https://doi.org/10.51220/hjssh.v16i1.2

Jansen, L. J. M. & Gregorio, A. Di. (2000). *Land Cover Classification System (LCCS): Classification Concepts and User Manual*. FAO, Rome, Italy.

Jozdani, S. E., Johnson, B. A. & Chen, D. (2019). Comparing deep neural networks, ensemble classifiers, and support vector machine algorithms for object-based urban land use/land cover classification. *Remote Sensing*, 11(14). https://doi.org/10.3390/rs11141713

Kebede, T. (2015). *Characterizing the Groundwater Potetial of Wabi-Shebelle River Basin.* MSc. Thesis, Addis Ababa University, Ethiopia.

Kutter, A., Nachtergaele, F. O. & Verheye, W. H. (2016). The new FAO approach to land use planning and management, and its application in Sierra Leone. *ITC Journal*, 3(4), 278-283. https://doi.org/https://www.researchgate.net/publication/290975923

Liang, X., Guan, Q., Clarke, K. C., Liu, S., Wang, B. & Yao, Y. (2021). Understanding the drivers of sustainable land expansion using a patch-generating land use simulation (PLUS) model: A case study in Wuhan, China. C*omputers, Environment and Urban Systems*, 85, 101569. https://doi.org/10.1016/j.compenvurbsys.2020.101569

Mulugeta, M., Tiruneh, G. & Alemu, Z. A. (2018). Magnitude and associated factors of household food insecurity in Fedis Woreda East Hararghe zone, Oromia region, Ethiopia. *Agriculture and Food Security*, 7(1), 1–8. https://doi.org/10.1186/s40066-017-0140-6

Munthali, M. G., Mustak, S., Adeola, A., Botai, J., Singh, S. K. & Davis, N. (2020). Modelling land use and land cover dynamics of Dedza district of Malawi using hybrid Cellular Automata and Markov model. Remote Sensing Applications: *Society and Environment*, 17. https://doi.org/10.1016/j.rsase.2019.100276

NWRC (National Water Resource Commission) (1973). *Soil Survey of the Wabi Shebelle Basin*. Addis Ababa, Ethiopia.

Olofsson, P., Foody, G. M., Herold, M., Stehman, S. V, Woodcock, C. E. & Wulder, M. A. (2014). Good practices for estimating area and assessing accuracy of land change. *Remote Sensing of Environment*, 148, 42–57. https://doi.org/10.1016/j.rse.2014.02.015

Pijanowski, B. C., Brown, D. G., Shellito, B. A. & Manik, G. A. (2002). Using neural networks and GIS to forecast land use changes: a Land Transformation Model. *Computers, Environment and Urban Systems*, 26(6), 553–575. https://doi.org/10.1016/S0198-9715(01)00015-1

Potapov, P., Hansen, M. C., Pickens, A., Hernandez-Serna, A., Tyukavina, A., Turubanova, S., Zalles, V., Li, X., Khan, A., Stolle, F., Harris, N., Song, X.-P., Baggett, A., Kommareddy, I. & Kommareddy, A. (2022). The Global 2000-2020 Land Cover and Land Use Change Dataset Derived from the Landsat Archive: First Results. *Frontiers in Remote Sensing*, 3. https://doi.org/10.3389/frsen.2022.856903

Puyravaud, J. P. (2003). Standardizing the calculation of the annual rate of deforestation. *Forest Ecology and Management*, 177(1–3), 593–596. https://doi.org/10.1016/S0378-1127(02)00335-3

Regasa, M. S., Nones, M. & Adeba, D. (2021). A review on land use and land cover change in ethiopian basins. *Land*, 10(6). https://doi.org/10.3390/land10060585

Roy, P. S., Ramachandran, R. M., Paul, O., Thakur, P. K., Ravan, S., Behera, M. D., Sarangi, C. & Kanawade, V. P. (2022). Anthropogenic Land Use and Land Cover Changes—A Review on Its Environmental Consequences and Climate Change. In *Journal of the Indian Society of Remote Sensing*, 50 (8), 1615–1640). https://doi.org/10.1007/s12524-022-01569-w

Rwanga, S. S. & Ndambuki, J. M. (2017). Accuracy Assessment of Land Use/Land Cover Classification Using Remote Sensing and GIS. *International Journal of Geosciences*, 8, 611–622. https://doi.org/https://doi.org/10.4236/ijg.2017.84033

Saigal, P. (2021). Introduction to Support Vector Machines. In P. Saigal (Ed.), *Support Vector Machines: Evolution and Application* (pp. 1–10). Nova Science Publishers, Inc.

Tofu, D. A., Mekuria, M. M. & Ogato, G. S. (2023). Climatic extremes' resilient livelihoods of rural households in the Eastern Ethiopia. *Agriculture and Food Security*, 12(1). https://doi.org/10.1186/s40066-023-00446-0

Toma, M. B., Belete, M. D. & Ulsido, M. D. (2023). Historical and future dynamics of land use land cover and its drivers in Ajora-Woybo watershed, Omo-Gibe basin, Ethiopia. *Natural Resource Modeling*, 36(1). https://doi.org/10.1111/nrm.12353

Toni, A. T., Malcherek, A. & Kassa, A. K. (2022). Agroclimatic Zone-Based Analysis of Rainfall Variability and Trends in the Wabi Shebele River Basin, Ethiopia. *Water*, 14(22). https://doi.org/10.3390/w14223699

van Vliet, J., Bregt, A. K. & Hagen-Zanker, A. (2011). Revisiting Kappa to account for change in the accuracy assessment of land-use change models. *Ecological Modelling*, 222(8), 1367–1375. https://doi.org/https://doi.org/10.1016/j.ecolmodel.2011.01.017

Verburg, P. H., Soepboer, W., Veldkamp, A., Limpiada, R., Espaldon, V. & Mastura, S. S. A. (2002). Modeling the spatial dynamics of regional land use: The CLUE-S model. *Environmental Management*, 30(3), 391–405. https://doi.org/10.1007/s00267-002-2630-x

Viera, A. J. & Garrett, J. M. (2005). Understanding Interobserver Agreement: The Kappa Statistic. *Research Series*, 35(5), 360–363.

Wang, Y., Zhao, X., Zuo, L., Zhang, Z., Wang, X., Yi, L., Liu, F. & Xu, J. (2020). Spatial differentiation of land use and landscape pattern changes in the Beijing-Tianjin-Hebei area. *Sustainability*, 12(7). https://doi.org/10.3390/su12073040

White, R. & Engelen, G. (1993). Cellular Automata and Fractal Urban Form: A Cellular Modelling Approach to the Evolution of Urban Land-Use Patterns. *Environment and Planning A*, 25(8), 1175–1199.

Wolde, B., Moges, A. & Grima, R. (2023). Assessment of the combined effects of land use/land cover and climate change on soil erosion in the Sile watershed, Ethiopian Rift Valley Lakes Basin. *Cogent Food and Agricultur*e, 9(2). https://doi.org/10.1080/23311932.2023.2273630.

Woldemariam, G. W. & Harka, A. E. (2020). Effect of land use and land cover change on soil erosion in erer sub-basin, Northeast Wabi-Shebelle Basin, Ethiopia. *Land*, 9(4), 1–25. https://doi.org/10.3390/land9040111

Woldemariam, G. W., Tibebe, D., Mengesha, T. E. & Gelete, T. B. (2022). Machine-learning algorithms for land use dynamics in Lake Haramaya Watershed, Ethiopia. *Modeling Earth Systems and Environment*, 8(3), 3719–3736. https://doi.org/10.1007/s40808-021-01296-0

Wudineh, F. A. (2023). Land-use and land-cover change and its impact on flood hazard occurrence in Wabi-Shebele River Basin of Ethiopia. *Hydrology Research*, 54(6), 756–769. https://doi.org/10.2166/nh.2023.121

Yohannes, H., Mohammed, A. & Elias, E. (2017). Land Use/Land Cover Dynamics and Its Impact on Biodiversity Resources in the Abijata Shalla National Park, Central Rift Valley Lakes Region, Ethiopia. *Environmental Science: An Indian Journal*, 13(5). www.tsijournals.com

Zhang, Y., Woodcock, C. E., Arévalo, P., Olofsson, P., Tang, X., Stanimirova, R., Bullock, E., Tarrio, K. R., Zhu, Z. & Friedl, M. A. (2022). A Global Analysis of the Spatial and Temporal Variability of Usable Landsat Observations at the Pixel Scale. *Frontiers in Remote Sensing*, 3. https://doi.org/10.3389/frsen.2022.894618

Zhao, Q., Wen, Z., Chen, S., Ding, S. & Zhang, M. (2020). Quantifying land use/land cover and landscape pattern changes and impacts on ecosystem services. *International Journal of Environmental Research and Public Health*, 17(1). https://doi.org/10.3390/ijerph17010126.

Journal of Science and Sustainable Development (JSSD), 2026, 14(2), 31-38

ISSN: 2304-2702 (print); 2414-4479 (online)
DOI: 10.20372/au.jssd.14.2.2026.0751

RESEARCH PAPER

Exploring the Nexus Between Prison Ecology and Behavioral Adaptations Among Convicted Individuals: A Case Study in Sheger City of Oromia Region, Ethiopia

Alemneh Birhanu Yirgu[1]

[1] *Department of Social Work, College of Social Sciences and Humanities, Ambo University, Ambo, Ethiopia*

***Corresponding author**: *Alemneh.birhanu@ambou.edu.et*

Abstract

This mixed-methods study explores the relationship between prison ecology and behavioral adaptations among convicted individuals in the Sheger City correctional system, Oromia Region, Ethiopia, addressing a critical empirical gap in localized carceral settings. A Convergent Parallel Mixed-Methods Design incorporating a cross-sectional survey was employed, utilizing a structured questionnaire with 341 convicted individuals (proportionally stratified across 120 cell units within 6 blocks across three municipal facilities) and supplemented by semi-structured key informant interviews and focus group discussions (2 sessions) for empirical triangulation. Quantitative survey results revealed that an overwhelming combined 86.3% of respondents agreed or strongly agreed that spatial overcrowding directly heightened interpersonal aggression, while 80.9% reported that severely restricted access to proper sanitation facilities compromised personal dignity. Furthermore, 66.8% rated institutional educational and vocational programs as ineffective or non-existent, and 47.8% attributed behavioral rebellion or emotional withdrawal to negative, security-centric staff interactions. Qualitative thematic analysis supported these trends, showing that inmates adapt through a dual mechanism: predominantly pro-social coping (90.3%, primarily spiritual practices and peer networks) and localized anti-social tactics (9.7%, including social isolation and defensive group affiliations). The study concludes that the current carceral ecology remains overly punitive, and recommends urgent administrative policy shifts toward infrastructural expansion, staff rehabilitative training, and structured inmate development programs.

Keywords: Prison ecology, behavioral adaptations, correctional facilities, Sheger City, rehabilitation, mixed-methods

Introduction

The concept of 'prison ecology' is defined in this study as an integrated tripartite framework encompassing physical infrastructure (housing, sanitation, and spatial density), the social environment (peer dynamics and staff-inmate relations), and institutional policies (governance, security protocols, and rehabilitation access). This comprehensive definition ensures that physical, social, and administrative environmental factors are systematically examined as interconnected determinants of inmate behavioral adaptations (Festa and Lancia, 2024). By treating these three dimensions as a unified ecological system, this framework examines how physical space, social interactions, and institutional governance jointly drive inmate behavioral adaptations, framing adaptation through the depth, weight, and tightness of modern imprisonment (Crewe, 2021; Festa and Lancia, 2024). Behavioral adaptations represent the functional and psychological coping mechanisms inmates employ to navigate these carceral pressures (Crewe, 2021).

Globally, carceral overcapacity triggers psychological distress and acute behavioral adaptations (World Prison Brief, 2024). In East Africa, rapid urbanization intensifies these pressures, with Ethiopian correctional facilities operating at average occupancy rates exceeding 140% (Ethiopian Ministry of Justice, 2022). Crucially, an explicit ecological-behavioral nexus exists: physical infrastructure deficits, social dynamics, and institutional policies directly dictate whether inmate adaptations manifest as constructive pro-social coping mechanisms or defensive anti-social survival tactics.

While international scholarship explores prison ecology (Pellow, 2020; Festa and Lancia, 2024), these insights stem predominantly from Western contexts and lack direct transferability to developing regions facing distinct socioeconomic constraints. Furthermore, literature frequently fragments carceral environments by examining physical overcrowding separately from institutional policies or social dynamics.

In Ethiopia, prior research has addressed isolated variables such as mental health distress or general facility overviews without applying a comprehensive ecological framework that bridges physical, social, and institutional dimensions (Alemayehu, 2022; Habtamu and Desalegn, 2022). Specifically, existing literature frequently examines physical overcapacity in isolation from administrative security policies and informal social networks, obscuring the combined institutional pressure on inmate adaptation. Regionally, studies in Oromia have overlooked the unique municipal pressures of newly established urban centers like Sheger City. Unless explicitly conceptualized as an integrated system, 'prison ecology' risks fragmented interpretation. In this study, prison ecology is operationalized as a unified system where physical spatial density, social peer-staff dynamics, and institutional governance interact continuously to shape individual inmate behavior. This study aimed to addresses this empirical gap through a mixed-methods case analysis in Sheger City, evaluating how integrated ecological pressures drive both pro-social coping mechanisms and anti-social survival strategies.

Materials and Methods

Research Design

A convergent parallel mixed-methods design incorporating a cross-sectional survey was employed. A cross-sectional approach was specifically chosen because it allows for the simultaneous assessment of institutional environmental stressors and inmate behavioral adaptations across diverse prison blocks at a single point in time. In volatile carceral settings characterized by sentence variations and potential inmate transfers, this design minimizes participant attrition, avoids ethical issues associated with longitudinal tracking in high-security facilities, and delivers an accurate snapshot of institutional conditions (Creswell and Creswell, 2018). Quantitative survey data and qualitative narrative accounts were collected concurrently and integrated during analysis for empirical triangulation.

Study Area and Population

The study was conducted in Sheger City, an administrative urban center surrounding Addis Ababa in the Oromia Region, Ethiopia. The Sheger City Correctional Administration governs three municipal correctional facilities: Facility A (Koye Feche Wing), Facility B (Burayu Wing), and Facility C (Sebata/Sheger Central Wing). At the time of data collection in early 2026, the target population comprised 3,000 officially convicted inmates serving sentences across three municipal facilities: Facility A (Koye Feche Wing, 1,100 inmates), Facility B (Burayu Wing, 1,000 inmates), and Facility C (Sebata/Sheger Central Wing, 900 inmates).

Sample Size Determination and Sampling Techniques

Utilizing Yamane's formula at a 95% confidence interval and a 5% margin of error, an initial base sample size of 353 was calculated from the target population of 3,000. Adjusting for a potential 5% non-response rate yielded a targeted sample of 370 respondents, of which 341 questionnaires were fully completed and analyzed (92.2% response rate).

A multi-stage proportional stratified sampling technique was implemented using official correctional registers as the sampling frame. The Sheger City carceral system comprises 3 facilities containing 6 residential blocks and 120 standardized cell units (averaging 25 inmates per cell). The sample of 341 respondents was allocated across facilities, blocks, and cell units using proportional stratified sampling:

Facility A (Koye Feche Wing): Block 1 (Cell Units 1–20); Block 2 (Cell Units 21–40).

Facility B (Burayu Wing): Block 1 (Cell Units 1–20); Block 2 (Cell Units 21–40).

Facility C (Sebata/Central Wing): Block 1 (Cell Units 1–20); Block 2 (Cell Units 21–40).

Systematic random sampling was then applied within each designated cell unit to select individual survey participants."

For qualitative inquiry, criterion-based purposive sampling selected 18 Key Informants (12 convicted inmates with sentence lengths to ensure deep institutional familiarity, and 6 senior correctional administrators). Additionally, 16 inmates participated in two gender-disaggregated Focus Group Discussions (FGD 1: 8 males; FGD 2: 8 females) to reach theoretical saturation regarding shared carceral experiences.

Data Collection Instruments and Procedures

Structured Questionnaire: Administered to 341 inmates, featuring sections on socio-demographics, carceral environmental conditions, and Likert-scale items measuring behavioral coping strategies.

Semi-Structured Interviews: Conducted with purposively selected inmates and staff to capture rich personal narratives regarding institutional culture and survival strategies.

Focus Group Discussions (FGDs): Two sessions held in secure facility rooms to explore collective experiences of overcrowding, staff dynamics, and peer socialization.

Non-Participant Observation: Systematic observation of common areas (courtyards, dining halls) to record unscripted staff-inmate interactions.

Validity and Reliability

Instrument reliability was evaluated through a pilot study of 35 inmates (excluded from the primary analysis). Scale internal consistency was confirmed with Cronbach's alpha () coefficients of 0.84 for the overall prison ecology scale, 0.82 for the pro-social adaptation subscale, and 0.79 for the anti-social adaptation subscale, all exceeding the acceptable 0.70 threshold. Content validity was verified by a panel of four criminologists at Ambo University, and construct validity was established through exploratory factor analysis (EFA), where all retained items demonstrated factor loadings above 0.65.

Data Analysis Procedures

Quantitative survey data were coded, entered, and analyzed using the Statistical Package for the Social Sciences (SPSS version 26). Descriptive statistics (frequencies, percentages, means, and standard deviations) were calculated and presented in standardized thematic tables. Qualitative data from interviews and FGDs were audio-recorded, transcribed verbatim, translated into English, and subjected to inductive thematic analysis (Braun and Clarke, 2021). Data were coded iteratively to generate core thematic clusters (e.g., structural neglect, security-driven containment, dual coping mechanisms), which were subsequently triangulated with the quantitative survey results.

Ethical Considerations

Ethical clearance was officially granted by the Ambo University Institutional Review Board Written institutional permission was secured from the Sheger City Correctional Administration prior to field entry. Informed consent was obtained from all participating inmates and correctional officers. Participants were explicitly informed of voluntary participation, complete anonymity, data confidentiality, and the right to withdraw at any stage without penalty.

Results

Ecological Characteristics of Sheger City Correctional Facility

Inmates perceive the physical and material environment of Sheger City Correctional Facility as severely deficient, with basic material deprivation (food, sanitation) and spatial overcrowding emerging as the primary environmental drivers of interpersonal aggression and loss of personal dignity.

Table 1. Inmate Perceptions of Prison Ecology by Thematic Clusters

Ecological Dimension & Variable Items	**Strongly Disagree (%)**	**Disagree**	**Neutral (%)**	**Agree**	**Strongly Agree (%)**	**Mean**	**SD |**
Basic Needs & Physical Infrastructure							
Insufficient food quantity and quality	5 (1.50)	7 (2.10)	11 (3.20)	121 (35.50)	197 (57.70)	4.46	0.78
Inadequate and untimely medical care	19 (5.50)	25 (7.30)	39 (11.50)	83 (24.40)	175 (51.30)	4.09	1.19
Unclean and poorly maintained sanitation facilities	13 (3.80)	28 (8.20)	45 (13.20)	87 (25.50)	168 (49.30)	4.08	1.14
Limited access to proper hygiene impacts dignity	9 (2.60)	18 (5.30)	38 (11.20)	128 (37.50)	148 (43.40)	4.14	0.99
Safety, Governance & Staff Relations							
Overcrowding leads to increased aggression	9 (2.60)	15 (4.40)	23 (6.70)	123 (36.10)	171 (50.20)	4.27	0.96
Safety & Fairness Inmates feel safe from violence and threats	130 (38.10)	95 (27.80)	65 (19.10)	38 (11.20)	13 (3.80)	2.15	1.16
Unfair and nontransparent administration of rules	155 (45.50)	92 (26.90)	50 (14.70)	25 (7.30)	19 (5.60)	2.01	1.18
Relationships with prison staff lack respect	90 (26.40)	85 (24.90)	78 (22.90)	62 (18.20)	26 (7.60)	2.56	1.27
Rehabilitation & Programs							
Effective educational and vocational training options	133 (39.00)	95 (27.80)	58 (17.10)	37 (10.80)	18 (5.30)	2.16	1.20
Lack of opportunities for recreation and exercise	45 (13.20)	112 (32.80)	89 (26.10)	65 (19.10)	30 (8.80)	2.77	1.18

Note: SD = Strongly Disagree, D = Disagree, N = Neutral, A = Agree, SA = Strongly Agree.

Quantitative survey results in Table 1 indicate an overwhelmingly negative appraisal of physical and infrastructural conditions. A combined 86.3% of respondents agreed or strongly agreed that spatial overcrowding directly heightens interpersonal aggression (Mean = 4.27, SD = 0.96), while 80.9% reported that restricted sanitation compromises personal dignity (Mean = 4.14, SD = 0.99). Furthermore, 66.8% of respondents indicated that effective rehabilitative and vocational programs were lacking (Mean = 2.16, SD = 1.20).

Qualitative thematic analysis strongly reinforced these statistical findings. Themes of physical compression and systemic neglect were prominent during interviews:

"The sleeping blocks are so packed that people sleep shoulder-to-shoulder, and tension over space sparks fights almost every night. Staff view us as security risks rather than human beings undergoing reform." (Inmate Interviewee 04, Male, Age 42, Facility A).

Nature of Staff-Inmate Interactions and Behavioral Influences

Table 2. Perceived Influence of Staff-Inmate Interactions on Behavioral Adaptations

Perceived Nature and Impact of Staff Interactions	Frequency	Percentage (%)
Staff treated us with respect and humanity (Positive)	31	9.10
Negative interactions, like constant harassment, made me more rebellious	26	7.60
The staff's focus on security over rehabilitation	131	38.40
The guards were often abusive and didn't care about our well-being	65	19.10
We were often ignored by staff	72	21.10
Staff-led programs and constructive dialogue helped me learn new skills	16	4.70
Total	**341**	**100.0**

As presented in Table 2, institutional operations are dominated by security containment (38.4%). Cumulative negative custodial experiences comprising emotional detachment (21.1%), abusive treatment (19.1%), and harassment-driven rebellion (7.6%) account for 47.8% of inmate responses. Positive rehabilitative engagement accounted for only 13.8% combined. Qualitative accounts corroborated these metrics, highlighting how custodial hostility fosters alienation and behavioral withdrawal:

"*When I first came here, I thought they were supposed to help us change. But all they talk about is security. If you try to ask for help, they say you're trying to breach security protocols. It makes you feel like a number... Honestly, that lack of trust makes some of us think, 'Why bother changing?*'" (Inmate Interviewee 12, Male, Age 42, Facility B).

Integrated Structure of Inmate Behavioral Coping Mechanisms

Convicted individuals display a dual adaptation model: while 90.3% adopt pro-social coping mechanisms primarily spiritual engagement and peer networks a distinct minority (9.7%) resort to anti-social survival strategies such as social withdrawal, aggressive postures, or protection group affiliations.

To operationalize these coping dynamics clearly, survey distributions were categorized into primary thematic clusters as detailed below (Table 3).

Table 3. Integrated Behavioral Coping Strategies Among Inmates

Adaptation Category	Specific Strategy	Frequency	Percentage (%)	Combined Category %
Pro-Social / Positive				**90.30%**
	Spiritual & Religious Engagement	121	35.40	
	Peer Support Networks & Friendships	87	25.50	
	Family Contact Maintenance	53	15.60	
	Physical Fitness & Recreation	29	8.40	
	Personal Reading & Development	18	5.40	
Anti-Social / Defensive				**9.70%**
	Social Withdrawal & Isolation	18	5.40	
	Aggressive Defensive Posture	8	2.40	

	Protection Group /Gang Association	7	2.00	
Total		**341**	**100.00**	**100.00**

As displayed in Table 3, behavioral adaptations divide into two primary pathways: dominant pro-social coping mechanisms and defensive anti-social survival strategies.

The high prevalence of pro-social adaptations indicates that inmates primarily rely on internal resilience structures. Faith-based participation serves as the primary psychological buffer. As one participant noted during an FGD:

'*Faith and mutual sharing inside the cell are what keep us sane. When food runs low or space becomes unbearable, we rely on our prayer groups and share whatever small items we receive from family visits.' (FGD 1, Participant 03, Male, Facility A*)

Conversely, defensive anti-social mechanisms, though less common, represent essential survival tactics in overcrowded spaces. An interviewee highlighted this dynamic:

'If you appear weak in the cell, you risk being exploited. Some guys isolate themselves completely, while others join informal cell groups just to make sure no one takes their sleeping space or provisions.' (Inmate Interviewee 09, Male, Age 31, Facility C)".

Discussion

Theoretical Integration of Carceral Stressors and Behavioral Adaptations

The empirical findings confirm that the carceral environment in Sheger City acts as a key determinant of inmate behavioral adaptation, supporting the tenets of prison ecology theory (Festa and Lancia, 2024; Pellow, 2020). These results align with carceral deprivation frameworks (Crewe, 2021) and modern reformulations of General Strain Theory in institutional settings (Agnew, 2022; van den Brink *et al*., 2023), demonstrating that physical and administrative stressors function as chronic institutional strains. Taken together, these findings suggest that Sheger City prisons replicate broader regional carceral challenges in Ethiopia, but with intensified behavioral effects due to rapid municipal urban expansion, acute resource constraints, and spatial overcrowding.

In Sheger City, severe overcrowding (86.3%) and material deficits generate environmental pressures that lead to peer conflict. The observed relationship between overcrowding (Mean = 4.27) and interpersonal aggression illustrates how spatial compression heightens emotional distress within residential blocks. The observed predominance of pro-social mechanisms (90.3%) highlights inmates' psychological resilience, whereas the persistence of anti-social survival tactics (9.7%) underscores the necessity of defensive coping where institutional governance is security-centric.

Furthermore, the finding that 66.8% of respondents view rehabilitation programs as ineffective directly aligns with the 38.4% rate of security-driven containment. When custodial institutions prioritize static security over human development, inmates lose faith in formal reform mechanisms, turning instead to informal peer networks and spiritual coping. To improve behavioral outcomes, institutional policies must transition from purely containment-based mandates to structured rehabilitative environments.

Determinants of Coping Adaptation Choice

The findings explain why inmates adopt specific pro-social or anti-social coping strategies. Spiritual engagement serves as a primary pro-social coping mechanism (35.4%) because it provides an internal locus of control and psychological resilience amid material deprivation. Conversely, anti-social adaptations such as defensive postures (2.4%) or protection group affiliations (1.8%) occur primarily when institutional governance fails to ensure physical safety, making collective defense a functional strategy for spatial survival. Where institutional security does not prevent peer victimization, defensive anti-social behaviors emerge as survival mechanisms to secure personal space.

Depth on Coping Mechanisms and Policy Implications

Inmates chose spirituality (35.4%) and peer networks (25.5%) primarily because institutional avenues for personal growth were lacking (66.8% reported ineffective programs). Spiritual practices serve as internal psychological buffers, restoring a sense of agency and personal dignity within an environment characterized by institutional deprivation. Conversely, anti-social tactics such as gang affiliation (1.9%) or defensive aggression (2.4%) emerge directly from structural insecurity and fear of victimization. When custodial governance is perceived as purely security-driven and punitive, informal cell hierarchies form to fill the administrative void, forcing vulnerable inmates to adopt aggressive postures for self-preservation.

Limitations of the Study

This study has several methodological limitations. First, its cross-sectional design captures inmate perceptions and behavioral adaptations at a single point in time, preventing causal inferences regarding how carceral adaptation evolves over prolonged sentences. Second, reliance on self-reported survey data introduces potential response biases, such as social desirability or fear of custodial retaliation, though anonymity protocols were strictly maintained. Third, the empirical focus was restricted to municipal facilities in Sheger City, which may limit the generalizability of findings to rural Ethiopian correctional facilities operating under different institutional dynamics.

Conclusion

This study establishes a clear empirical link between prison ecology and inmate behavioral adaptation within the Sheger City carceral system. Physical overcapacity, severe sanitation deficits, and security-heavy administrative policies create an environment characterized by systemic stress. In response, convicted individuals demonstrate notable psychological resilience, relying overwhelmingly on pro-social coping mechanisms such as spiritual practice and peer support. However, custodial hostility (47.8% negative custodial interactions) and a pronounced lack of rehabilitative programming (66.8% rating programs as non-existent or ineffective) force a subset of inmates into defensive anti-social survival tactics (9.7%). Transforming these carceral spaces from punitive holding facilities into genuine centers for rehabilitation requires immediate infrastructural expansion, administrative policy shifts, and institutionalized human rights training for correctional personnel.

Recommendations

1. Infrastructural Decompression & Facility Expansion: To mitigate the 86.3% rate of

overcrowding-induced aggression and severe sanitation deficits (80.9%), regional justice bureaus should prioritize expanding residential block capacities and upgrading sanitation facilities.

2. Custodial Staff Training Reform: Addressing the 47.8% negative custodial interaction rate requires shifting staff training from static security containment (38.4%) toward dynamic security, human rights principles, and rehabilitative communication strategies.

3. Structured Vocational & Educational Programs: To counter the 66.8% perceived insufficiency of reformative programs, municipal correctional administration should partner with local TVET institutes and NGOs to establish certified skill-building options.

4. Institutional Integration of Pro-Social Support Networks: Given that 90.3% of inmates adapt through pro-social mechanisms—predominantly spiritual engagement (35.4%) and peer networks (25.5%)—facility management should formally accommodate faith-based and peer-mentorship initiatives as core rehabilitative frameworks

Acknowledgments

The authors are grateful for the collaboration of those who participated in this study.

Funding

This research is fully funded by Ambo University

Declaration of conflict of interest

The author declares that there is no potential conflict of interest with respect to the research, authorship, and/or publication of this article.

References

Agnew, R. (2022). General strain theory and carceral adaptation: Unpacking institutional environmental stressors. *Journal of Quantitative Criminology*, 38(2), 245–269. https://doi.org/10.1007/s10940-021-09512-3

Alemayehu, G. (2022). Institutional challenges and human rights compliance in Ethiopian correctional facilities: A regional overview. *Ethiopian Journal of Human Rights*, 14(1), 88–12.

Braun, V. & Clarke, V. (2021). *To thematic analysis: Conceptual foundations and practical guidelines*. Sage Publications.

Creswell, J. W. & Creswell, J. D. (2018). *Research design: Qualitative, quantitative, and mixed methods approaches*. 5th edition, Sage Publications.

Crewe, B. (2021). The depth, weight, tightness, and breadth of imprisonment in modern penal systems. *Theoretical Criminology*, 25(3), 339–361. https://doi.org/10.1177/13624806211018382.

Ethiopian Ministry of Justice. (2022). *Annual national correctional administration statistics and facilities report*. FDRE Ministry of Justice.

Festa, M. & Lancia, M. (2024). Prison ecology and institutional dynamics: A systematic review of carceral spatial impacts on behavior. *Criminology & Criminal Justice*, 24(1), 102–124. https://doi.org/10.1177/17488958231182901.

Habtamu, T. & Desalegn, M. (2022). Overcrowding and inmate mental health outcomes in regional correctional centers in Oromia, Ethiopia. *African Journal of Criminology and Security Studies*, 9(2), 45–61.

Pellow, D. N. (2020). Toward a critical environmental justice approach to carceral spaces and prison ecology. *Environmental Justice*, 13(5), 160–168. https://doi.org/10.1089/env.2020.0028.

van den Brink, Y., van der Laan, A. & de Keijser, J. (2023). Strain, coping, and behavioral adaptations in institutionalized populations: Testing strain theory in carceral contexts. *Crime & Delinquency*, 69(4), 512–538. https://doi.org/10.1177/00111287221083921.

World Prison Brief. (2024). *World prison population list.* 14th edition, Institute for Crime & Justice Policy Research.

Journal of Science and Sustainable Development (JSSD), 2026, 14(2), 39-59

ISSN: 2304-2702 (print); 2414-4479 (online)
DOI: 10.20372/au.jssd.14.2.2026.0752

RESEARCH PAPER

Integrated Assessment of Land Use/Land Cover Dynamics and Climate Change Impacts on Watershed Hydrology in the Dawe Watershed, Ethiopia

Birhanu Legesse Wakjira[1]*, Asfaw Kebede Kassa[2], Awdenegest Moges[3], Olkeba Tolessa Leta[4]

[1]*Ph.D. candidate, Department of Natural Resources Management, Ambo University, Ethiopia. birelegesse2000@gmail.com, https://orcid.org/0009-0008-7237-4315*
[2]*Haramaya Institute of Technology, Ethiopia. asfaw649@gmail.com, https://orcid.org/0000-0002-6496-7216*
[3]*Department of Agricultural Engineering, Hawassa University, Ethiopia. awde_moges@yahoo.co.uk, https://orcid.org/0000-0001-6084-8327*
[4]*St. Johns River Water Management District, Palatka, FL, United States. olkebat2005@gmail.com, https://orcid.org/0000-0003-3479-901X*

***Corresponding author**: *birelegesse2000@gmail.com*

Abstract

Freshwater sustainability is increasingly threatened by the impacts of land use/land cover (LULC) dynamics and climate changes, mainly in arid and semi-arid data-scarce watersheds of developing countries. This study assessed the separate and combined effects of predicted LULC dynamics and climate changes on the water resources in the Dawe watershed, Ethiopia. Future LULC was projected using a Cellular Automata (CA)-Markov model, while climate projections were derived from an ensemble of six CMIP6 Global Climate Models (GCMs) under the shared socioeconomic pathways (SSPs) SSP2–4.5 and SSP5–8.5. Hydrological responses were simulated using the Soil and Water Assessment Tool Plus (SWAT+) under nine scenarios (S0–S8), integrating projected LULC conditions (2024 and 2062) with mid-century (2024–2055) and late-century (2056–2085) climate projections. With Nash-Sutcliffe efficiency (NSE) and Kling-Gupta efficiency (KGE) values surpassing 0.8 during both calibration and validation, the model demonstrated strong performance. The simulations demonstrate a consistent increase in evapotranspiration (ET) under all scenarios, ranging from 13.0% under climate change alone (S1) to 23.4% under the combined LULC and climate change scenario (S8). In contrast, water yield (WY), surface runoff (SR), and groundwater recharge (GWR) will decline under all future scenarios, with the greatest reduction occurring under the combined effects of LULC and climate change. Under the worst-case scenario (S8: SSP5–8.5, 2062 LULC, and late-century climate), WY decreased by 34.5%, SR by 32.9%, and GWR by 23.2%. The continued land expansion and warming will alter watershed hydrology. Climate change is the main driver of hydrological shifts, amplified by LULC change. The worst impacts occur under combined SSP5–8.5 and 2062 LULC, so assessing drivers separately underestimates risks, underscoring the need for integrated modeling. These results highlight the necessity of integrated land and water resource management strategies to enhance water security and strengthen climate resilience.

Keywords: CMIP6, SWAT+, SSP, LULC dynamics, climate change, Dawe watershed.

Introduction

Freshwater resource is fundamental to sustain life on the globe. However, it is increasingly threatened by the effect of land use/land cover (LULC) dynamics and climate change. According to the Intergovernmental Panel on Climate Change (IPCC), rising temperatures, altered precipitation regimes, increasing climate variability, rapid population growth, and accelerating land degradation are intensifying water scarcity worldwide, with the greatest impacts occurring in semi-arid and arid regions (IPCC, 2023).

The impacts of these environmental changes are particularly pronounced in Sub-Saharan Africa, where livelihoods and national economies depend heavily on climate-sensitive sectors such as rain-fed agriculture (Shah et al., 2008). Moreover, limited adaptive capacity, rapid population growth, and increasing pressure on natural resources further heighten the vulnerability of the region to hydrological extremes (IPCC, 2023). Ethiopia is the most climate change affected nation in the region, mainly because of its dependence on rain-fed agriculture (Feleke *et al*., 2025; Gebrechorkos *et al*., 2019). In recent decades, the country has experienced recurrent droughts, increasing erratic rainfall, rising temperatures, and continuous degradation of natural vegetation, resulting in declining water availability, reduced agricultural productivity and increasing food insecurity (Amsalu, 2019; Aragaw *et al*., 2021).

Beyond climate change, LULC dynamics have emerged as major drivers of hydrological change. Human-induced land transformations, including agricultural expansion, deforestation, urbanization, and overgrazing, substantially modify watershed hydrological processes by altering interception, infiltration, evapotranspiration, runoff generation, and groundwater recharge (Birhanu *et al*., 2022; Kuma *et al*., 2022). In Ethiopia, the rapid conversion of forests, shrublands, and wetlands into cultivated and built-up areas has accelerated over the last few decades (Ayalew and Nigussie, 2023; Wudineh, 2023). The prevailing water resources scarcity is being exacerbated by the intensified soil erosion, reduced ecosystem resilience, and diminished capacity of watersheds to regulate stream flow and recharge groundwater.

Climate change and LULC change are closely interrelated and often reinforce each other. Climate change influences LULC through changes in vegetation distribution, agricultural practices, drought frequency, and land degradation. However, LULC changes contribute to climate change by altering surface energy balance, reducing carbon sequestration, and increasing greenhouse gas emissions through deforestation and urban expansion (Bikeko and Venkatesham, 2024; FAO, 2023; Yang *et al*., 2024). Their combined impacts produce nonlinear hydrological responses that differ substantially from the impacts of either driver alone. As a result, assessing these factors separately could underestimate future shifts in watershed hydrology and water availability.

The Dawe watershed, located in the northeastern Wabi-Shebelle River Basin (WSRB) in eastern Ethiopia, is experiencing the impact of LULC dynamics and climate changes (Harka *et al*., 2020). The watershed is facing water scarcity because of the combined influence of climate variability, rapid urbanization, agricultural expansion, and environmental degradation (Engdaw, 2016). The expansions of cultivated and built-up regions at the expense of forest and shrublands has been affected by fast population growth and rising agricultural land demand (Eva *et al*., 2024; Siraj *et al*., 2023). These changes have reduced the natural water retention capacity, increased surface runoff, and accelerated soil erosion. Subsequently, the long-term viability of water supplies and ecosystem services within the watershed are threatened.

Numerous studies have investigated the effects of climate change and/or LULC change on watershed hydrology in Ethiopia. However, their separate and combined consequences were not evaluated using advanced hydrological models and next-generation climate projections. Most previous studies relied on earlier generations of climate models the Coupled Model Intercomparison Project Phase five (CMIP5), which considered a limited number of climate scenarios, or assessed LULC and climate change separately. As a result, they overlooked the combined effects of these drivers on the watershed hydrology. Moreover, studies that integrate future LULC simulations, CMIP6 climate projections, and the recently restructured SWAT+ model remain limited in Ethiopian watersheds, especially in data-scarce semi-arid watersheds like the Dawe watershed.

Advances in spatial modeling and climate science provide an opportunity to address these limitations. The Cellular Automata-Markov (CA-Markov) model has demonstrated strong capability in simulating future LULC changes by capturing both temporal trends and spatial allocation patterns derived from historical satellite observations (Atulley, 2023; Semegnew *et al*., 2021). Similarly, the latest CMIP6 provides an improved representation of future climate variability and extremes under different projection scenarios compared with previous generations of Global Climate Models (GCMs) (Gebisa and Dibaba, 2024; Yilmaz *et al*., 2024). These variables are used as a robust input for hydrological simulations. These methods allow for thorough evaluation of future watershed responses under various land use and climate change scenarios when incorporated into hydrological models like SWAT+.

The purpose of this study was to evaluate the separate and combined impacts of future LULC change and climate change on the hydrological processes of the Dawe watershed, Ethiopia. Specifically, future LULC change patterns were simulated using the CA-Markov model; climate projections were derived from an ensemble of six CMIP6 GCMs under Shared Socioeconomic Pathways (SSP) SSP2–4.5 and SSP5–8.5 scenarios; and watershed hydrological responses were evaluated using the SWAT+ model. By integrating state-of-the-art land use modeling, future climate projections, and advanced hydrological simulation, this paper offers a comprehensive evaluation of potential water balance dynamics and generates scientific evidence to help sustainable management of watershed, climate change adaptation, and water security planning in semi-arid regions facing similar challenges.

Materials and Methods

Description of the Study Area

The study was conducted in the Dawe watershed, located in the northeast WSRB, Ethiopia. Geographically, it is situated between 9°13.5’ and 9°28.5' N and 41°42’ and 41°53’ E (Fig. 1). Its elevation ranges from 1695–3313 m above sea level, with the western part being mountainous and the eastern part being flat, predominantly agricultural land. The majority of the watershed is a sub-humid agro-ecological zone with an average yearly precipitation of 833 mm. Fig. 2 shows that the mean yearly high and low temperatures were 24.14°C and 10.99°C, respectively. The watershed has a low drainage density (0.55 km/km^2), which is the ratio of the sum of all stream lengths (202.133 km) to the watershed area (368.94 km^2). Lower drainage density indicates higher infiltration capacity, low runoff generation, and greater potential for groundwater recharge.

The watershed is distinguished by a mixed farming system that combines the production of livestock with crop cultivation (Zeleke *et al*., 2021). Agriculture is the dominant LULC type, followed by shrub land, with farmland covering more than 80% of the watershed. Soil and water conservation practices, including contour farming, soil bunds, and strip cropping (e.g., khat or coffee intercropped with sorghum, maize, or vegetables), are widely practiced (Roba *et al*., 2021). The predominant soil types are Rendzic Leptosols, Chromic Luvisols, Eutric Leptosols, and Humic Nitisols (Fig. 3).

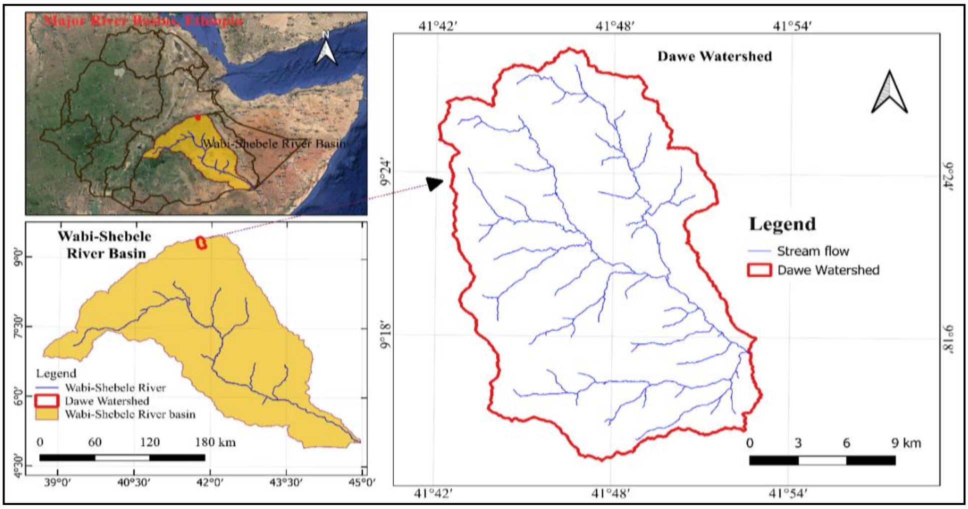

Figure 5. Location of the Dawe watershed in the northeast of the Wabi-Shebelle River basin.

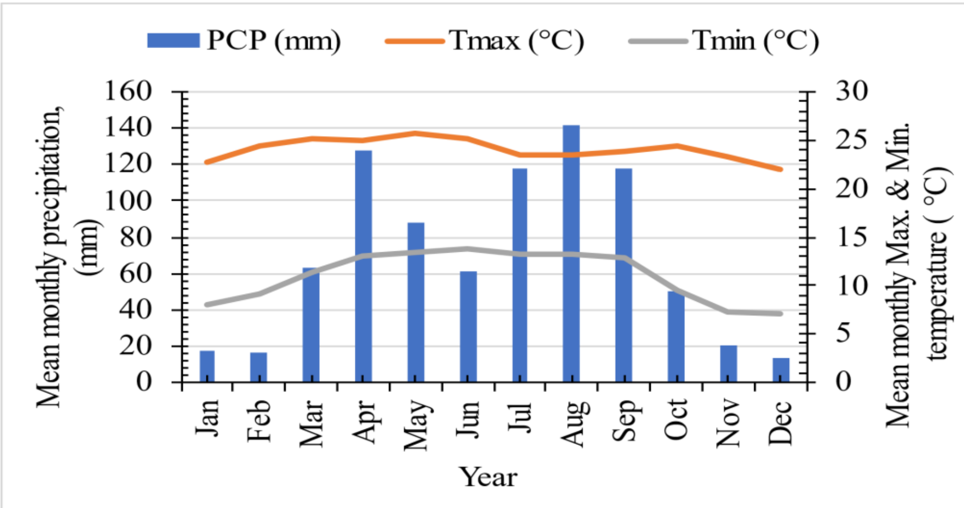

Figure 6. Historical monthly precipitation (mm), maximum, and minimum temperature (°C)

Database

Geospatial and hydrometeorological data

Landsat imageries (Table 1) (https://glovis.usgs.gov), DEM (https://search.earthdata.nasa.gov/), street network (https://www.openstreetmap.org/), stream network (derived from the DEM in SWAT+), and city center were used for LULC classification and prediction. Fig. 3 shows the DEM, soil (Harmonized World Soil Database), and LULC maps of the Dawe watershed. Meteorological (1988–2013) (Table 2) and hydrological data (1997–2013) were obtained from the Ethiopian Meteorology Institute (EMI) and Ministry of Water and Energy (MoWE) of Ethiopia, respectively.

Table 10. Landsat images and their characteristics, where MSS (Multispectral Scanner), ETM+ (Enhanced Thematic Mapper Plus), OLI (Operational Land Imager), and TIRS (the Thermal Infrared Sensor).

Product	Sensor	Acquisition Date (yyyy/mm/dd)	Path/Row	Resolution (m)	Day/night
Landsat 3	MSS	1985/01/20 1985/01/20	166/54,55	30	Day
Landsat 7	ETM+	2000/12/23 2000/12/07	166/54,55	30	Day
Landsat 8	OLI/TIRS	2022/01/26	166/54,55	30	Day

Sources*:* (https://glovis.usgs.gov)

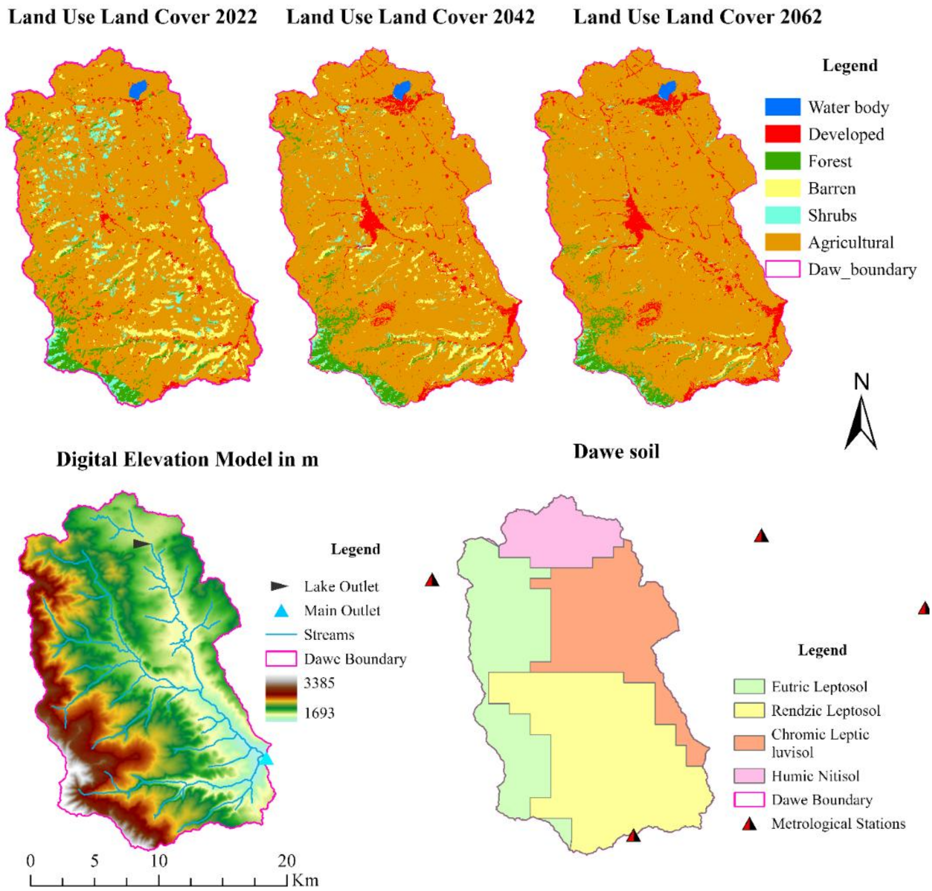

Figure 7. Digital elevation model, soils, LULC maps, and the meteorological station of the Dawe watershed.

Table 11. Meteorological stations and their geographic locations

ID	Station name	Latitude (decimal degree)	Longitude (decimal degrees)	Elevation (m)
1	Haramaya	9.40	42.03	2020
2	Dengego	9.45	41.92	2078
3	Harar	9.31	42.09	1977

4	Kullubi	9.42	41.68	2436

Climate model data

The ensemble of six CMIP6 GCMs' data for SSP2–4.5 and SSP5–8.5 (Table 3) for the period 2024–2085 was used for the simulation of hydrological data. The models were chosen based on the accessibility of the required variables (pr, tasmax, tasmin) and their capacity to reproduce Ethiopia in East African monsoon dynamics and seasonal rainfall patterns (Berhanu *et al*., 2023; Omay *et al*., 2023; Seifu and Eshetu, 2024). The SSP2–4.5 (moderate emissions) and SSP5–8.5 (fossil fuel-driven high-emissions) pathways were used because they represent contrasting yet widely used climate futures, thereby capturing a broad range of potential climate outcomes.

Table 12. Description of climate models for SSP2-4.5 and SSP5-8.5 emission scenarios

Model	Description	Institution	Spatial Resolution
ACCESS-CM2	Australian Community Climate and Earth System Simulator Coupled Model v2	CSIRO/Bureau of Meteorology	1° x 1°
CMCC-ESM2	Euro-Mediterranean Center on Climate Change Earth System Model v2	CMCC, Italy	1.875° x 1.875°
GFDL-ESM4	Geophysical Fluid Dynamics Laboratory Earth System Model Version 4	NOAA/GFDL, USA	1° x 1°
MPI-ESM1-2-LR	Max Planck Institute Earth System Model v1.2 Low Resolution	Max Planck Institute, Germany	1.875° x 1.875°
MRI-ESM2-0	Meteorological Research Institute Earth System Model v2.0	MRI, Japan	1.4° x 1.4°
NorESM2-MM	Norwegian Earth System Model v2 Medium Resolution	Norwegian Climate Centre (NCC)	2° x 2°

Source: https://cds.climate.copernicus.eu.

Bias Correction and Statistical Evaluation

Bias in GCM-simulated precipitation and temperature was corrected using the bias-correction algorithms implemented in the CMhyd (Rathjens *et al*., 2016). CMhyd is the most frequently used bias correction technique for analyzing how climate change affects water resources at the watershed level (Seifu and Eshetu, 2024).

The Linear–scaling approach was used in the bias correction. It assumes that the historical model–observation bias remains sufficiently stable for the correction factors to be applicable to future simulations. The observed station data were used as the reference dataset. Monthly correction factors were derived from the past period and applied separately to precipitation and temperature. A multiplicative correction was used for precipitation, while an additive correction was applied to temperature. Using Root Mean Squared Error (RMSE), Mean Absolute Error (MAE), and PBIAS, the efficacy of the bias correction was assessed by comparing raw and bias-corrected simulations with observations for each station–GCM combination.

Methods

General Framework

Fig. 4 presents the conceptual framework of the study. It integrates remote sensing-based LULC analysis, hydrological modeling, and climate modeling to assess how the hydrology of the Dawe watershed will be affected by potential change in LULC and climate.

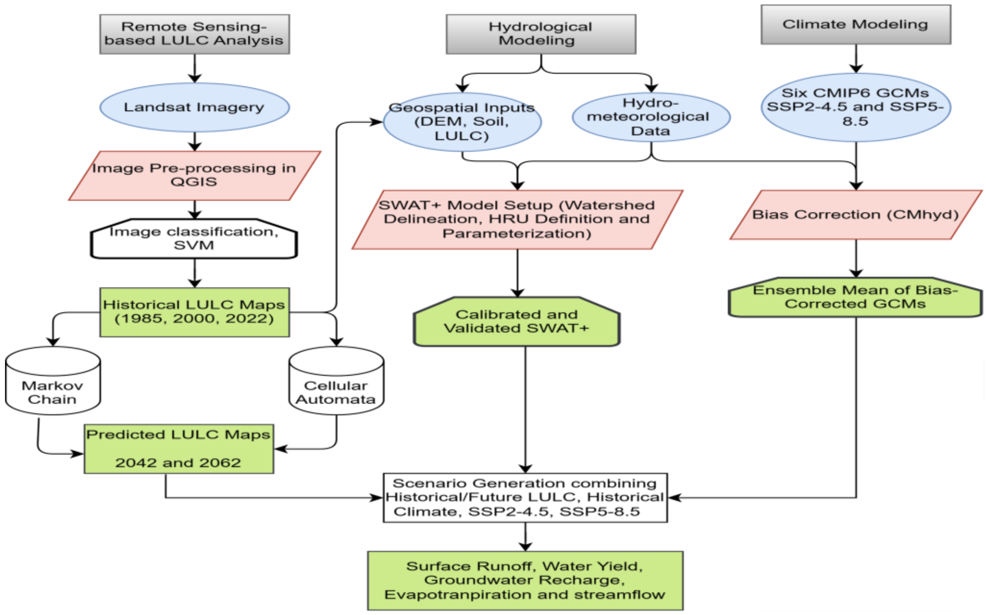

Figure 8. A framework to estimate watershed hydrology by integrating LULC prediction, SWAT+ hydrological modeling, and an ensemble of six CMIP6 GCMs to estimate watershed hydrology. Blue represents input datasets, pink denotes data processing and model setup, white indicates analytical/modeling processes, and green represents intermediate and final outputs.

Land Use/Land Cover Classification and Prediction

The historical LULC was classified from Landsat imageries (2000 and 2022) using a Support Vector Machine (SVM) algorithm in ArcGIS Pro. The error matrix was used to generate the overall accuracy (OA), which represents the overall classification accuracy across all LULC classes (Congalton and Green, 2019). The land use classification by chance was taken into account using Cohen's Kappa coefficient (K), a robust nonparametric statistical measure (Rwanga and Ndambuki, 2017). The kappa value varies from –1 to 1. A kappa of –1, 0, and 1 denotes disagreement, agreement by chance, and perfect agreement, respectively. The SVM was chosen because of its track record of outperforming other machine learning (ML) algorithms in terms of overall classification accuracy (Siraj *et al.*, 2023).

A CA-Markov model within the Land Change Modeler (LCM) in Idris TerrSet was used to predict the LULC of 2042 and 2062. The CA-Markov model was used to project future LULC based on historical transition patterns. It integrates the temporal transition probabilities of the Markov chain with the spatial allocation capabilities of CA to simulate future LULC patterns (Gebresellase *et al.*, 2023).

Hydrological Model

The SWAT model, a large-scale basin model, is most commonly used globally due to ease of obtaining input, high computational efficiency, its capability of long-term watershed simulation, and its being in the public domain (Arnold *et al.*, 1998). SWAT+, a completely redesigned version of SWAT, a powerful distributed hydrological model with several uses, was employed in this investigation (Bieger *et al.*, 2017).

Model Setup

The Dawe watershed was divided into 25 sub-basins, 73 landscape units (LSUs), and 1631 hydrological response units (HRUs) using QSWAT+ following its delineation. The Muskingum method was used to simulate monthly stream flow, and Penman–Monteith was used for PET estimation (Bieger *et al*., 2017).

Model parameter sensitivity analysis

The SWAT+ Toolbox was employed to perform the sensitivity of model parameters, and the model calibration and validation. Due to the existence of hundreds of parameters describing hydrological, soil, land-use and management processes 18 commonly used were chosen through a combination of literature information and the researchers' expertise. The impact of these parameters on the model's results was assessed utilizing Random Balance Designs–Fourier Amplitude Sensitivity Test (RBD-FAST) within the SWAT+ Toolbox version. RBD-FAST is a comprehensive sensitivity analysis method that employs the Fourier amplitude sensitivity test through a random balance design strategy (Xiang *et al*., 2022). The parameters were ranked depending on how they affected the model's simulation after the sensitivity study was finished. The parameter with the greatest impact was assigned the first rank, indicating its significant effect on the model results, while the parameter with the lowest impact was ranked last. Subsequently, the top 12 parameters from the sensitivity ranking were selected for the tasting and verifying the model.

Calibration and Validation

The SWAT+ model development covered the period from 1998–2013. The model was calibrated for the period from 2000 to 2008; the first two years were used for model warm-up. Then, the model was validated for the period from 2009–2013. Automatic calibration was performed using the 'Calibration by Latin-hypercube Sampling Iterations (CALSI)' algorithm. Based on the value of the objective function, the alignment between the observed and simulated stream flow hydrograph, and the water balance ratios, the model parameters were manually calibrated (Arnold *et al*., 2012).

Nash-Sutcliffe Efficiency (NSE) (Nash and Sutcliffe, 1970), Kling-Gupta Efficiency (KGE), PBIAS, and coefficient of determination (R^2) (Arnold *et al*., 2012) were used to assess the hydrological model performance during calibration and validation. The NSE shows how well the 1:1 line fits the plots of the simulated and observed stream flow data. The NSE measures how well the two data values agree. It ranges from -∞ to 1, with a value closer to 1, demonstrating better model performance. NSE of 0 shows poor model performance, which is no better than the observed mean, while values less than 0 indicate that its performance is worse than the observed mean.

The average tendency of the simulated data to match the observed data was compared using PBIAS. The ideal PBIAS value is zero. For stream flow model simulations, NSE > 0.50 and PBIAS < ±25% were deemed acceptable (Moriasi *et al*., 2007). R^2 is the degree to which the simulated and observed values have a linear relationship. Greater model performance is shown by higher values on the R^2 scale, which ranges from 0 to 1.

Furthermore, KGE was used, which combines correlation coefficient, variability ratio, and bias ratio to create a single measure of model performance. The constraints of NSE and R^2 were overcome by KGE's capacity to replicate the timing and variability of the observed data (Gupta *et al*., 2009). The range of KGE is −∞ to 1, where 1 denotes perfect agreement and more than 0.75 is being considered acceptable.

LULC and climate change impact assessment

This study used a comparative scenario-based method to measure the separate and combined impacts of LULC dynamics and climate changes on hydrological components (SR, GWR, WY, and ET). The combination of two climate projections (SSP2–4.5 and SSP5–8.5) and two predicted LULC maps (LULC 2042 and 2062) was considered across two time periods: mid-century (2024–2055) and late-century (2056–

2085). Nine scenarios, spanning from S0–S8, were developed, as summarized in Table 4.

Two climate projections were selected because these emission scenarios capture a broad range of plausible climate futures, from intermediate to worst-case conditions. SSP2–4.5 corresponds to a moderate emission trajectory, assuming sustainable development and partial mitigation, while SSP5–8.5, on the other hand, represents a development route with high emissions and a strong reliance on fossil fuels (Riahi *et al*., 2017). The LULC map of 2022 was used as a reference, while the LULC 2042 and LULC 2062 projections were used to capture the future land cover dynamics within 2022–2055 and 2056–2085, respectively. The selected time horizons were aligned with the standard climate assessment periods recommended by the IPCC. This makes it possible to assess long-term hydrological threats and short- to mid-term adaptation requirements.

The impact of LULC alteration on hydrological components was assessed using a differential scenario-based approach. In hydrological impact assessments, this method is frequently employed to determine the overall impact of LULC change under stationary climate assumptions. We recognize that this assumption does not take into consideration possible feedbacks (e.g., LULC-induced changes in local evapotranspiration altering regional rainfall patterns). However, considering the limits of the SWAT+ framework with respect to independent LULC-only simulations under future climatic forcing, the differential approach is still suitable for this investigation. Therefore, rather than focusing on absolute attribution, the data are interpreted cautiously, emphasizing the direction and relative size of LULC-driven changes.

Table 13. Summary of the scenario matrix. "Mid" stands for mid-century (2024–2055), and "Late" for late-century (2056–2085).

Scenario	**LULC**	**Climate**
S0	2022	Baseline
S1	2022	SSP2-4.5 Mid
S2	2022	SSP2-4.5 Late
S3	2022	SSP5-8.5 Mid
S4	2022	SSP5-8.5 Late
S5	2042	SSP2-4.5 Mid
S6	2042	SSP5-8.5 Mid
S7	2062	SSP2-4.5 Late
S8	2062	SSP5-8.5 Late

Source: Own Study

RESULTS

Projected LULC Change

The CA-Markov model in Idrisi software was employed to predict the LULC maps for 2042 and 2062 (Table 5). The model's ability to predict LULC change was evaluated using three Kappa statistics: Klocation (0.82), Kstandard (0.75), and Kno (0.84). OA of 89% and κ of 0.87, the historical classification reveals a high degree of agreement between the classified map and the reference material. PA ranging from 82.0% to 96.5% and UA ranging from 86.5% to 92.5% (Table 6) demonstrate strong classification performance.

Table 14. Present and predicted LULC of the northeast WSRB. LULC 2022 is based on Landsat 8 image classification using a support vector machine (SVM).

LULC	**Area (km²)**			**Change in %**		
	2022	2042	2062	2042-2022	2062-2042	2062-2022
Water	6.8	5.31	4.06	-21.90	-23.50	-40.25
Developed	137.8	406.93	918.18	195.31	125.63	566.31
Forest	329.8	228.83	197.44	-30.62	-13.72	-40.13
Barren	2853.5	2898.71	2992.33	1.58	3.23	4.87
Shrubs	7615.9	7079.92	6111.63	-7.04	-13.68	-19.75
Agriculture	3883.8	4208.20	4603.70	8.35	9.40	18.54

Table 15. Confusion matrix showing the accuracy assessment of historical land use/land cover classification.

LULCC	**Water**	**Developed**	**Forest**	**Barren**	**Shrubs**	**Agriculture**	**Total**	**UA**
Water	74	0	3.00	0.50	1.50	1.00	80	0.925
Developed	0	80	0.50	6.00	0.50	3.50	90	0.885
Forest	4.5	0	84.50	1.00	6.00	1.50	97	0.865
Barren	0.5	2	0.00	92.50	3.50	4.00	102	0.895
Shrubs	1.5	1	9.00	9.00	173	3.00	196	0.88
Agriculture	0.5	0	2.00	3.50	9	113.50	128	0.885
Total	81	83	99.00	112.50	193.5	126.50	693	713
PA	0.915	0.97	0.86	0.82	0.89	0.90		
Kappa coefficient = 0.87 and Overall accuracy = 0.89								

where PA = Producer's Accuracy, UA = User's Accuracy.

Climate Model Bias Correction

The bias-correction results (Table 7) show substantial improvements in the CMIP6 simulations. For rainfall, RMSE decreased by 33.1%, MAE by 11.9%, and PBIAS by 87.6%. On the other hand, Tmax RMSE and MAE decreased by 48.7% and 57.9%, while Tmin showed reductions of 66.8% and 73.7%, respectively. Absolute systematic bias was reduced by 99.3% for Tmax and 97.9% for Tmin. Aggregates of post-bias-correction by stations and GCMs are given in Table 7, 8 & 9.

Table 16. Post-bias correction performance aggregated by station (mean and range across all six GCMs).

Station	**Variable**	**RMSE (Mean ± Range)**	**MAE (Mean ± Range)**	**PBIAS (Mean ± Range)**
Dengego	Precip	7.94 (7.37 – 8.71)	3.33 (2.83 – 3.80)	-2.73 (-8.27 – 1.38)
	Tmax	3.56 (2.55 – 4.16)	2.34 (2.00 – 2.80)	-0.10 (-0.92 – 0.17)
	Tmin	3.80 (3.56 – 4.62)	2.31 (2.01 – 3.49)	3.59 (0.00 – 19.77)
Haramaya	Precip	7.66 (7.08 – 8.45)	3.18 (2.83 – 3.79)	-2.86 (-8.55 – 0.00)
	Tmax	2.68 (2.34 – 3.17)	2.10 (1.84 – 2.48)	0.97 (0.00 – 5.84)

	Tmin	3.63 (3.41 – 4.29)	2.75 (2.53 – 3.06)	0.01 (0.00 – 0.02)
Harar	Precip	7.38 (6.81 – 8.20)	3.10 (2.81 – 3.70)	-3.18 (-10.89 – 0.00)
	Tmax	3.07 (2.59 – 4.01)	2.24 (1.91 – 2.70)	0.79 (-0.01 – 4.80)
	Tmin	2.45 (2.29 – 2.47)	1.79 (1.68 – 1.92)	0.00 (-0.01 – 0.00)
Kulubi	Precip	8.73 (8.31 – 9.36)	3.60 (3.40 – 4.14)	-4.30 (-12.09 – 0.34)
	Tmax	3.98 (3.61 – 4.52)	2.28 (1.98 – 2.86)	-0.85 (-8.90 – 0.35)
	Tmin	2.34 (1.88 – 3.33)	1.82 (1.41 – 2.72)	-2.28 (-18.53 – 0.00)

Table 17. Post-bias correction performance aggregated by GCM (mean across all four stations).

GCM	**Precip RMSE**	**Precip PBIAS**	**Tmax RMSE**	**Tmax PBIAS**	**Tmin RMSE**	**Tmin PBIAS**
ACCESS-CM2	7.88	-0.74	3.05	0.13	2.98	0.11
GFDL-ESM4	8.65	0.13	3.30	0.13	3.08	0.11
MPI-ESM1-2-LR	7.39	-9.95	3.65	2.79	3.29	0.72
MRI-ESM2-0	8.30	-0.01	3.78	0.00	2.86	0.00
NESM3	7.39	-9.43	3.01	-1.74	3.15	-4.63
NorESM2-MM	7.92	0.00	2.69	-0.14	3.23	4.94

Table 18. Summary of bias-correction performance for rainfall and temperature maximum (T_{max}) and minimum (T_{min}) across all stations and GCMs, showing RMSE, MAE, and PBIAS before (Raw) and after (BC) correction.

Variable	RMSE Raw → BC	MAE Raw → BC	PBIAS Raw → BC
Rainfall	11.74 → 7.85	3.95 → 3.48	−33.73 → −4.17%
Tmax	6.31 → 3.24	5.18 → 2.18	20.93 → 0.14%
Tmin	9.30 → 3.09	8.39 → 2.21	75.92 → 1.63%

Climate Change Trend

The projected climate data from the six-GCM ensemble from CMIP6 projects a significant warming trend by the late 21st century (Fig. 5). The average yearly temperature under the SSP2–4.5 and SSP5–8.5 scenarios is predicted to rise by 2.54°C and 3.44°C, respectively, over the baseline period (1988–2013).

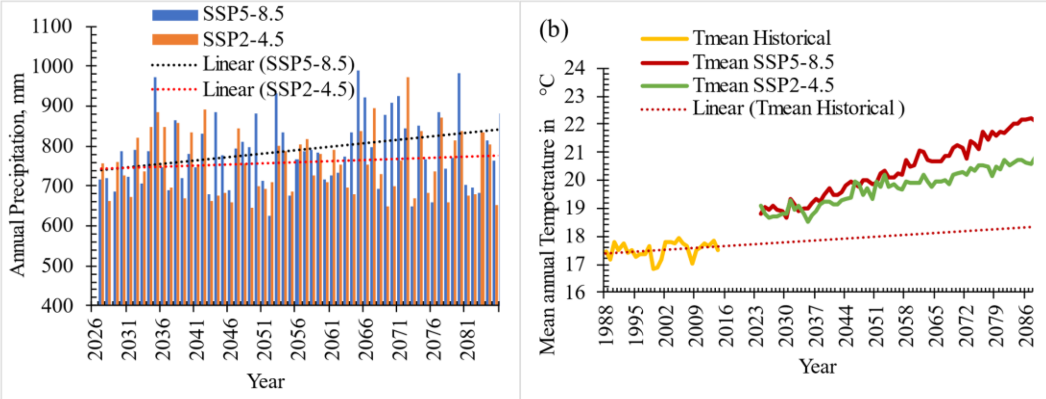

Figure 9. Projected annual precipitation (a) and average annual temperature (b) for the 2024–2085 SSP2–4.5 and SSP5–8.5 scenarios.

Calibrated and Validated QSWAT+

The calibrated parameters with their range of values, sensitivity order, and auto- and manual-fitted values are listed in Table 10. The sensitivity analysis showed that CN2 was most sensitive, followed by the soil evaporation compensation factor (ESCO) and percolation coefficient (PERCO). This implies that land use and soil type are the most important variables controlling the water flow in the area.

Table 19. Sensitivity analysis and calibrated values of key hydrological parameters showing their relative influence on model performance, allowable ranges, parameter adjustments, and final fitted values.

Parameters	**Descriptions**	**Value Range**	**Sensitivity order**	**Adjustment value**	**Fitted Value**
p_CN2	SCS curve number for moisture condition II	±20	1.535	3.652	78.776
r_ESCO	Soil Evaporation Compensation Factor	0 - 1	0.277	0.206	0.206
r_PERCO	Percolation Coefficient	0 - 1	0.228	0.684	0.684
p_BD	Soil Bulk Density	±20	0.198	11.448	1.337
r_REVAP_CO	Groundwater "revap" coefficient	0.02 – 0.2	0.039	0.115	0.115
p_AWC	Available water capacity of the soil layer	±10	0.007	5.292	0.097
p_SURLAG	Surface Runoff Lag Coefficient	±30	0.005	4.007	13.729
p_FLO_MIN	Threshold depth for groundwater flow	0 - 20	0.0003	0.407	0.973
r_ALPHA	Baseflow Alpha Factor	0.01-0.9	-0.0013	0.583	0.583
p_K	Saturated Hydraulic Conductivity	±10	-0.007	13.981	23.047
r_CN3_SWF	Soil Water Factor for Curve Number III	0 – 1	-0.079	0.189	0.189
r_CANMX	Maximum Canopy Storage	1 - 100	-0.118	17.728	17.728

p represents the percent of change of the default value of parameters, and r represents changes of parameters in which the existing value is replaced by the new value. Negative sensitivity values for K, CN3_SWF, and CANMX indicate inverse relationships with stream flow.

The SWAT+ demonstrated a strong association between the simulated and observed streamflow. as indicated by the KGE, NSE, R^2, and PBIAS values during both the calibration and validation periods. The results show that the SWAT+ model is trustworthy for upcoming evaluations of the effects of climate change (Fig. 6).

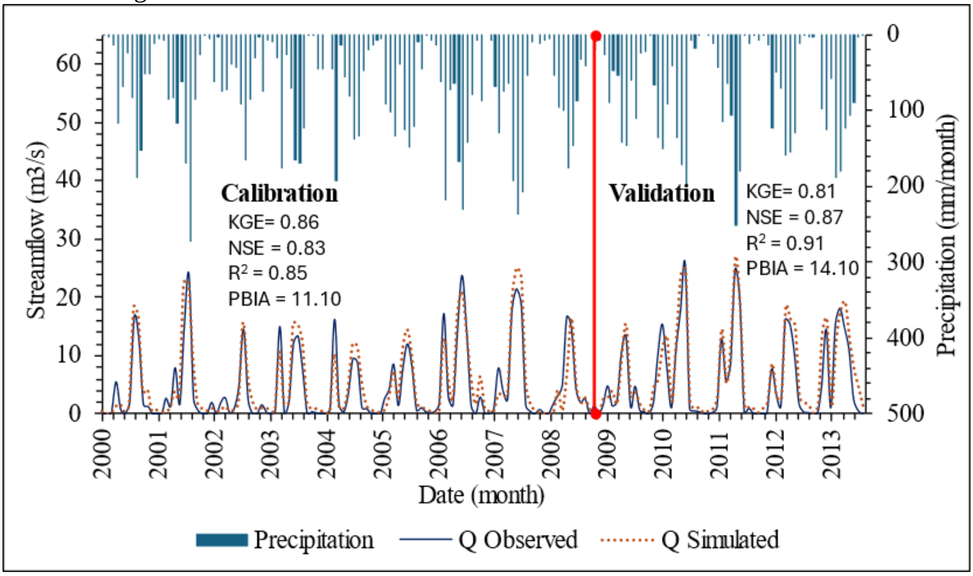

Figure 10. Hydrograph of measured and simulated streamflow (Q) during testing (2000–2008) and verification (2009–2013) at the Dawe watershed.

Impact of LULC and Climate Change on Hydrological Components

Climate change impacts

Table 11 reveals the effects of climate change on water balance elements like SR, GWR, WY, and ET. The individual impacts of climate change under both SSP2–4.5 and SSP5–8.5 with constant LULC (2022) are represented in S1–S4. The projected WY and SR will decline by 17.16% and 21.75% in the late century (S2) and 19.10% and 23.22% in the mid-century (S1) under SSP2–4.5, respectively. Groundwater recharge's response to climate change showed inconsistency under different scenarios. GWR under S1 and S2 increased by 7.90% and 10.07%, respectively, whereas under S4, it decreased by 19.82%. In contrast, ET consistently increased (by 13.00 to 23.4%) under all scenarios (S1 to S4) in response to climate change.

Table 20. The simulated annual mean hydrological components

Scenario	SR	ΔSR %	GWR	ΔGWR %	WY	ΔWY%	ET	ΔET %
So	134.00	-	73.94	-	381.62	-	602.43	-
S1	108.40	-19.10	79.38	7.36	293.02	-23.22	682.96	13.37
S2	111.00	-17.16	81.38	10.07	299.31	-21.57	702.8	16.66
S3	116.30	-13.21	78.66	6.38	313.49	-17.85	703.53	16.78
S4	93.77	-30.02	59.29	-19.82	276.69	-27.50	744.41	23.57
S5	109.20	-18.51	77.53	4.85	295.11	-22.67	680.66	12.99
S6	117.10	-12.61	76.80	3.87	315.67	-17.28	703.09	16.71

S7	92.77	-30.77	59.29	-19.82	302.23	-20.8	700.19	16.23
S8	89.95	-32.87	56.78	-23.21	249.95	-34.5	743.76	23.46

Combined Impacts of LULC and Climate Change

The combined impact of future LULC and climate change scenarios altered all major hydrological components (Table 9). Compared with the baseline, surface runoff decreased by 12.61–32.87%, groundwater recharge ranged from a 4.85% increase to a 23.21% decrease, water yield declined by 20.80–34.50%, and evapotranspiration increased by 12.99–23.46%. The largest changes were observed under Scenario S8 (2062 LULC + SSP5–8.5), which recorded a 32.87% reduction in surface runoff, a 23.21% reduction in groundwater recharge, a 34.50% reduction in water yield, and a 23.46% increase in evapotranspiration.

Fig. 7 illustrates the effects of both LULC and climate changes on annual mean stream flow under the baseline scenario (S0) and late-century scenario (S8). Under the S8 scenario, stream flow reductions were widespread, with the highest flows dropping from 3.45–4.45 m^3/s in the baseline scenario to 1.97–2.51 m^3/s, indicating reduced base flow contributions and diminished upstream water availability. These declines threaten household water supplies, irrigation potential, ecological water needs, and the sustainability of dry-season flows along the mainstream.

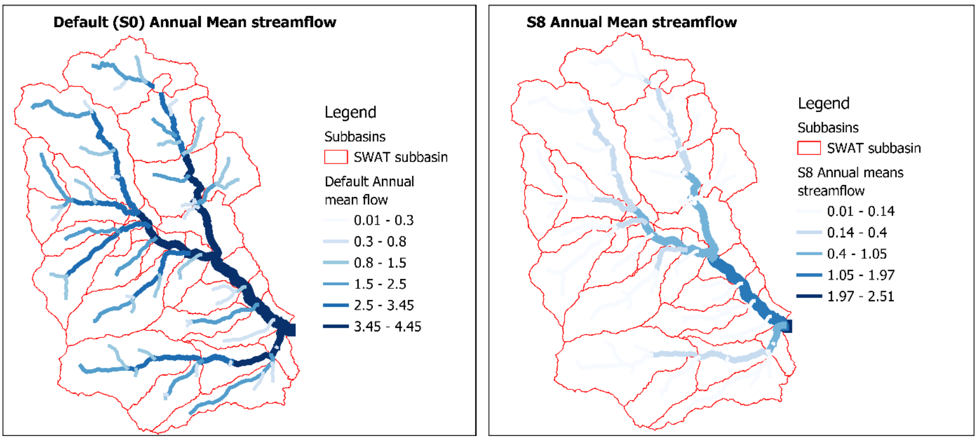

Figure 11. Spatial comparison between the annual average streamflow for S8 and S0 scenarios in response to the LULC and climate changes.

LULC impacts

To determine the incremental impacts of LULC dynamics on hydrological components, the combined scenarios' effects were compared to their respective climate impact equivalents. For instance, the SR difference between S5 and S1 is minimal (–18.51% vs. –19.10%), which may indicate that in SSP2–4.5, LULC has limited additional influence. However, the GWR dropped from +7.36% (S1) to +4.85% (S5), suggesting that future LULC may limit infiltration slightly because of the expansion of developed and barren land. Similar to this, WY differences between S6 and S3 in SSP5 are minimal (–17.28% vs. –17.85%), but ET is still substantial and dominated by warming.

In the late-century scenarios (S7 and S8), the combined impact is more apparent. For example, SR decreased from –30.02% in S4 (climate only) to –32.87% in S8 (with 2062 LULC), and WY decreased further (–27.5% to –34.5%). This implies that the drying effect of extreme climate change is amplified by landscape degradation.

DISCUSSIONS

Impacts of Projected LULC Dynamics on Hydrological Processes

The predicted LULC changes in the Dawe watershed for 2042 and 2062 indicate substantial transformation, marked by swift growth of the urban area and agricultural land. These changes significantly affect hydrological processes by modifying infiltration, runoff generation, and evapotranspiration. The expansion of built-up area increases impermeable surfaces, which raises the risk of flash flooding, soil erosion, and sedimentation. Similarly, because of decreased interception and soil water retention, the growth of agricultural land at the cost of natural vegetation tends to increase SR and decrease GWR (Aragaw and Kura, 2024; Lukas *et al*., 2025).

Nevertheless, the Dawe watershed is predominantly agricultural, with farmland encompassing more than 80% of the total land area. On the farmlands, conservation techniques for soil and water (Fig. 8), like contour farming, bunds, and strip cropping (khat or coffee and sorghum or maize or vegetables), might have contributed to the reduction of surface runoff and increase in GWR and ET, particularly under S1 and S2. This result is in line with earlier research. showing that soil and water conservation interventions can substantially modify watershed hydrological responses by improving soil moisture retention and reducing overland flow (Woldemariam *et al*., 2018; Yaekob *et al*., 2022).

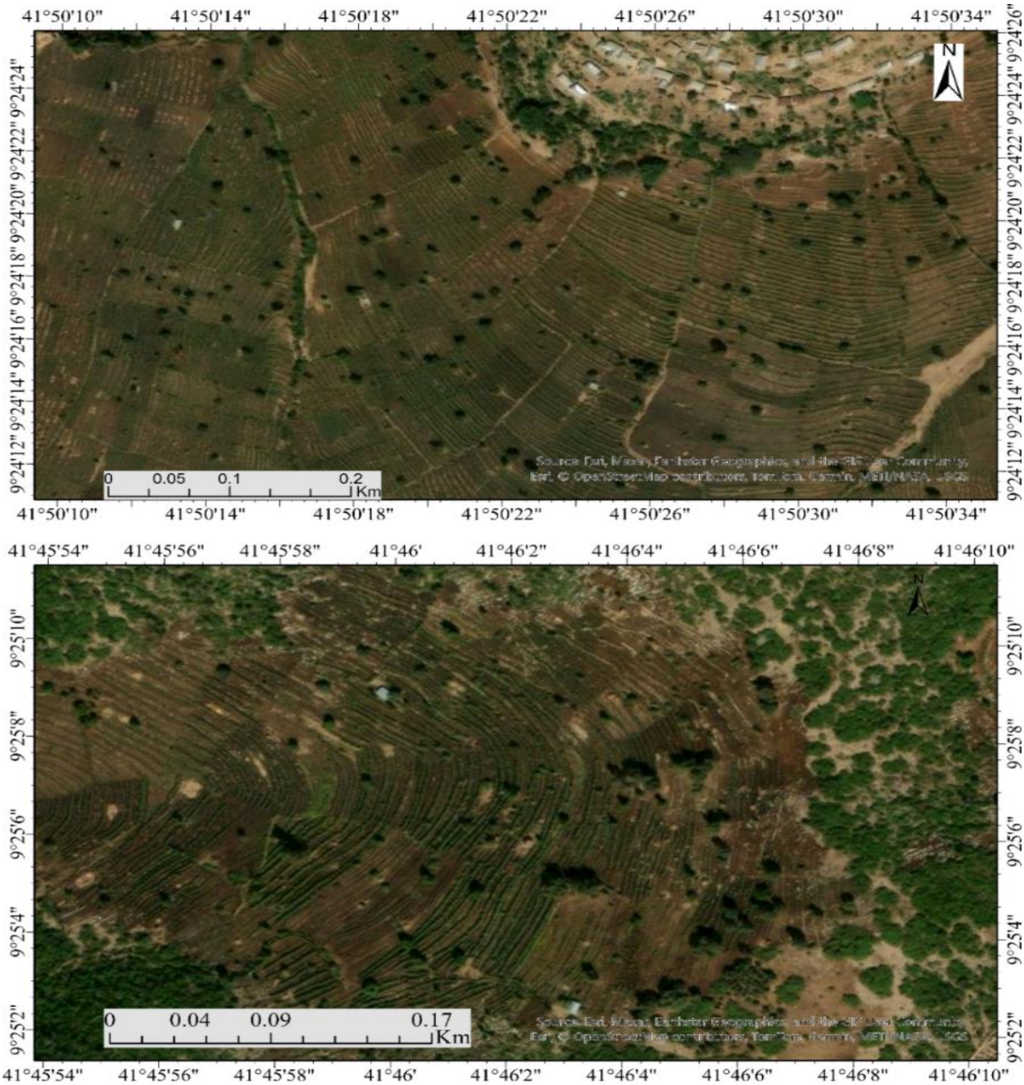

Figure 12. Images of soil water conservation practices on the cultivated area (image source: Google Earth Pro, accessed on July 23, 2025).

Projected Climate Change Patterns in the Dawe Watershed

The findings of this investigation align with the projected global mean average warming rate, which projected average surface temperature will exceed 2–4°C under intermediate to high-emission pathways (IPCC, 2023a). The projected warming is also comparable to regional findings by Tikuye *et al.* (2024), who reported an ensemble temperature increase of 4.9°C in the Upper Blue Nile Basin under RCP8.5 by the end of the century, consistently indicating substantial warming under high-emission scenarios. The slight variation in projected warming can be attributed to differences in emission scenarios (CMIP6 SSPs versus CMIP5 RCPs), climate models, bias-correction methods, and the distinct geographical and topographic characteristics of the study regions. Moreover, these findings agree with regional projections for East Africa, which consistently indicate accelerated warming and increasing exposure to extreme heat (Babaousmail e*t al*., 2024; Choi *et al*., 2023).

Although mean annual precipitation is projected to increase slightly, substantial interannual variability, particularly under the SSP5–8.5 scenario, introduces considerable uncertainty in future water availability. These results are consistent with recent climate studies conducted in Ethiopia, which show strong and steady warming trends but geographically and temporally varied precipitation responses to climate change (Feleke *et al*., 2025). Increased precipitation does not always equate to improved water security. Droughts and floods may become more likely if rainfall patterns shift and precipitation events become more extreme. Future hydrological regimes will therefore probably be more erratic, which will present serious difficulties for managing water supplies, increasing agricultural output, and adapting to climate change.

Combined Impacts on Watershed Hydrological Processes

The findings showed rising ET and falling SR, WY, and GWR, which indicate a drop in the watershed's total water supply and a rise in atmospheric water demand. Similar ET increases have been reported in several Ethiopian watersheds. For instance, Mechal and Bayisa (2025) and Balcha *et al.* (2023) concluded that future warming substantially increased ET and altered basin water balance components in the Central Rift Valley Lakes Basin. Daniel (2023) and Truneh *et al*. (2024) also reported that agricultural expansion and urbanization enhanced ET by increasing atmospheric water demand and modifying land surface characteristics. However, contrasting findings from some studies indicate that ET responses remain highly dependent on local agro-ecological conditions, land management practices, and climate variability (Ayalew *et al.*, 2024).

The projected declines in SR and WY align with findings from major Ethiopian basins such as the Wabi-Shebelle and Upper Blue Nile basins. These studies revealed that the combined impact of LULC and climate change reduces stream flow and alters flow duration characteristics, particularly low flows (Fita and Abate, 2022). By contrast, studies in neighbouring watersheds have demonstrated that deforestation and cropland expansion may locally increase runoff and stream flow due to reduced infiltration and interception (Abdule *et al*., 2023; Chanie, 2024). These conflicting results highlight how local watershed management, land-cover dynamics, and climate forcing interact to significantly impact hydrological responses throughout watersheds.

It is anticipated that future LULC and climate change scenarios will drastically lower GWR, making shallow groundwater resources more vulnerable to drought and intensifying competition. This finding is consistent with several studies conducted across Ethiopia. For instance, Chuko and Abdissa (2023) and Woldu *et al*. (2024) reported that conversion of natural vegetation to agricultural land and built-up area reduces recharge through impaired infiltration and increased surface sealing. Although soil and water conservation measures and moderate climate shifts may locally buffer GWR (Tofu *et al*., 2023), the overall trajectory for the Dawe watershed indicates a net reduction in groundwater replenishment. Concurrent depletion of surface and groundwater resources may have detrimental effects on household water supplies, agricultural productivity, and ecosystem sustainability.

Conclusions and Recommendations

This study integrated the CA-Markov land-use change model, an ensemble of six CMIP6 GCMs, and the SWAT+ hydrological model to examine the effects of potential LULC and climate changes on the hydrological processes of the Dawe watershed. By integrating these complementary models, the study provides a comprehensive framework for evaluating watershed responses under change scenarios. The findings reveal the value of integrated assessments for supporting long-term water resource planning.

The results indicate that agricultural land and developed areas will continue to broaden, while forests and shrub lands will decline. These changes will be reinforced by rising temperatures. Consequently, the watershed hydrological regime will be substantially altered. Climate change was identified as the primary driver of future hydrological change, while LULC change further amplified its effects. Across all future scenarios, evapotranspiration increased, whereas water yield, surface runoff, and groundwater recharge declined. The SSP5-8.5 and 2062 LULC scenarios resulted in the greatest hydrological decline. This finding highlights the importance of considering the combined effects of land-use change and climate change on future water availability.

The findings suggest that sustainable water resource management should integrate climate adaptation with land-use planning rather than addressing these drivers independently. Protecting remaining forests, restoring degraded shrub lands, implementing soil and water conservation measures, and promoting agroforestry should be prioritized to enhance infiltration, groundwater recharge, and watershed resilience. Increasing the effectiveness of agricultural water use through water-saving irrigation technologies, rainwater harvesting, and drought-tolerant crop varieties will also be essential to reduce pressure on increasingly limited water resources.

Future research should improve integrated assessments by incorporating socioeconomic drivers of land-use change, coupling surface water and groundwater models (e.g., SWAT-MODFLOW). The cumulative downstream impacts across the Wabi-Shebelle River Basin need to be evaluated. Additionally, uncertainty analyses using multiple climate and hydrological models would also support the scientific basis for managing water resources in an adaptable and sustainable manner under future environmental changes.

Declarations

Competing interests: The authors have no competing interests to declare that are relevant to the content of this article.

Ethics and Consent to Participate declarations

|Not applicable

Funding

The study received funds from Haramaya University and Ethiopian Ministry of Education.

Data Availability Statement

The datasets generated and/or analyzed during the current study are available from the corresponding author on reasonable request.

Author contributions

All the authors contributed to the conceptualization and design of the study. The corresponding author, Birhanu Legesse Wakjira, acquired and analyzed the data and wrote the manuscript. The other authors, Asfaw Kebede Kassa, Awdenegest Moges, and Olkeba Tolessa Leta, critically revised and strengthened the overall manuscript.

Acknowledgments

I would like to express my gratitude to the Ethiopian Ministry of Education and Haramaya University for funding this research work. The majority of the materials and information utilized were gathered from the Ministry of Water and Energy and the National Meteorological Agency of Ethiopia and are gratefully acknowledged for granting access to the data.

References

Abdule, A. M., Muluneh, A. & Woldemichael, A. (2023). Impact of Climate and Land Use/Cover Changes on Streamflow in Yadot Watershed, Genale Dawa Basin, Ethiopia. *Air, Soil and Water Research*, 16. https://doi.org/10.1177/11786221231200106

Amsalu, S. (2019). Review on the Cause and Effects of Recurrent Drought on Ethiopian Agriculture Productivity. *International Journal of Horticulture, Agriculture and Food Science*, 3(5), 292–298. https://doi.org/10.22161/ijhaf.3.5.7

Aragaw, H. M., Goel, M. K. & Mishra, S. K. (2021). Hydrological Responses to Human-Induced Land Use/Land Cover Changes in the Gidabo River Basin, Ethiopia. *Hydrological Sciences Journal*, 66(4), 640–655. https://doi.org/10.1080/02626667.2021.1890328

Aragaw, H. M. & Kura, A. L. (2024). Hydrological Response to Land Use/Land Cover Changes in Ethiopian Basins: A Review. *Hydrological Sciences Journal*, 69(7), 986–996). https://doi.org/10.1080/02626667.2024.2349272.

Arnold, J. G., Moriasi, D. N., Gassman, P. W., Abbaspour, K. C., White, M. J., Srinivasan, R., Santhi, C., Harmel, R. D., Van Griensven, A., Van Liew, M. W., Kannan, N. & Jha, M. K. (2012). SWAT: Model Use, Calibration, and Validation. *Transactions of the ASABE*, 55(4), 1491–1508. https://doi.org/10.13031/2013.42259

Arnold, J. G., Srinivasan, R., Muttiah, R. S. & Williams, J. R. (1998). Large Area Hydrologic Modeling and Assessment — Part I: Model Development. *Journal of the American Water Resources Association*, 34(1), 73–89.

Atulley, J. A. (2023). Simulating future land cover change in the Tono catchment using the CA-Markov model. *Research Square*, https://doi.org/https://doi.org/10.21203/rs.3.rs-2401213/v1.

Ayalew, A. D., Wagner, P. D., Sahlu, D. & Fohrer, N. (2024). Unveiling hydrological dynamics in data-scarce regions: Experiences from the Ethiopian Rift Valley Lakes Basin. *Hydrology and Earth System Sciences*, 28(8), 1853–1872. https://doi.org/10.5194/hess-28-1853-2024

Ayalew, S. E. & Nigussie, T. A. (2023). Historical and projected land-use / land cover changes of the Welmel River Watershed, Genale Dawa Basin, Ethiopia. *Journal of Water and Land Development*, (58), 89–98. https://doi.org/10.24425/jwld.2023.146601

Babaousmail, H., Ayugi, B. O., Lim Kam Sian, K. T. C., Randriatsara, H. H. R. H. & Mumo, R. (2024). How Do CMIP6 HighResMIP Models Perform in Simulating Precipitation Extremes over East Africa? *Hydrology*, 11(7). https://doi.org/10.3390/hydrology11070106

Balcha, S. K., Awass, A. A., Hulluka, T. A., Bantider, A. & Ayele, G. T. (2023). Assessment of future climate change impact on water balance components in Central Rift Valley Lakes Basin, Ethiopia. *Journal of Water and Climate Change*, 14(1), 175–199. https://doi.org/10.2166/wcc.2022.249

Berhanu, D., Alamirew, T., Taye, M. T., Tibebe, D., Gebrehiwot, S. & Zeleke, G. (2023). Evaluation of CMIP6 models in reproducing observed rainfall over Ethiopia. *Journal of Water and Climate Change*, 14(8), 2583–2605. https://doi.org/10.2166/wcc.2023.502

Bieger, K., Arnold, J. G., Rathjens, H., White, M. J., Bosch, D. D., Allen, P. M., Volk, M. & Srinivasan, R. (2017). Introduction to SWAT+, A Completely Restructured Version of the Soil and Water Assessment Tool. *Journal of the American Water Resources Association*, 53(1), 115–130. https://doi.org/10.1111/1752-1688.12482

Bikeko, S. S. & Venkatesham, E. (2024). Land use land cover change as a casual factor for climate variability and trends in the Bilate Watershed, Ethiopia. *Environmental Monitoring and Assessment*, 196(12), 1250. https://doi.org/10.1007/s10661-024-13435-y

Birhan Getachew, T., Ray, R. L., Gebeyehu, K. & Teshome, M. (2024). Assessing the influence of land use/land cover dynamics and climate change on water resources in Upper Blue Nile, Ethiopia. *Journal of Water and Climate Change*, 15(9), 4745–4774. https://doi.org/10.2166/wcc.2024.319

Birhanu, S. Y., Moges, M. A., Sinshaw, B. G., Tefera, A. K., Atinkut, H. B., Fenta, H. M. & Berihun, M. L. (2022). Hydrological modeling, impact of land-use and land-cover change on hydrological process and sediment yield; case study in Jedeb and Chemoga watersheds. *Energy Nexus*, 5, 100051.

https://doi.org/https://doi.org/10.1016/j.nexus.2022.100051

Chanie, K. M. (2024). Hydro-meteorological response to climate change impact in Ethiopia: a review. *Journal of Water and Climate Change*, 15 (4), 1922–1932. https://doi.org/10.2166/wcc.2024.711

Choi, Y. W., Campbell, D. J. & Eltahir, E. A. B. (2023). Near-term regional climate change in East Africa. *Climate Dynamics*, 61, 961–978. https://doi.org/10.1007/s00382-022-06591-9

Chuko, F. W. & Abdissa, A. G. (2023). Impact of land-use dynamics and climate change scenarios on Groundwater recharge in the case of Anger watershed, Ethiopia. *Heliyon*, 9(8). https://doi.org/10.1016/j.heliyon.2023.e18467

Congalton, R. G. & Green, K. (2019). *Assessing the Accuracy of Remotely Sensed Data: Principles and Practices (3rd ed.).* CRC Press, Taylor & Francis Group, LLC.

Daniel, H. (2023). Hydrological response to climate change in the Deme watershed, Omo-Gibe Basin, Ethiopia. *Journal of Water and Climate Change*, 14(4), 1112–1131. https://doi.org/10.2166/wcc.2023.248

Engdaw, K. (2016). *Assessment on Surface Water Potential and Demands of Wabi-shebele Basin in Ethiopia*. MSc. Thesis, Addis Ababa University.

Eva, E. A., Marzen, L. J., Lamba, J., Ahsanullah, S. M. & Mitra, C. (2024). Projection of land use and land cover changes based on land change modeler and integrating both land use land cover and climate change on the hydrological response of Big Creek Lake Watershed, South Alabama. *Journal of Environmental Management*, 370. https://doi.org/10.1016/j.jenvman.2024.122923

FAO. (2023). The State of Food Security and Nutrition in the World 2023. *The State of Food Security and Nutrition in the World 2023*. FAO; IFAD; UNICEF; WFP; WHO; https://doi.org/10.4060/cc3017en.

Feleke, H. G., Amdie, T. A., Rasche, F., Mersha, S. Y. & Brandt, C. (2025). Climate on the Edge: Impacts and Adaptation in Ethiopia's Agriculture. *Sustainability*, 17(11). https://doi.org/10.3390/su17115119

Fita, T. & Abate, B. (2022). Impact of climate change on streamflow of Melka Wakena catchment, Upper Wabi Shebelle sub-basin, south-eastern Ethiopia. *Journal of Water and Climate Change*, 13(5), 1995–2010. https://doi.org/10.2166/wcc.2022.191

Gebisa, B. T. & Dibaba, W. T. (2024). Ensemble modeling of the hydrological impacts of climate change: A case study of the Baro River sub-basin, Ethiopia. *Hydrology Research*, 55(11), 1143–1160. https://doi.org/10.2166/nh.2024.066

Gebrechorkos, S. H., Hülsmann, S. & Bernhofer, C. (2019). Regional climate projections for impact assessment studies in East Africa. *Environmental Research Letters*, 14(4). https://doi.org/10.1088/1748-9326/ab055a.

Gebresellase, S. H., Wu, Z., Xu, H. & Muhammad, W. I. (2023). Scenario-Based LULC Dynamics Projection Using the CA–Markov Model on Upper Awash Basin (UAB), Ethiopia. *Sustainability*, 15(2). https://doi.org/10.3390/su15021683

Gupta, H. V, Kling, H., Yilmaz, K. K. & Martinez, G. F. (2009). Decomposition of the mean squared error and NSE performance criteria : Implications for improving hydrological modelling. *Journal of Hydrology*, 377(1–2), 80–91. https://doi.org/10.1016/j.jhydrol.2009.08.003

Harka, A. E., Roba, N. T. & Kassa, A. K. (2020). Modelling rainfall runoff for identification of suitable water harvesting sites in Dawe River watershed, Wabe Shebelle River basin, Ethiopia. *Journal of Water and Land Development*, 47(1), 186–195. https://doi.org/10.24425/jwld.2020.135313

IPCC (2023). Climate Change 2023: Synthesis Report. Contribution of Working Groups I, II and III to the Sixth Assessment Report of the Intergovernmental Panel on Climate Change. In: P. Arias, M. Bustamante, I. Elgizouli, G. Flato, M. Howden, C. Méndez-Vallejo, J. J. Pereira, R. Pichs-Madruga, S. K. Rose, Y. Saheb, R. Sánchez Rodríguez, D. Ürge-Vorsatz, C. Xiao, N. Yassaa, J. Romero, J. Kim, E. F. Haites, Y. Jung, R. Stavins, … C. Péan (Eds.), *Climate Change 2023 Synthesis Report* (p. 35-51). https://doi.org/10.59327/IPCC/AR6-9789291691647

Kuma, H. G., Feyessa, F. F. & Demissie, T. A. (2022). Land-use/land-cover changes and implications in Southern Ethiopia: evidence from remote sensing and informants. *Heliyon*, 8(3). https://doi.org/10.1016/j.heliyon.2022.e09071.

Lukas, P., Melesse, A. M. & Kenea, T. T. (2025). Integrating Land Use/Land Cover and Climate Change Projections to Assess Future Hydrological Responses: A CMIP6-Based Multi-Scenario Approach in the Omo–Gibe River Basin, Ethiopia. *Climate*, 13(3). https://doi.org/10.3390/cli13030051

Mechal, A. & Bayisa, A. (2025). Modeling the Impacts of Climate Change on Watershed Hydrology Using Climate and Hydrological Models: The Case of the Ziway Lake Watershed, Ethiopian Rift. *Environmental Modeling and Assessment*, 30(3), 515–541. https://doi.org/10.1007/s10666-024-10010-0

Moriasi, D. N., Arnold, J. G., Liew, M. W. Van, Bingner, R. L., Harmel, R. D. & Veith, T. L. (2007). Model Evaluation Guidelines for Systematic Quantification of Accuracy in Watershed Simulations. *ASABE*, 50(3), 885–900.

Nash, J. E. & Sutcliffe, I. V. (1970). River Flow Forecasting Through Conceptual Models Part I - A Discussion of Principles. *Journal of Hydrology*, 10, 82–290.

Omay, P. O., Muthama, N. J., Oludhe, C., Kinama, J. M., Artan, G. & Atheru, Z. (2023). Evaluation of CMIP6 historical simulations over IGAD region of Eastern Africa. *Discover Environment*, 1(1). https://doi.org/10.1007/s44274-023-00012-2

Rathjens, H., Bieger, K., Srinivasan, R., Chaubey, I. & Arnold, J. G. (2016). *CMhyd User Manual: Documentation for preparing simulated climate change data for hydrologic impact studies*. http://swat.tamu.edu/software/cmhyd/.

Riahi, K., van Vuuren, D. P., Kriegler, E., Edmonds, J., O'Neill, B. C., Fujimori, S., Bauer, N., Calvin, K., Dellink, R., Fricko, O., Lutz, W., Popp, A., Cuaresma, J. C., KC, S., Leimbach, M., Jiang, L., Kram, T., Rao, S., Emmerling, J., …Tavoni, M. (2017). The Shared Socioeconomic Pathways and their energy, land use, and greenhouse gas emissions implications: An overview. *Global Environmental Change*, 42, 153–168. https://doi.org/10.1016/j.gloenvcha.2016.05.009

Roba, N. T., Kassa, A. K., Geleta, D. Y. & Harka, A. E. (2021). Streamflow and sediment yield estimation, and area prioritization for better conservation planning in the Dawe River watershed of the Wabi Shebelle River Basin, Ethiopia. *Heliyon*, 7(12). https://doi.org/10.1016/j.heliyon.2021.e08509

Rwanga, S. S. & Ndambuki, J. M. (2017). Accuracy Assessment of Land Use/Land Cover Classification Using Remote Sensing and GIS. *International Journal of Geosciences*, 8, 611–622. https://doi.org/https://doi.org/10.4236/ijg.2017.84033

Seifu, T. K. & Eshetu, K. D. (2024). Characterizing the aridity indices and potential evapotranspiration using CMIP6-GCMs in two distinct regions of Ethiopia. *Journal of Water and Climate Change*, 15(4), 1507–1531. https://doi.org/10.2166/wcc.2024.394

Semegnew, T., Soromessa, T. & Bekele, T. (2021). Analysis of the Current and Future Prediction of Land Use/Land Cover Change Using Remote Sensing and the CA-Markov Model in Majang Forest Biosphere Reserves of Gambella, Southwestern Ethiopia. *Scientific World Journal*, 2021. https://doi.org/https://doi.org/10.1155/2021/6685045

Shah, M. M., Fischer, G., & van Velthuizen, H. (2008). Food security and sustainable agriculture: The challenges of climate change in Sub-Saharan Africa.

Siraj, B., Moges, A. & Dananto, M. (2023). Trend analysis, past dynamics and future prediction of land use and land cover change in upper Wabe-Shebele river basin. *Heliyon*, 9(9). https://doi.org/10.1016/j.heliyon.2023.e19128

Tofu, D. A., Mekuria, M. M. & Ogato, G. S. (2023). Climatic extremes' resilient livelihoods of rural households in the Eastern Ethiopia. *Agriculture and Food Security*, 12(1). https://doi.org/https://doi.org/10.1186/s40066-023-00446-0.

Truneh, L. A., Matula, S. & Báťková, K. (2024). An analysis of the impacts of land use change on the components of the water balance in the Central Rift Valley sub-basins in Ethiopia. *Sustainable Water Resources*

Management, 10(2). https://doi.org/10.1007/s40899-024-01050-1

Woldemariam, G. W., Iguala, A. D., Tekalign, S. & Reddy, R. U. (2018). Spatial Modeling of Soil Erosion Risk and Its Implication for Conservation Planning: The Case of the Gobele Watershed, East Hararghe Zone, Ethiopia. *Land*, 7(25). https://doi.org/10.3390/land7010025

Woldu, T. T., Ayenew, T., Baychken, B. & Birhanu, B. (2024). Spatiotemporal recharge estimation in the upper Awash sub-basin, central Ethiopia. *Hydrology Research*, 55(7), 711–727. https://doi.org/10.2166/nh.2024.164

Wudineh, F. A. (2023). Land-use and land-cover change and its impact on flood hazard occurrence in Wabi Shebele River Basin of Ethiopia. *Hydrology Research*, 54(6), 756–769. https://doi.org/https://doi.org/10.2166/nh.2023.121

Xiang, X., Ao, T., Xiao, Q., Li, X., Zhou, L., Chen, Y., Bi, Y. & Guo, J. (2022). Parameter Sensitivity Analysis of SWAT Modeling in the Upper Heihe River Basin Using Four Typical Approaches. *Applied Sciences*, 12(19). https://doi.org/10.3390/app12199862

Yaekob, T., Tamene, L., Gebrehiwot, S. G., Demissie, S. S., Adimassu, Z., Woldearegay, K., Mekonnen, K., Amede, T., Abera, W., Recha, J. W., Solomon, D. & Thorne, P. (2022). Assessing the impacts of different land uses and soil and water conservation interventions on runoff and sediment yield at different scales in the central highlands of Ethiopia. *Renewable Agriculture and Food Systems*, 37, S73–S87. https://doi.org/10.1017/S1742170520000010

Yang, L., Shi, L., Li, J. & Kong, H. (2024). Spatio-temporal pattern change of LULC and its response to climate in the Loess Plateau, China. *Scientific Reports*, 14(1). https://doi.org/10.1038/s41598-024-73945-0

Yilmaz, B., Aras, E. & Nacar, S. (2024). A CMIP6-ensemble-based evaluation of precipitation and temperature projections. *Theoretical and Applied Climatology*, 155(8), 7377–7401. https://doi.org/10.1007/s00704-024-05066-7.

Zeleke, T., Beyene, F., Deressa, T., Yousuf, J. & Kebede, T. (2021). Vulnerability of smallholder farmers to climate change-induced shocks in east hararghe zone, ethiopia. *Sustainability*, 13(4), 1–19. https://doi.org/10.3390/su1304216.

Journal of Science and Sustainable Development (JSSD), 2026, 14 (1), 60-81

ISSN: 2304-2702 (print); 2414-4479 (online)
DOI: 10.20372/au.jssd.14.2.2026.0753

RESEARCH PAPER

Chickpea Fusarium Wilt (*Fusarium oxysporum* f. sp. *ciceri*): Distribution and Pathogen Characterization in the West and Southwest Shewa Zones in the Oromia Regional State, Ethiopia

Tsegaye Dabessa[1*], Alemu Lencho[1], Thangavel Selvaraj[1], Jemal Tola[2], and Gezahegne Getaneh[3]
[1]*Department of plant Sciences, Ambo University, Ethiopia*
[2]*Ambo Agricultural Research Center, Ethiopian Institute of Agricultural Research (EIAR);*
[3]*Debre Zeit Agricultural Research Center, Ethiopian Institute of Agricultural Research*
[*]*Corresponding Author Email: tsegayedabessa05@gmail.com; ORCID: 0009-0007-2293-7039*

Abstract

Fusarium oxysporum f. sp. ciceri, a soil-borne hemi-biotrophic hyphomycete that produces vascular Fusarium wilt,, represents a principal biotic danger affecting the productivity and economic sustainability of chickpea (Cicer arietinum L) production system in Ethiopia. This study studied the contemporary spatiotemporal distribution, field prevalence, environmental causes, and pathogen features of the disease among key smallholder agriculture tracts spanning the West and Southwest Shewa Zones of the Oromia Regional State. Field diagnostic survey data collected from 216 district smallholder plots over two consecutive production cycles (2023/24 and 2024/25) were analyzed using multi-stage cluster descriptive modeling, overlaying disease parameters against localized biophysical parameters, cropping timelines, and host cultivar choices. Survey results confirmed widespread distribution of vascular wilt, with mean disease incidence levels fluctuating markedly between 10.01% and 34.75% across the six investigated districts, demonstrating that intensive monocropping and delayed sowing act as key drivers accelerating regional wilt epidemics. Symptomatic root and stem vascular stands obtained during field samplings identified 70 pure monoconidial fungus cultures on Potato Dextrose Agar (PDA). Quantitative in-vitro radial colony development velocities and microscopic reproductive dimensions were examined via one-way Analysis of Variance (ANOVA) utilizing SAS software's General Linear Models (GLM) method (Version 9.4). The findings indicated that highly significant differences ($p < 0.001$) in radial colony growth velocities on PDA (Grand Mean = 58.42 mm) and colony topography and pigmentation. Diagnostic taxonomic features, such as a large number of oval aseptate microconidia on short monophylies and gently curved macroconidia with 3 to 5 septations, were confirmed by microscopic analyzes. One-way ANOVA for conidial length ($df = 19$, $F = 6940.63$, $p \leq 0.001$) and conidial width ($df = 19$, $F = 647.78$, $p < 0.001$) confirmed deep morphological variability, with mean establishing at 15.82 μm and 5.76 μm respectively. Using the highly susceptible tester line "JG-62" in a Completely Randomized Design (CRD) with three replications, in-vivo pathogenicity testing effectively satisfied Koch's postulates. With grand averages increasing from 8.29% at 30 DAI to 25.61% at 45 DAI and finishing at 44.40% at 60 DAI, two-way ANOVA revealed extremely significant differences ($p < 0.001$) in virulence development. Factorial analysis classified the local isolates into distinct pathogenic groups based on terminal values: 20 highly aggressive (> 70% incidence; maxing out at 93.35%), 40 moderately aggressive (20% - 70% incidence), and 10 weakly aggressive (< 20% incidence) isolates. This study significantly contributes to existing knowledge by shifting from broad, pooled regional pulse disease descriptions to providing the first high-resolution, spatiotemporally mapped micro-level epidemiological blueprint of pathodynamic in Central Ethiopia: Fusarium oxysporum f. sp. ciceri, isolating hyper-virulent local reference standards for targeted, site-specific marker-assisted resistance breeding and sustainable integrated disease management (IDM) frameworks.

Keywords: *Cicer arietinum*, disease survey, host resistance, Koch's postulates, vascular wilt

Introduction

The second most produced pulse crop is the chickpea (*Cicer arietinum* L.) globally, trailing only dry beans, with an international output reaching 17 million tons over a global footprint that has expanded to approximately 14.56 million hectares (FAOSTAT, 2025). Globally, India remains the dominant producer of chickpea, contributing over 73% of the total global production volume (FAOSTAT, 2024). As a dense nutritional repository, chickpea seeds provide an essential, affordable source of plant-based proteins (ranging from 15% to 39% or wider based on cultivar variability), complex carbohydrates, dietary fibers, vitamins, and bioavailable minerals like iron and zinc (Getahun *et al.,* 2021). This comprehensive biochemical profile serves as a critical dietary asset in developing nations combating protein-energy malnutrition (Merga and Haji, 2022). Within the African continent, Ethiopia represents the primary powerhouse for chickpea (*Cicer arietinum* L.) cultivation, processing, and export, commanding approximately 46% of total continental volumetric output (ICARDA, 2019). Nationally, chickpea accounts for more than 12% of the total acreage designated for pulse crops and holds a 14% share of aggregate national pulse production volumes (CSA, 2021), stands as one of the country's most vital food security components (Getahun *et al.,* 2021). Vascular Fusarium wilt caused by the soil-borne, hemi-biotrophic F. oxysporum f. sp. *ciceri* stands out as the yield-limiting threat countrywide, and it is the main cause of this severe productivity gap (Yilma et al., 2026). The epidemiological consequences of this disease are profound; wide-spread localized field surveys reveal baseline disease incidence rates commonly fluctuating between 5% and 58% across major production regions (Yilma eta al., 2026). Depending on the crop phenological stage at initial infection, environmental variables, and cultivar susceptibility, total localized yield losses frequently reach up to100%, often driving smallholders into complete crop failure (Teklu *et al.,* 2024; Yilma *et al.,* 2026).

Resent empirical survey indicate that vascular Fusarium wilt is expanding aggressively in both geographic range and epidemic severity across Ethiopian chickpea-growing jurisdictions (Yimer *et al.,* 2025). Comparative epidemiological investigations conducted across the high-production highland tracs of the Gonder and Gojjam zones documented a parallel, climate-driven intensification of soil-borne fungal complexes, demonstrating that shifts in terminal soil moisture deficits are altering regional Patho system baselines (Yilma *et al.,* 2026). Furthermore, broad-scale surveillance across East African legume ecologies confirms that this aggressive spatial expansion is not isolated to Central Ethiopia; rather, it represents a wider Sub-Saharan phenomenon where rising ambient temperatures during host reproductive phases systematically accelerate xylem colonization rates and shorten the pathogen's incubation window (Assfaw and Negash, 2020). When contrasted with these adjacent regional datasets, the high field intensities documented within the heavy Vertisols of the West and Southwest Shewa Zones underscore an urgent requirement for localized, high-resolution diagnostic mapping. In the West and Southwest Shewa Zones of Oromia, Ethiopia, some attempts were made to understand current status, distribution, and characterization of the chickpea Fusarium wilt pathogen along with the biophysical factors that influence it. In addition, quantitative information on the current status of chickpea Fusarium wilt pathogen disease is lacking and also, due to variability amongst the pathogens, updated information regarding the Fusarium wilt pathogen of chickpeas could be needed. Given the high evolutionary variability, shifting aggressive pathotypes, and persistent nature of this soil-borne hyphomycete, updated regional monitoring is vital for targeted resistance breeding and sustainable integrated disease management (IDM) frameworks. To address these critical epidemiological knowledge gaps, these field, laboratory, and *in-vivo* investigations were initiated to achieve three specific objectives: (i) Determine the contemporary prevalence, field incidence, and internal vascular tissue severity of chickpea Fusarium wilt across the primary production districts of the West and Southwest Shewa

Zones. (ii) Isolate, purify, and morphologically characterize local *F. oxysporum* f. sp. *ciceri* isolates while systematically validating their individual virulence profiles via standard in-vivo pathogenicity testing. (iii) Assess associations between diseases intensity and selected agronomic and environmental factors.

Methods and Materials

Study areas' description

The survey chickpea fields were located in the primary administrative zones of West and Southwest Shewa in the Oromia Regional State, Ethiopia, and ranged in elevation from 2,060 to 2,303 meters above sea level. Six districts from the Southwest and West Shewa administrative zones for this field survey during the October-to-February windows of the 2023/24 and 2024/25 cropping seasons, aligning with the chickpea cultivation cycle in Ethiopia. Three districts were selected from the West Shewa Zone (Dendi, Ejere, and Ejersa Lafo) and three from the Southwest Shewa zone (Sebeta Hawas, Becho, Ilu).

The Agro-ecological and spatial profiles of the surveyed districts were characterized systematically across their respective geographic bounds. In the West Shewa Zone, the study area of Dendi district is bounded by latitudes 09°00.938′ N to 09°02.278′ N and longitudes 38°04.937′ E to 38°12.011′ E, spanning an altitudinal range of 2,199-2,303 m a.s.l., around 85 km to the west of Addis Ababa. The monitored fields in the Ejere district, which is about 46 km west of Addis Ababa, covered elevations between 2,081 and 2,180 m a.s.l. and were bounded by latitudes 08°58.244′ N to 09°01.555′ N and longitudes 38°19.738′ E to 38°20.996′ E within the same zone. Sown chickpea stands were found at an altitudinal range of 2,110 to 2,170 m a.s.l. in the nearby Ejersa Lafo district, which is roughly 60 km west of Addis Ababa. Their coordinates fell between latitudes 08°59.154′ N and 09°00.443′ N and longitudes 38°13.820′ E and 38°17.758′ E. At the same time, different Agro-climatic clusters were identified using spatial monitoring throughout the Southwest Shewa Zone. Sown stands in the Becho district, situated approximately 82 km Southwest of Addis Ababa, featured an altitudinal profile ranging from 2,112 to 2,156 m a.s.l., and were bounded by altitudes 08°40.233′ N to 08°43.105′ N and longitudes 38°13.587′ E to 38°16.112′ E. Moving closer to the capital, the field assessment points in the Ilu district fell within narrow altitudinal bands of 2,060 to 2,091 m a.s.l., bounded by latitudes 08°46.731′ N to 08°49.332′ N and longitudes 38°19.220′ E to 38°22.545′ E, situated roughly 55 km Southwest of Addis Ababa. Finally, the Sebeta Hawas district, positioned approximatel y 26 km southwest of Addis Ababa, contained monitored production fields at altitudinal elevations between 2064 and 2083 m a.s.l., traversing a spatial grid bounded by latitudes 08°49.162′ N to 08°50.205′ N and longitudes 038°30.457′ E to 038°31.854′ E (Fig. 1).

Survey design and sampling strategy

The multi-stage purposive sampling framework was executed systematically across the selected districts by targeting three major kebeles (farmer associations) per administrative unit based on intensive chickpea production histories. Field monitoring was carried out in the kebeles of Yubido Legebatu, Dano Ejersa Gibe, and Awash Bolo within the Dendi district; Kimoye, Enaftu, and Tulu Korma within the Ejere district; and Jemijem Legebatu, Cheleleka Bobe, and Serewa Debisa in the neighborhood of Ejersa Lafo.

At the same time, agricultural monitoring in the nearby Southwest Shewa Zone monitored production fields in the districts of Becho (Batu, Kobo, and Awash Bune); Ilu (Bili, Keta Asgori, and Buti Talgo); and Sebeta Hawas (Borohiro, Debelyohans, and Nanotefki). This spatial distribution guaranteed an even geographical spread across both administrative zones, capturing localized smallholder farming micro-climates and management variations cleanly. Within each designed kebeles, twelve smallholder production fields were evaluated.

Field monitoring operations were stratified equally across two consecutive cultivation cycles, tracking 108 production fields in the 2023/24 season and an additional 108 fields in the 2024/25 season. This framework generated a cumulative national sample matrix of 216 unique production environments for statistical evaluation. The structural allocation of the cumulative sample size (N = 216) was mathematically derived via a multi-stage cluster configuration according to the following sampling hierarchy:

2Administrative zones × 3districts per zone × 3kebeles per district × 6fields per kebele per year × 2cropping cycles = 216 fields.

The multi-year sample footprint of 216 unique production environments was considered highly adequate to rigorously represent the targeted epidemiological landscape based on three interconnected spatial-statistical parameters. First, the purposive selection of these specific fields across an altitudinal gradient of 2,060 to 2,303 m a.s.l. ensured the saturation of biophysical variation, effectively capturing the full range of microclimatic regimes, soil-moisture variations, and thermal zones that govern *Fusarium oxysporum* f. sp. *ciceri* pathodynamic in Central Ethiopia. Second, this sampling scale strictly fulfills established epidemiological replication guidelines; according to foundational plant disease epidemiology survey principles (Campbell and Madden, 1990; Yimer *et al.*, 2025), a multi-seasonal matrix exceeding 150 to 200 field observation points generates sufficient degrees of freedom (df) within the statistical Analysis of Variance (ANOVA) error matrix to cleanly isolate genuine pathotypic, agronomic, and geographic effects from confounding environmental noise. Finally, by tracking precisely 12 smallholder fields per kebele over two consecutive years, the framework achieved a thorough representation of localized farming practices, successfully integrating the diverse sowing chronologies, micro-plot organic amendment application rates, and historical cereal-legume crop rotation sequences (predominantly involving teff and wheat) that directly dictate soil-borne chlamydospore inoculum densities and suppressive rhizosphere dynamics within these high-intensity chickpea production belts.

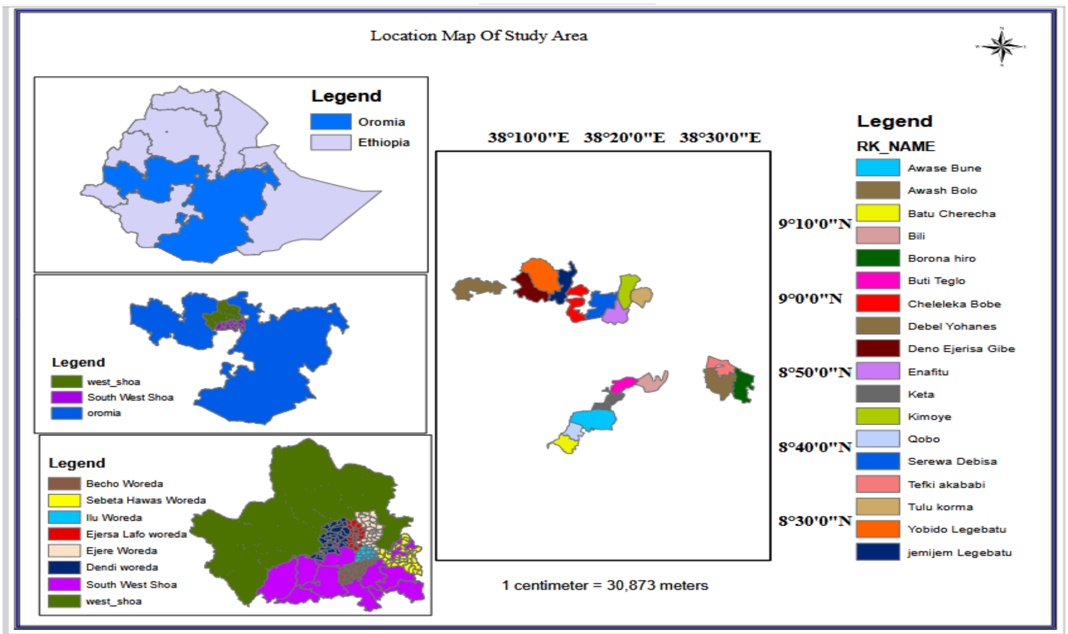

Figure 1. Geographic location map of the study districts and sampled smallholder chickpea fields across the West and Southwest Shewa Zones of the Oromia Regional State, Ethiopia.

Map borders are delineated in standard geographic coordinates using North (N) and East (E) directional suffixes (RK: Rural Kebeles, indicating the lowest local administrative tier in the rural districts of Ethiopia).

Survey procedures and biophysical factors tracking

Monitored smallholder fields within each target district were intercepted along primary and secondary feeder agricultural transit roads at predetermined linear intervals of at least 5 km in order to guaranty a representative and non-overlapping spatial distribution. To fully monitor seasonal epidemics, field surveys started in the early host vegetative phase and continued through the complete crop pod-setting growth phases. A portable Geographical Position System (GPS) receiver was used at each diagnostic sampling site to record exact altitudinal measurements and geographic coordinates. In order to monitor local biophysical factors, a structured agronomic ledger was created concurrently.

Based on morphological characteristics, the host crop type was classified as either conventional Desi or improved, large-seeded Kabuli kinds. Furthermore, in order to clearly distinguish between continuous monocropping and varied cereal-legume rotations, local cropping histories were recorded to capture the immediately previous crop rotation cycles. Visual and textural classification were also used to assess soil matrix profiles, and it was found that heavy clay Vertisols predominated in the areas under observation. Lastly, crop phenological growth stages were methodically assessed, and the exact host growth phase during each observation window was ascertained using conventional decimal keys (Fig. 2).

Figure 2. Photos taken at the research locations in 2023 and 2024 G.C. during the field survey, sample collection (A), and GPS data recording (B).

Qualitative disease sampling was accomplished by systematically touring each producing fields using an inverted diagonal “W” transect pattern to reduce edge effects and minimize spatial bias. At five randomized equidistant places along the transect, a 1 m^2 quadrat was deployed to quantify disease parameters. Individual quadrat metrics were subsequently pooled and synthesized to derive a single, mathematically robust mean value for each operational farm matrix. Symptomatic root and lower stem specimens exhibiting definitive diagnostic indicators of vascular wilting such as severe chlorosis, downward epinasty, and internal xylem browning were carefully excavated along with healthily control plants from each site.

Collected tissue specimens were immediately transferred into clean, breathable paper envelopes, placed inside labeled polyethylene storage bags, and maintained within insulated coolers at 4ºC to arrest secondary decay. All specimens were transported to the Plant Pathology Laboratory at Ambo University.

Disease assessment

The spatiotemporal distribution, prevalence, and field intensities of the wilt epidemics were quantified across all 216 monitored farms using three standardized epidemiological parameters:

Disease prevalence

The disease prevalence was calculated by dividing the number of quadrats showing the disease by the total number of quadrats evaluated in each field, and this value was subsequently converted to a percentage. The subsequent description details the method used to calculate the disease prevalence. The ratio of the number of quadrats impacted by the disease to the total number of quadrats evaluated in each field, multiplied by 100.

Prevalence of disease (%) = The count of quadrats impacted by the disease / The total count of quadrats evaluated in each field × 100.

Incidence of disease

The incidence of chickpea Fusarium wilt was calculated by dividing the number of infected plants in a chosen quadrat by the total number of plants assessed within that quadrat and expressing the result as a percentage. The average incidence of disease across the five quadrats in each field was calculated. The incidence of disease (%) is calculated as follows: The total of withered chickpea plants within a quadrat / the total of plants evaluated within that quadrat × 100.

To assess the severity of the disease, five chickpea plants were randomly uprooted from each quadrat and examined for internal vascular discoloration. The percentage of root vascular bundle necrosis was scored using a modified 0-4 descriptive scale, where Grade 0 represented 0% vascular infection (completely symptomless), Grade 1 indicated 1-25% vascular infection or slightly discoloration, Grade 2 signified 26-50% vascular infection or moderate discoloration, Grade 3 denoted 51-75% vascular infection or extensive discoloration, and Grade 4 represented 76-100% vascular necrosis, characterized by complete tissue death or absolute structural wilt. The individual plant scores were subsequently averaged per quadrat and aggregated to establish a structurally sound estimate of disease severity per field. This rigorous scoring framework builds upon foundational visual indices modified for recent pulse crop pathodynamic (Teklu *et al*., 2024).

Meteorological data acquisition

To model regional macro-climatic influences on wilt progression, localized monthly weather records covering the 2023 and 2024 growing seasons were obtained from the National Meteorology Agency of Ethiopia. The gathered datasets included cumulative monthly precipitation, mean relative humidity, and monthly maximum/minimum ambient temperatures. Environmental profiling targeted the window from August to December to capture pre-planting soil moisture retention through to critical host phenological development phases (Table 1).

Table 1. Meteorological profiles recorded from surveyed zones during 2023/24 and 2024/25 cropping seasons.

Year	Parameter	Aug.	Sept.	Oct.	Nov.	Dec.	Jan.	Feb.	Mean
2023/24	Mean RF (mm)	257.10	140.52	89.95	36.76	12.88	6.46	20.17	85.60
	Mean RH (%)	73.56	72.63	66.03	63.28	57.44	57.40	59.29	64.20
	Max. Temp. (ºC)	28.30	28.40	28.40	29.40	29.30	29.90	31.30	29.20
	Min. Temp. (ºC)	2.10	3.20	2.20	2.10	0.10	2.40	4.10	2.30
2024/25	Mean RF (mm)	200.34	119.06	67.64	30.67	13.87	1.96	4.18	62.50
	Mean RH (%)	67.90	67.89	59.35	59.67	55.05	51.75	49.35	58.70
	Max. Temp.(ºC)	31.00	29.50	30.70	30.00	29.70	31.00	32.00	31.50
	Min. Temp. (ºC)	2.90	5.80	5.30	3.30	1.00	-0.20	5.20	3.30

Source: - From Ethiopia National Metrology Agency.

Isolation and characterization of the fungal pathogen

To isolate the causal phytopathogens, systematic chickpea plants exhibiting pathognomonic vascular wilt indicators were collected from 108 production fields across the West and Southwest Shewa Zones of the Oromia Regional State, Ethiopia. The root system were meticulously washed under distilled water to dislodge adhering rhizosphere soil and structural debris, followed by blot-drying between sterile filter paper layers. Tissue fragments measuring approximately 2-3 mm were excised from the advancing margins of internal vascular discoloration using a sterile scalpel blade. To eliminate superficial saprophytic microorganisms, the root segments were surface sterilized for one minute in a 2% sodium hypochlorite (NaOCl) solution. Any leftover chemical residue was then rinsed three times in sterile distilled water before being blotted dry. Five tissue segments were equally spaced throughout standard Potato Dextrose Agar (PDA) matrices. The plates were incubated at 28 ± 2ºC for seven days in order to encourage early hyphal growth (Aneja, 2003). Single-spore isolation and hyphal-tip extraction methods were used to create axenic fungal cultures. Active mycelial disks from the advancing colony boundaries were transferred onto new PDA plates using a flamed inoculating loop to do sub-culturing under aseptic conditions. This purification process was carried out repeatedly until clean, morphologically homogeneous parental colonies were produced. For further research, pure cultures were kept at 4 °C on PDA slants in sterile screw-capped test tubes (Kurt *et al.*, 2002). In accordance with the standard foundational guidelines for Fusarium species, the pure Fusarium oxysporum f. sp. ciceri isolates were taxonomically confirmed using diagnostic culture and macro-morphological criteria, such as radial mycelial growth velocities, colony margin architecture, surface coloration, and reverse pigmentation matrices (Leslie and Summerell, 2006).

Fungal spores were aseptically put on glass slides for microscopic characterization, dyed with lactophenol cotton blue (or methyl blue), covered with a coverslip, and examined using a stereo binocular microscope at 40× and 100× magnifications at the Ambo Agricultural Research Centre. Diagnostic parameters captured included macro-conidial geometric curvature, micro-conidial arrangements on short monophylies, and the presence, position, or wall texture of chlamydospores. The recorded morphological profiles were cross-referenced against established mycological diagnostic keys and standard taxonomic criteria to confirm definitive placement within the *Fusarium oxysporum* species complex (Leslie and Summerell, 2006).

Inoculum mass multiplication and pathogenicity verification

Mass multiplication of *Fusarium oxysporum* f. sp. *ciceri* on sorghum grains

Axenic cultures of the purified *Fusarium oxysporum* f. sp. *ciceri* isolates were mass-multiplied on whole sorghum (*Sorghum bicolor* L.) grains as a solid substrate. The sorghum grains were soaked overnight in distilled water, drained of excess moisture, and transferred into (500 mL) conical flasks. The flasks were sealed with non-absorbent cotton plugs and sequentially autoclaved at 121°C (15 psi) for 30 min over two consecutive days. Upon cooling to room temperature, each flask was aseptically inoculated with a 5mm mycelial disc excised from the advancing margins of actively growing 5-day-old Potato Dextrose Agar (PDA) cultures. The inoculated flasks were incubated at 25 ± 2°C for 15 days in the Plant Pathology Laboratory at Ambo University. To ensure uniform fungal colonization, prevent particle clumping, and accelerate substrate penetration, the flasks were manually agitated daily throughout the incubation window. Fully colonized grain substrates were deployed for downstream pathodynamic validation (Fig. 3).

Figure 3. Mass Multiplications of *Fusarium oxysporum* f. sp. *ciceri* inoculum on Sorghum grains that were used for pathogenicity test at Ambo University, plant pathology laboratory.

Pathogenicity testing and Koch's postulates verification

Greenhouse pathogenicity tests were conducted to systematically verify fulfillment of Koch's postulates using the highly susceptible tester variety 'JG-62'. Steam-sterilized soil matrix (2 kg) was put into plastic pots with a diameter of 25 cm. The solid-state sorghum inoculum was thoroughly incorporated into the soil profile at a standardized amendment rate of (200 g kg^{-1}) of soil achieving a target population density of approximately (10^8cfug^{-1}). The infested soil mixtures were lightly moistened and incubated for 4 days prior to planting to facilitate initial fungal stabilization. In three separate biological replications, five surface-sterilized "JG-62" seeds were planted per pot. To maintain a uniform moisture profile ideal for symptoms of disease while preventing saturated conditions, the pots were watered once a week. Symptomatic progress characterized by leaf chlorosis, downward epinasty, and progressive wilting was quantitatively monitored at 30, 45, and 60 days post-sowing. Causal pathogen identity was systematically confirmed by re-isolating the fungal agent from the vascular tissues of symptomatic host roots exhibiting characteristic internal xylem discoloration, which verified compliance with Koch's postulates by matching the cultural and macro-morphological traits of the parental axenic stock (Jamil and Ashraf, 2020).

Pathogenicity screening and inoculation protocol

The pathogenic variability of 70 isolates of F. oxysporum f. sp. ciceri and one uninoculated sterile soil with three replications in two cycles (September-December 2024 and 2525), totaling 213 pots, was investigated at room temperature in a controlled greenhouse at Ambo University using plastic pots (30 cm in diameter) arranged in a Completely Randomized Design (CRD). Healthy seeds originating from the extremely vulnerable chickpea cultivar "JG-62" were surface sterilized for three minutes using 1% sodium hypochlorite (NaOCl), thoroughly rinsed 3 times with sterile distilled water, and air dried. The fungus was grow on a sand-maize meal medium (9:1 w/w ratio) for 14 days at 25±2°C until a large number of chlamydospores and conidia were formed in order to prepare the inoculum for each isolated strain. The substrate was added to an autoclaved soil mix (soil: sand: peat moss at 2:1:1 v/v/v) at a consistent rate of 10% (w/w). The control block consisted of non-inoculated pots that contained only the autoclaved soil mix. The 25 cm diameter plastic pots have been filled with two kg of steam-sterilized soil. To ensure equitable distribution, the mass-multiplied fungus was added to these pots at a rate of 200 g kg^{-1} (10^8 $cfug^{-1}$) soil and thoroughly mixed. The pots were incubated for four days and, if needed, occasionally watered. Each pot sown 5 surface-sterilized seeds of the chickpea cultivar "JG-62," for a total of 15 plants per treatment in each of the three replicates (Fig. 4). The minimal moisture requirements of the plants were satisfied by watering the containers once a week.

Figure 4. Pathogenicity test activity in chickpea cultivar ‘JG-62’ at Ambo University, greenhouse conditions**.**

Spatiotemporal disease monitoring and incidence computation

At 30, 45, and 60 Days After Inoculation (DAI), the progressive spatiotemporal expansion of Fusarium wilt symptoms which were initially characterized by lower leaf yellowing, flaccidity, marginal necrosis, petiole drooping, and ultimately Fusarium vascular wilting was methodically observed and recorded. The disease incidence percentage (PDI) within each replicate pot was calculated as the proportion of plants displaying visible localized or systemic wilt symptoms in relation to the total number of plants that emerged. The following conventional epidemiological formula was used to compute the spatiotemporal progress of chickpea Fusarium wilt incidence (%) for each replication matrix (Jamil and Ashraf, 2020).

$$\text{PDI} = \frac{\text{Number of wilted plants per pot}}{\text{Total number of plants per pot}} \times 100$$

Statistical analysis

In order to describe the spatiotemporal distribution and relative importance of chickpea wilt diseases across the districts, survey data were summarized and analyzed using descriptive statistics. Based on the approximate similarity of the variables to the total assessed fields in each zone, class boundaries were chosen for disease incidence and severity data separately. To analyze the relationship between wilt disease pathogen and biophysical factors, disease incidence and severity were classified into district class boundaries (Yuen, 2006). The effect of the independent variables on the disease's incidence and severity has been evaluated twice. The relationship between the incidence, severity, temperatures, relative humidity, and rainfall during the survey period in 2023 and 2024 was investigated in order to classify and rank districts into wilt risk areas. SAS version 9.4 (SAS Institute Inc., 2017) was used for the statistical analyzes in this study. Either the Analysis of Variance (ANOVA) or General Linear Models (GLM) methods were used to examine the data. Duncan's Multiple Range test and Fisher's Protected Least Significant Difference (LSD) test with $P \leq 0.05$ were utilized for comparing means. To assess variations in disease intensity among districts, cropping seasons, and host varieties, descriptive statistics were used to summarize spatiotemporal survey data and biophysical factors, which were then submitted to Analysis of Variance (ANOVA). Pearson correlation coefficients r was computed to quantify relationships between environmental drivers (meteorological profiles, elevation, crop rotation sequences) and disease metrics (Teklu *et al.*, 2024). Using the Linear Model recommendations for a Completely Randomized Design, a conventional Analysis of Variance (ANOVA) was performed on all accumulated spatiotemporal replication percentages. Localized replicate fluctuations (e.g., scoring variations of 40% and 46.66% inside certain blocks) were kept to compute the correct Mean Square Error (MSE) in order to satisfy mathematical compliance for hypothesis testing and correct structural zero-variance bounds. The Least Significant Difference (LSD) test at a 95% Confidence Level ($\alpha = 0.05$) was used to distinguish treatment. The experimental reliability and degree of precision were determined by computing the Coefficient of Variation (CV %) for each chronological window:

$$\text{CV (\%)} = \sqrt{\frac{\text{Mean Square Error}}{\text{Grand Mean}}} \times 100$$

All generated pathodynamic percentage datasets were subjected to standard checking procedures to verify normal distribution variance assumptions. Factorial Analysis of Variance (ANOVA) procedures utilizing SAS software (version 9.4) were used to process the data. Terminal disease incidence means recorded at the final 60 DAI evaluation boundary were utilized to cluster the isolates into four distinct pathotype categories: Highly Pathogenic (>70%) final wilt incidence), Moderately Pathogenic (20% - 70%), Slightly Pathogenic (<20%), and non-pathogenic (0%).

Results

Spatiotemporal distribution and intensity of Fusarium wilt

Systematic diagnostic field surveys demonstrated that vascular wilt symptoms were distributed throughout the major chickpea-producing belts of Central Ethiopia. The target pathogen was detected in 152 out of the 216 fields assessed across the 2023 and 2024 cropping seasons, establishing an overall regional prevalence of 70.36%, a mean disease incidence of 23.96%, and an average severity rate of 21.43%. ANOVA showed statistically significant differences ($P < 0.05$) in disease parameters across the six surveyed districts (Table 2 and Fig. 5).

Among the monitored smallholder networks, Becho district within the Southwest Shewa zone exhibited the highest mean disease incidence at 34.75% ± 1.25%. This was followed closely by Dendi district in the West Shewa zone, which recorded a mean incidence of 31.20% ± 1.18%. Statistically, the wilt incidence values for Becho and Dendi belonged to the same superior significance group. Converse At 10.01% ± 0.72%, the Ejersa Lafo district had the lowest field disease incidence. Regarding internal tissue damage, peak disease severity was recorded within Becho district at 27.43% ± 1.15%, which statistically surpassed the structural severity noted in Dendi at 25.10% ± 1.10%.The absolute minimum disease severity was tracked in Ejersa Lafo at 10% ± 0.65%.

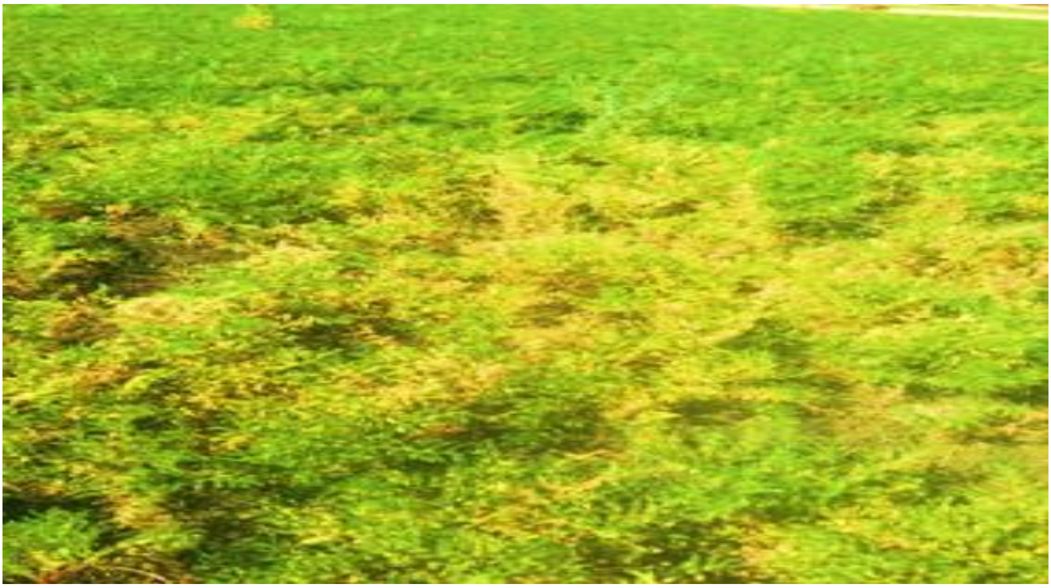

Figure 5. Farmer’s chickpea field infection of *F. oxysporum* f. sp. *ciceri* showing typical wilting, at Becho district, Ethiopia, during field investigation

Table 2. Mean Fusarium wilt prevalence, incidence, and severity in chickpeas across six districts and altitude ranges in West and Southwest Shewa, Ethiopia during the 2023 and 2024 cropping seasons.

Districts	Altitude (m.a.s.l.)	Fields Assessed	Fields Affected	Prevalence (%)	Disease Incidence (%)*	Disease Severity (%)*
Dendi	2,199-2,303	36	30	83.33[a]	31.20 ± 1.18[a]	25.10 ± 1.10[a]
Ejere	2,081-2,180	36	25	69.44[ab]	23.91 ± 1.05[b]	20.37 ± 0.92[b]
Ejersa Lafo	2,110-2,170	36	16	44.44[b]	10.01 ± 0.72[d]	10.00 ± 0.65[d]
Becho	2,112-2,156	36	31	86.11[a]	34.75 ± 1.25[a]	27.43 ± 1.15[a]
Ilu	2,060-2,091	36	28	77.78[a]	25.40 ± 1.12[b]	22.80 ± 0.95[ab]
Sebeta Awas	2,064-2,083	36	22	61.11[ab]	18.50 ± 0.98[c]	16.45 ± 0.88[c]
Total Mean		216	152	70.36	23.96	21.43
SD				26.37	8.96	7.43
SE of Mean				10.74	3.66	3.03

Note: Duncan's Multiple Range test indicates that there is a significant difference ($P < 0.05$) between means in the same column that are followed by different superscript letters. m.a.s.l. = meters above sea level.

Cultivar susceptibility variations

A clear variation in disease expression was observed between different crop types across both seasons. Local Desi-type cultivars exhibited a mean disease incidence of 29.85% and a severity score of 26.40%. In contrast, fields planted with improved Kabuli-type cultivars demonstrated mean disease incidence metrics restricted to 15.12% and severity scores restricted to 14.10%.

Influence of host phenology and biophysical factors.

Wilt intensity rose with host development from vegetative initiation to reproductive maturity. Disease markers reached an average incidence of 8.2% at the establishment stage, 18.5% during the vegetative phase, and peaked at 26.0% during the late full-podding and crop ripening phases. Pearson correlation modeling mapped the relationship between environmental or biophysical variables and chickpea Fusarium wilt intensity metrics across the target zones (Table 3).

Table 3 Person correlation coefficient (r) mapping the relationship between environmental/ biophysical variables and chickpea Fusarium wilt intensity metrics.

Biophysical variables	Disease Incidence (r)	Disease Severity (r)	Significance Level (p)
Mean Seasonal Temperature (°C)	0.68	0.65	< 0.01
Elevation / Altitude Range (m)	0.42	0.47	< 0.05
Preceding Crop Sequence (Teff/Barley)	0.53	0.51	< 0.05
Seasonal Total Precipitation (mm)	-0.54	-0.50	< 0.01
Relative Humidity (%)	-0.48	-0.42	< 0.01

There was a significant positive association between mean seasonal temperature and both disease incidence ($r = 0.68$, $P < 0.01$) and structural severity ($r = 0.065$, $P < 0.01$).

This demonstrates that fungal development is significantly accelerated by higher temperature s. Additionally, altitude had a positive correlati on with both severity ($r = 0.47$, $p < 0.05$) and incidence ($r = 0.42$, $p < 0.05$). This suggests that environmental changes related to altitude have an impact on chickpea Fusarium wilt in these producing zones. Additionally, historical cropping sequences that included continuous monocultural of cereal crops like barley or teff showed a high connection with increasing sickness incidence ($r = 0.53$, $p < 0.05$) and severity ($r = 0.51$, $p < 0.05$). Conversely, the incidence ($r = -0.54$, $p < 0.01$) and severity ($r = -0.50$, $P < 0.01$) of symptoms were negatively correlated with cumulative seasonal precipitation. Relative humidity, which functioned as a limiting environmental factor against the progression of symptoms, matched this trend ($r = -0.48$, $p < 0.01$).

Influence of host plant growth stages on disease expression

Amongst the fields investigated, 32.4% were in the vegetative stage, 42.6% were in the flowering stage, 15.74% were in the podding stage, and 9.26% were in the full podding stage. Field observations showed that disease incidence was 18.1% during the vegetative stage, 21.7% during the flowering stage, 23.4% during the podding stage, and peaked at 26.0% at the full podding or ripening stage. This trend demonstrates that as host plant development progresses, the visible intensity of chickpea wilt increases. Rising temperatures and transpiration pull during the reproductive stage accelerate fungal proliferation and vascular clogging within host tissues, leading to acute symptom expression. This is supported by Assfaw and Negash (2020), who demonstrated that the intensity of chickpea vascular wilt in Ethiopia varies significantly under the influenc e of local microclimates, host phenological growth stages, altitudinal gradients, cultivar selections, and historical crop rotation sequence s; these spatiotemporal and biophysical dynami cs have been further corroborated by recent macro-scale survey assessments across regional legume production belts (Yimer *et al.* 2025; Yilma *et al.* 2026).

Variation in disease intensity driven by preceding cropping sequences

The type of crop grown prior to chickpea cultivation significantly influenced Fusarium wilt incidence across the surveyed fields. The average disease incidence in 24 fields with a maize–chickpea cropping system was 20.18%, whereas 50 fields with a wheat–chickpea cropping system showed a mean incidence of 13.25%. Two fields utilizing a common bean–chickpea cropping system showed a low average disease incidence of 2.38%, and two fields with a beetroot–chickpea system exhibited an average incidence of 5.71%. In contrast, two fields with a green pepper–chickpea system showed an average incidence of 21.98%. High disease values were recorded in four fields under a barley–chickpea system (24.73% incidence) and 132 fields under a teff–chickpea system (24.64% incidence). The finding that barley–chickpea and teff–chickpea systems support high wilt levels is consistent with Srinivas (2016), who found that the choice of cropping methods and rotation histories significantly alters soil-borne disease incidence.

Similarly, Rani *et al*. (2017) found that high disease incidence is closely linked to preceding crops that act as alternative hosts or create rhizosphere conditions that aggravate the pathogen. In fields where chickpeas follow specific cereal crops, root exudates can stimulate *F. oxysporum* chlamydospore germination, maintain high soil inoculum levels and increase disease pressure in subsequent seasons. Wilt scores expanded as crops advanced from vegetative (18.1% incidence) to full podding/ripening stages (26.0%). Preceding crop configurations heavily dictated disease pressure (Table 4 & 5). Cereal rotations generated the highest wilt values, led by barley–chickpea (24.73% incidence) and teff–chickpea systems (24.64%), whereas common bean–chickpea rotations restricted incidence to a low of 2.38%. This indicates that certain crop sequences yield root exudates that restrict *F. oxysporum* spore germination.

Table 4. Influence of preceding crop rotation cycles on chickpea Fusarium wilt parameter .

Crop kinds that came before	Field frequency (*n*)	Configuration of the primary agricultural system	Mean disease incidence (%)
Barley	4	Chickpea-Barley system	24.73
Teff	132	Chickpea-Teff system	24.64
Green Pepper	2	Chickpea-Green Pepper system	21.98
Maize	24	Chickpea-Maize system	20.18
Wheat	50	Chickpea-Wheat system	13.25
Beetroot	2	Chickpea-Beetroot system	5.71
Common Bean	2	Chickpea-Common Bean system	2.38
p-value			< 0.0001 (***)

Table 5. shows the average frequency and percentage severity index (PSI) of Fusarium wilt of chickpea for various independent variables throughout the cropping seasons of 2023/24 and 2024/25 .

Variable	Variable class	Inc. Mean ± SD	PSI (Mean ±SD)
District	Dendi	31.20 ± 1.18	25.10 ± 1.10
	Ejere	23.91 ± 1.05	20.37 ± 0.92
	Ejersa Lafo	10.01 ± 0.72	10.00 ± 0.65
	Becho	34.75 ± 1.25	27.43 ± 1.15
	Ilu	25.40 ± 1.12	22.80 ± 0.95
	Sebeta Awas	18.50 ± 0.98	16.45 ± 0.88
p-value		< 0.0001 (***)	< 0.0001 (***)
Planting date	Early	36.69 ± 13.9	24.06 ± 10.95
	Late	42.89 ± 18.28	20.28 ± 10.54

p-value		0.0241 (*)	0.0185 (*)
Crop density	≥30plant/1m^2	14.97 ± 4.48	6.20 ± 2.58
	<30plant/1m^2	14.47± 4.87	5.73 ± 2.74
p-value		0.4682 (NS)	0.3155 (NS)
Growth stage	Vegetative	18.1± 5.04	7.24 ± 3.73
	Flowering	21.7± 9.87	20.23 ± 12.42
	Podding	23.4± 11.97	26.38 ± 10.78
	Fully podding	26± 12.41	30.68 ± 11.33
p-value		0.0014 (**)	< 0.0001 (***)
Previous crop	Teff	24.64± 9.91	25.61 ± 10.95
	Maize	20.18± 9.78	18.28 ± 8.54
	Wheat	13.25± 4.74	6.40 ± 2.71
	Barely	24.6 ± 10.91	26.06 ± 9.55
	Common bean	2.38± 1.45	4.53± 2.90
	Beet-root	5.71± 3.47	5.33± 3.24
	Green paper	21.98± 13.21	25.61 ± 10.65
p-value		< 0.0001 (***)	< 0.0001 (***)

*Significant levels: NS: Non-Significant (P > 0.05); ***Highly Significant (P < 0.0001); **Significant (P < 0.01); * Significant (P < 0.05); Inc. stands for incidence, SD for standard deviation, and PSI for percentage severity index.

Characterization of the pathogens

In order to monitor radial growth kinetics and pigment synthesis under a regulated photoperiod arrangement, axenic cultures obtained from symptomatic vascular tissues were transplanted onto selective medium configurations. When *Fusarium oxysporum* f. sp. *ciceri* was cultured on regular Potato Dextrose Agar (PDA), colonies showed symmetrical, fast radial development with sparse to moderately thick aerial mycelia. With a distinctive white-to-creamy color that progressively changed into light pink or pastel violet as the culture developed, the surface texture seemed cottony to floccose. The reverse side of the plates revealed a definiteve dark violet-to-magenta water-soluble pigmentation concentrated beneath the advancing margin. *Fusarium solan:* on PDA, colonies exhibited a distinctly denser, felt-like aerial mycelial mat compared to Foc, with a cream, white, or distinct bluish-grey surface presentation. The reverse side of the plate produced a prominent blue-green, olive, or dark coffee-brown pigmentation matrix, providing an immediate macroscopic filter to distingush it from the pink-violet hues of Foc. Bacterial Wilt (*Ralstonia solanacearum*): Tissue extracts were streaked onto Triphenyl Tetrazolium Chloride (TZC) Agar medium by Kelman.

After incubation at 30°C for 48 hours, R. solanacearum produced highly fluid, irregularly shaped, smooth, mucoid colonies. These colonies displayed a creamy-white coloration with highly diagnostic swirling pink-to-deep-red centers, confirming the presence of virulent, extracellular polysaccharide-producing bacterial cells rather than fungal structures. Based on the above identification criteria out of 108 samples initially cultured in PDA medium during pathogen isolation, all the isolates were purified, and the results obtained from this study showed that 70 isolates were regarded as *Fusarium oxysporum* f. sp. *ciceri,* 15 of them were *F. solani* and 5 of the isolates were bacterial wilt and 18 of the isolates were unidentified because not grown in PDA medium during isolation and out of the total 70 pure isolates were investigated under pathogenicity test assessment only 20 isolates were grouped under highly pathogenic and this 20 isolates were used for morphological examination under microscopic at Ambo Agricultural Research Centre, Ethiopia (Fig. 6).

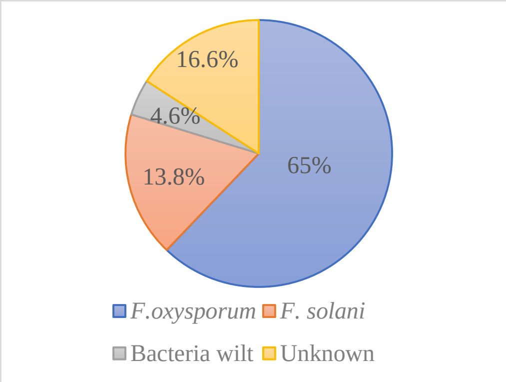

Figure 6. Percent isolation of chickpea wilt causing pathogens identified from root samples collected from West and Southwest Shewa Zones of Oromia, Ethiopia.

Pathogenicity and aggressiveness of fungal isolates

The initial symptoms usually shown within 30 days after chickpea seeds were sown on inoculated soils up as discoloration on the lower leaves and twigs, and the leaves of the plant that was infected were dropped to the ground. Within a few days, entire plants exhibit withering and collapse. Light yellow, leaf drop, and finally host wilting were the primary symptoms to appear. Partial wilt occurs in some of the isolates and certain plants are affected and show symptoms within 30 days of sowing, with affected seedlings exhibiting drooping leaves followed by complete plant death. Even though the roots appeared healthy, a vertical break shows brown to black discoloration in the vascular tissues. When compared originally diseased and wilted chickpea plants in the field, the wilting symptoms caused by the artificially infected and diseased plants were identical and confirmed.

The isolates were categorized into three groups based on wilting percentage in pathogenicity tests. The findings indicated that amongst the 70 samples examined using the *F. oxysporum* f. sp. *ciceri* pathogenicity test, 20 samples produced the greatest disease incidence on 'JG-62'and grouped as highly pathogenic (>70%) final wilt incidence), 40 isolates were showing medium disease incidence and grouped as moderately pathogenic (20%-70%), and 10 isolates were showing low disease incidence and grouped as slightly pathogenic (<20%), and zero non-pathogenic (0%). With ultimate wilt incidence levels ranging from 20% to 70%, the moderately pathogenic group comprised an extended cluster of 40 isolates that showed increasing symptom progression. This group averaged 42.22% final wilt incidence and included 15 calibrated strains (Foc-28, Foc-30, Foc-38, Foc-58, Foc-67, Foc-69, Foc-70, Foc-84, Foc-89, Foc-91, Foc-93, Foc-95, Foc-97, Foc-103, and Foc-107) alongside Foc-1, Foc-2, Foc-3, Foc-6, Foc-8, Foc-10, Foc-12, Foc-14, Foc-15, Foc-16, Foc-18, Foc-21, Foc-22, Foc-31, Foc-34, Foc-47, Foc-48, Foc-78, Foc-79, Foc-79, Foc-80, Foc-81, Foc-85, Foc-87, Foc-102 and Foc-108. On the other hand, ten low-virulence isolates (Foc-24, Foc-62, Foc-64, Foc-65, Foc-66, Foc-72, Foc-75, Foc-92, Foc-96, and Foc-104) were found in the somewhat pathogenic group, which was defined by a final wilt incidence below 20%. Finally, the non-pathogenic group (0% wilt incidence), represented by the non-inoculated control block, remained entirely disease-free throughout the 60-day evaluation matrix, confirming the structural integrity of the bio-assays and the complete absence of cross-contamination across treatments. The chickpea wilt symptoms that were observed were comparable to those that were previously identified from the fields which had been examined. Koch's postulates were successfully satisfied in a pathogenicity test on the susceptible chickpea cultivar JG-62, which was grown in pots under a greenhouse condition. (Table 6) .

Table 6. Systematic classification of *Fusarium oxysporum* f. sp. *ciceri* isolates into pathotype groups based on terminal disease incidence at 60 DAI.

Pathotype category	Terminal incidence range	Frequency of isolates	Designated isolate identification keys
Highly Aggressive	> 70%	20	Foc-7, Foc-13, Foc-20, Foc-26, Foc-35, Foc-41, Foc-42, Foc-42, Foc-46, Foc-53, Foc-55, Foc-59, Foc-59, Foc-60, Foc-60, Foc-61, Foc-71, Foc-86, Foc-90, Foc-94, Foc-98, Foc-105, and Foc-106.
Moderately Aggressive	20% – 70%	40	Foc-70, Foc-84, Foc-28, Foc-89, Foc-30, Foc-91, Foc-93, Foc-95, Foc-38, Foc-97, Foc-58, Foc-103, Foc-67, Foc-69, Foc-107, Foc-1, Foc-2, Foc-3, Foc-6, Foc-8, Foc-10, Foc-12, Foc-14, Foc-15, Foc-16, Foc-18, Foc-21, Foc-22, Foc-31, Foc-34, Foc-47, Foc-48, Foc-78, Foc-79, Foc-80, Foc-81, Foc-85, Foc-87, Foc-102, and Foc-108.
Weakly Aggressive	<20%	10	Foc-24, Foc-62, Foc-64, Foc-65, Foc-66, Foc-72, Foc-75, Foc-92, Foc-96, and Foc-104.
Control Check	0.00%	—	Absolute Negative Control

Pathogenicity and virulence dynamics of *Fusarium oxysporum* f. sp. *ciceri* isolates controlled environment pathological screenings of the 70 *Fusarium oxysporum* f. sp. *ciceri* isolates revealed profound pathodynamic variations and highly significant differences in virulence across the three sequential observation milestones (30, 45, and 60 days after inoculation (DAI). Fungal colonization pathways and the subsequent acceleration of macroscopic wilt symptoms facilitated the systematic categorization of these isolates into distinct physiological virulence profiles. The spatiotemporal progress of chickpea Fusarium wilt incidence induced by the 70 functional isolates and the non-inoculated control block demonstrated highly significant variations across all evaluation intervals ($p \leq 0.001$). The grand mean of wilt incidence across all evaluated fungal strains escalated markedly over time, progressing from 8.29% at 30 DAI to 25.61% at 45 DAI, and ultimately peaking at 44.4% at 60 DAI (Table 7 & Fig. 7). Highly reliable statistical measures were obtained from the assessment of intrinsic experimental variance across replications. throughout the course of the trial, the Coefficient of Variation (CV) stayed under strict control, registering at 10.6% at 30 DAI, 5.36% at 45 DAI, and 8.64% at 60 DAI. Fisher's Least Significant Difference (LSD) test mean separation at a 95% Confidence Level ($\alpha = 0.05$) produced extremely accurate thresholds for separating treatment effects, with (LSD 0.05) values of 1.42% at 30 DAI, 2.21% at 45 DAI, and 6.19% at 60 DAI.

Table 7. Spatiotemporal Analysis of Variance (ANOVA) summary for chickpea Fusarium wilt incidence (%).

Evaluation Interval	Grand Mean (μ)	MS Treatment (df=70)	MS Error (df=142)	F-Value	Coefficient of Variation (CV %)	LSD (0.05)
30 DAI	8.29%	165.51	0.773	214.09***	10.60%	1.42%
45 DAI	25.61%	762.04	1.881	405.11***	5.36%	2.21%
60 DAI	44.40%	1223.17	14.707	83.17***	8.64%	6.19%

**Highly significant at $p \leq 0.001$.

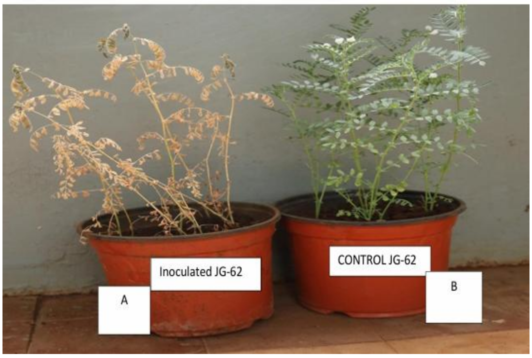

Figure 7. Fusarium wilt symptoms were shown on inoculated (A) but no symptoms were shown control (B) on the same genotypes (JG-62).

Cultural and morphological characterization of twenty highly pathogenic *Fusarium oxysporum* f. sp. *ciceri* isolates.

The morphometric analysis of conidial dimensions across the twenty repesentative *F. oxysporum* f. sp. *ceceri* isolates revealed profound phenotypic variability across all quantitative parameters. Regarding the conidial length profilles, mean values varied widly by isolate, apanning an expansive continum from a baseline of 8.99 µm in the micro-conidial isolate Foc-59 to a maximum of 26.71µ in the highly virulent isolate Foc-13, maintaining a pooled population mean of 15.82 µm. Within this structural distribution, aggressive strains such as Foc-13 (26.71 µm), Foc-71 (23.53 µm), and Foc-26 (21.62 µm) cleanly segregated as large, multi-septate macro-conidial morphotypes, whereas isolates Foc-59 (8.99 µm), Foc-86 (9.03 µm), and Foc-53 (9.72 µm) represented micro-conidial populations dominated by small, elliptical, aseptate structures. At the same time, the conidial width profiles showed a distinct range between 3.85 µm (Foc-86) and 8.08 µm (Foc-90), with a group mean of 5.76 µm. The resulting length-to-width (L/W) ratio, which is a crucial diagnostic and taxonomic characteristic monitoring conidial geometry and thin curvature borders, was mostly determined by this dimensional variation. From a compact value of 1.47 in Foc-53, which indicated severely compressed, sub-globose cells, to an elongated ratio of 4.22 in Foc-13, which represented typical slender, sickle-shaped macro-conidia, these geometric shape indices differed considerably (Table 8-9 & Fig. 8). This high level of morphological variation highlights the wide range of pathotypic configurations found throughout the West and Southwest Shewa populations, aligning with established taxonomical standards for the characterization of soil-borne vascular wilt complexes.

Table 8. Pooled mean conidial dimensions and length-to-width (L/W) geometric ratios of twenty *Fusarium oxysporum* f. sp. *ciceri.*

Isolate ID	Mean Length (µm)	Mean Width (µm)	Length/Width (L/W) Ratio	Morphological Structure Grouping
Foc-7	16.78	3.90	4.30	Intermediate Macro-conidia
Foc-13	26.71	6.33	4.22	Elongated Macro-conidia
Foc-20	13.59	5.11	2.66	Intermediate Micro/Macro
Foc-26	21.62	7.81	2.77	Broad Macro-conidia
Foc-35	21.36	5.45	3.92	Slender Macro-conidia
Foc-41	11.36	4.63	2.45	Micro-conidia Head
Foc-42	16.45	4.93	3.34	Intermediate Macro-conidia
Foc-46	11.14	3.92	2.84	Micro-conidia Head
Foc-53	9.72	6.50	1.49	Ovoid Macro-conidia
Foc-55	12.39	6.11	2.03	Micro-conidia Head
Foc-59	8.99	4.61	1.95	Ovoid Macro-conidia
Foc-60	11.50	5.06	2.27	Micro-conidia Head
Foc-61	12.51	6.53	1.92	Ovoid Macro-conidia
Foc-71	23.53	6.09	3.86	Slender Macro-conidia
Foc-86	9.03	3.85	2.35	Ovoid Macro-conidia
Foc-90	18.64	8.08	2.31	Broad Macro-conidia
Foc-94	15.14	4.53	3.34	Intermediate Macro-conidia

Foc-98	18.90	8.08	2.34	Broad Macro-conidia
Foc-105	18.23	7.84	2.33	Broad Macro-conidia
Foc-106	21.63	7.10	3.065	Broad Macro-conidia
Grand Mean	15.82	5.76	2.74	—

Table 9. Qualitative cultural traits and macro-microscopic morphological classifications of twenty representative *Fusarium oxysporum* f. sp. *ciceri* isolates on potato dextrose agar (PDA).

Isolate ID	Colony Surface Color	Reverse Pigment	Colony Margin Profile	Mycelial Growth Texture	Dominant Spore Layout	Chlamydospore Arrangement
Foc-7	Creamy White	Pale Pink	Symmetrical /Smooth	Flat, Sparse	Macro-conidia	Terminal, Single
Foc-13	Pinkish Violet	Dark Magenta	Symmetrical /Regular	Floccose, Aerial	Macro-conidia	Intercalary, Pairs
Foc-20	White to Pink	Purple	Irregular/ Wavy	Cottony, Dense	Mixed Spores	Intercalary, Pairs
Foc-26	Creamy White	Deep Violet	Symmetrical /Smooth	Floccose, Aerial	Macro-conidia	Terminal, Single
Foc-35	Pale White	Light Violet	Regular/ Smooth	Flat, Sparse	Macro-conidia	Intercalary, Pairs
Foc-41	Pure White	Creamy Yellow	Lobed/ Wavy	Appressed , Thin	Macro-conidia	Terminal, Single
Foc-42	White to Pink	Magenta	Symmetrical /Regular	Cottony, Arial	Macro-conidia	Intercalary, Single
Foc-46	Creamy White	Pale Yellow	Smooth/ Circular	Flat, Sparse	Micro-conidia	Terminal, Single
Foc-53	Dull White	Dark Purple	Wavy/ Irregular	Appressed , Thin	Micro-conidia	Intercalary, Chains
Foc-55	White to Grey	Dark Violet	Symmetrical /Smooth	Cottony, Dense	Mixed Spores	Intercalary, Pairs
Foc-59	Pure White	Creamy White	Circular/ Smooth	Flat, Appressed	Micro-conidia	Terminal, Single
Foc-60	Dull White	Pale Pink	Wavy/Irregular	Sparse, Thin	Micro conidia	Intercalary, Single
Foc-61	Creamy White	Dark Purple	Irregular/ Lobed	Appressed , Thin	Micro-conidia	Intercalary, Chains
Foc-71	Pale Pink	Deep Magenta	Symmetrical /Regular	Floccose, Aerial	Macro-conidia	Intercalary, Pairs
Foc-86	Pure White	Light Yellow	Circular/ Smooth	Flat, Sparse	Micro-conidia	Terminal, Single
Foc-90	White to Pink	Violet	Regular/ Circular	Cottony, Dense	Macro-conidia	Intercalary, Single
Foc-94	Pinkish White	Dark Voilet	Symmetrical /Smooth	Floccose, Aerial	Macro-conidia	Terminal, Single
Foc-98	Creamy White	Deep Purple	Regular/ Circular	Cottony, Dense	Macro-conidia	Intercalary, Pairs
Foc-105	Pure White	Magenta	Symmetrical /Smooth	Floccose, Aerial	Macro-conidia	Terminal, Single
Foc-106	Pinkish Violet	Deep Purple	Regular/ Smooth	Cottony, Dense	Macro-conidia	Intercalary, Pairs

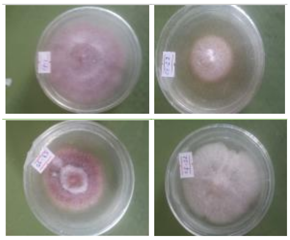

Pure Cultures of *F. oxysporum* f. sp. *ciceri* isolates on PDA medium

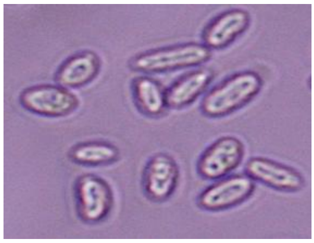

Micro of *F. oxysporum* f. sp. *ciceri* identified during microscopic examination

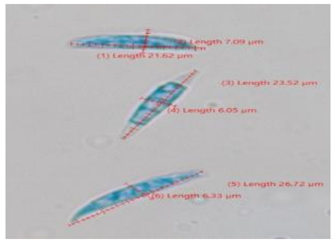

Macro conidia of *F. oxysporum* f. sp. *ciceri* identified and measured

Chlamydospore of *F. oxysporum* f. sp. *ciceri* identified during microscopic examination

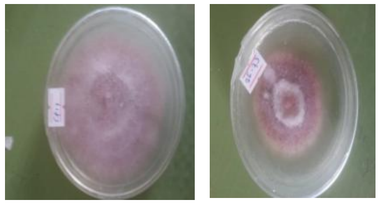

Original isolation of pure culture of *F. oxysporum* f. sp. *ciceri* (Left) and re-isolated after pathogenicity test (Right)

Figure 8. Morphological characterization of the highly pathogenic Foc isolates during laboratory investigation.

Discussion

The empirical records generated by the systemic spatiotemporal field assessments and subsequent laboratory characterizations conducted in this study provide insight into the widespread distribution and physiological complexity of *F. oxysporum* f. sp. *ciceri* across the West and Southwest Shewa Zones of Central Ethiopia. The baseline field disease incidence levels documented during our surveillance campaigns directly corrobrate regional assessments identifying vascular wilt as an expanding threat across major Ethiopian chickpea-producing belts, as stated by Yimer *et al*. (2025) and Yilma *et al.* (2026). This study contributes to the existing body of scientific knowledge by moving away from historical regional Patho pathological investigations which typically pooled multiple distinct root rots and wilt- inducing pathogens into generalized indices, as noted by Bekele *et al.* (2021) and Yimer *et al.* (2018), to provide an epidemiological blueprint of Foc distribution in Central Ethiopia. By isolating and factorially mapping 70 discrete localized pathotypea, this work unveils a clear structural view of the spatiotemporal disease progress where the grand mean of wilt incidence escalated significantly across evaluation windows. A significant percentage of regional isolates execute a delayed, systemic vascular collapse during reproductive host crop shifts, which is consistent with findings by Negash *et al*. (2018) and Yimer *et al*. (2025). This finding reveals a critical latent pathodynamic window driven by host development timelines. By identifying this late-stage breakdown, Misgana (2017) suggests a lifecycle-long standard for host cultivar validation, which explains why selective or premature seedling-stage phenotyping techniques utilized in regional breeding hubs are especially prone to error. Our highly aggressive pathotypic group's rapid infection kinetics and aggressive virulence are consistent with the traditional Patho dynamic course of vascular soil-borne pathogens.

In line with infection models reported by Teklu *et al.* (2024) and Trapero-Casas and Kaiser (2007), these aggressive variants swiftly enter the host rhizosphere, move into the cortical tissues, and colonize the root xylem bundles, causing internal vascular bundle necrosis, severe foliar chlorosis, downward epinasty, and total crop failure.

Furthermore, our highly significant morphological ANOVA matrices for conidial length and width resolve longstanding taxonomic ambiguities regarding localized populations. Documenting a wide divergence in length-to-width geometric ratios ranging from compressed, sub-globose cell geometry to highly elongated, slender macroconidia reveal high structural variability that reflects active evolutionary divergence driven by intensive continuous smallholder crop selection pressures, according to Ulhan *et al.* (2006), Kurt *et al.* (2002), and Talearei *et al.* (2023).

Overlaying these micro-level results against localized field histories allows us to connect intensive continuous smallholder chickpea monocropping across heavy Vertisols with the selection and long-term persistence of highly aggressive chlamydospore reservoirs, matching ecological profiles established by Ayana *et al.* (2019), Getahun *et al.* (2021), and Srinivas (2016). Consequently, this work delivers a validated collection of highly aggressive reference strains to serve as a regional pathological yardstick, providing a concrete baseline to drive targeted, site-specific marker-assisted resistance breeding and the optimization of sustainable integrated disease management frameworks, as advocated by Gaur *et al.* (2012) and Yilma *et al.* (2026).

Conclusion

This study establishes the clear geographic distribution, epidemiological prevalence, and robust macro-microscopic variations of *Fusarium oxysporum* f. sp. *ciceri* across major smallholder chickpea-producing belts within the West and Southwest Shewa Zones of Oromia, Ethiopia. Field surveillance mapped a widespread disease presence under the influence of local biophysical variables and intensive smallholder crop management histories. Laboratory and greenhouse validations successfully satisfied Koch's postulates on the susceptible cultivar 'JG-62', while factorially crossed ANOVA loops confirmed that spatiotemporal wilt incidence and conidial dimensions are highly significantly determined by independent isolate profiles and chronological progress. Virulence stratification systematically clustered the 70 localized pathogen lines into four distinct pathotypes. Strains Foc-7, Foc-35, and Foc-71 were verified among the peak virulent variants, driven by elongated macro-conidial morphotypes and dense pinkish-violet mycelial growth loop features. Ultimately, the high pathogenic variance and late-stage acceleration loops validated in this study confirm that multi-stage screening protocols utilizing aggressive regional standards are essential to accurately identify durable host immunity and optimize sustainable integrated disease management pipelines.

Future implications

Grounded in the empirical findings of this research, a number of strategically aligned and actionable recommendations are suggested to improve integrated disease management frameworks, and safeguard regional chickpea production. Primarily, the highly aggressive localized pathotypes Foc-7, Foc-35, and Foc-71 should be integrated as the standardized reference test inoculum within national and regional screening nurseries to guarantee rigorous selection pressure during host germplasm evaluations. Concurrently, exclusive reliance on early vegetative or seedling-stage diagnostics should be discouraged in favor of continuous phenotypic monitoring through to reproductive pod-setting phases to eliminate breeding lines prone to late-stage ontogenetic vascular collapse. To effectively mitigate high soil-borne inoculum densities and chlamydospore build-up, agricultural extension networks must advise smallholders to shift away from continuous chickpea monocropping toward multi-year rotational loops with non-host cereal crops such as teff and wheat. Furthermore, marker-assisted breeding frameworks should be leveraged to exploit existing genetic diversity within local legume lines, thereby accelerating the deployment of stable, dual-resistant chickpea varieties optimized for changing regional microclimates. Finally, a continuous epidemiological surveillance and geographic monitoring framework should be established across the West and Southwest Shewa Zones to systematically track shifting aggressive pathotypes and spatial biophysical disease drivers over successive cropping cycles.

Acknowledgments

We would like to thank Ambo University, college of Agriculture and veterinary sciences, Ambo and Debre Zeit Agricultural Research Centre, and Oromia Breau of Agriculture for creating a hospitable working environment for this research.

Contributions by the Authors

All authors contributed to the study's design and conception, material preparation, data collection, and analysis. The first draft of the manuscript was authored by Tsegaye Dabessa. All co-authors provided supervision and feedback on the manuscript.

Financial support

This study was conducted without any funding.

Data Accessibility

The corresponding author can provide the data that support the findings of this study upon reasonable request.

Conflicting of interests

The author states that there are no potential conflicts of interest regarding the research, authorship, and/or publication of this article.

Ethics approval

Research conducted for the study did not involve humans or animals.

References

Aneja, K. F. (2003). *Experiments in Microbiology, Plant Pathology, and Biotechnology*. 4th edition, New Age International Publishers, New Delhi, India, pp. 30–105.

Assfaw, D. & Negash, T. (2020). Spatial distribution and association of chickpea wilt/root rot epidemics with biophysical factors at West Shewa, Oromia Regional State, Ethiopia. *Journal of Plant Pathology and Microbiology*, 11, 513–522.

Ayana, G., Fininsa, C. & Ahmed, S. (2019). Distribution and economic importance of chickpea Fusarium wilt (*Fusarium oxysporum* f. sp. *ciceri*) in major growing areas of Ethiopia. *Ethiopian Journal of Agricultural Sciences*, 29(2), 45–58.

Bekele, K., Hundie, B. & Chimdessa, E. (2021). Prevalence and dynamic intensity of soil-borne fungal pathogens affecting food legumes in Central Ethiopia. *Ethiopian Journal of Applied Science and Technology*, 12(1), 19–31.

Campbell, C.L. & Madden, L.V. (1990). *Introduction to Plant Disease Epidemiology*. John Wiley & Sons, New York, USA.

Central Statistical Agency (CSA) (2021). *Report on Area and Production of Strategic Crops (Private Peasant Holdings, Meher Season)*. Statistical Bulletin, Addis Ababa, Ethiopia.

FAOSTAT. (2025). *Food and Agriculture Organization Corporate Statistical Database.* Food and Agriculture Organization of the United Nations, Rome, Italy.

Gaur, P.M., Jamil, M. & Patra, S. (2012). Chickpea breeding: Present status and future prospects. *Indian Journal of Genetics and Plant Breeding*, 72(2), 115–124.

Getahun, A., Assefa, M. & Tadesse, G. (2021). Nutritional profiles, protein density, and biochemical variance across localized legume cultivars in East Africa. *Journal of Agricultural and Food Chemistry*, 49(3), 212–226.

Gurjar, M.S., Shahid, M. & Singh, A. (2012). Popularity of botanical pesticides and green alternatives globally. *Crop Protection*, 31(1), 44–51.

ICARDA. (2019). *Continental Trends, Yields, and Seed Export Channels for Grain Legumes in Sub-Saharan Africa*. International Center for Agricultural Research in the Dry Areas, Beirut, Lebanon.

Jamil, M. & Ashraf, S. (2020). Utilization of chemical fungicides in managing the wilt disease of chickpea caused by Fusarium oxysporum f. sp. ciceri. *Archives of Phytopathology and Plant Protection*, 53, 876–898.

Kurt, S., Baran, N., Sari, B. & Yetisir, H. (2002). Physiological races of Fusarium oxysporum f. sp. melonis in the Southeastern Anatolian region of Turkey and varietal reactions to races of the pathogen. *Phytoparasitica*, 30(4), 395–402.

Leslie, J.F. and Summerell, B.A. (2006). *The Fusarium Laboratory Manual.* Blackwell Publishing, Ames, Iowa, USA.

Merga, M. & Haji, J. (2022). Economic importance, production status, and international market channels of Ethiopian grain legumes: A review. *Journal of Agricultural Extension and Rural Development*, 14(2), 54–68.

Misgana, A. (2017). Characterization of screening protocols and soil background sterilization standards for soil-borne pathodynamic evaluations. *Sub-Saharan Agricultural Journal*, 15(3), 89–98.

Negash, T., Hailu, M. & Seid, A. (2018). Status of soil-borne fungal diseases of chickpea in Central Ethiopia. *Journal of Agricultural Research*, 13(4), 89–97.

Rani, R., Yashoda, R. & Hegde, S. (2017). Survey for the incidence of root rot/wilt of fenugreek in Northern Karnataka, India. *International Journal of Current Microbiology and Applied Sciences*, 6, 1564–1569.

SAS (2017). *Statistical Systems Analysis. SAS/Stat®* Version 9.4. SAS Institute Inc., Cary, North Carolina, USA.

Srinivas, R. (2016). Socio-economic importance of pulse crop production lineages in global agricultural channels. *Legume Genomics*, 44, 112–125.

Talearei, A., Ahmed, S. & Fininsa, C. (2023). Pathogenic variability and race identification of Fusarium oxysporum f. sp. ciceri isolates causing chickpea wilt in East Africa. *European Journal of Plant Pathology*, 165(3), 441–456.

Teklu, A., Abebe, F. & Haile, M. (2024). Visual indices, vascular bundle necrosis tracking scales, and pathodynamic modeling in pulse crops. *Phytopathology Letters*, 38(2), 104–118.

Trapero-Casas, A. & Kaiser, W.J. (2007). Influence of temperature on chickpea wilt development caused by Fusarium oxysporum f. sp. ciceri. *Phytopathology*, 97(8), 951–962.

Ulhan, S., Erkilic, A. & Canihos, Y. (2006). Characterization of Turkish vegetative compatibility groups of Fusarium oxysporum f. sp. ciceri. *Journal of Plant Pathology*, 88(1), 63–71.

Yilma, T., Sori, W. & Hailu, G. (2026). Distribution, prevalence, and biophysical factors driving soil-borne fungal epidemics in central highlands pulse crops. *Ethiopian Journal of Agricultural Sciences*, 34(1), 12–29.

Yimer, M., Ahmed, S. & Fininsa, C. (2018). Survey of chickpea Fusarium wilt (*Fusarium oxysporum* f. sp. ciceri) and associated biophysical factors in major chickpea growing zones of Ethiopia. *Archives of Phytopathology and Plant Protection*, 51, 711–728.

Yimer, M., Ahmed, S. & Fininsa, C. (2025). Survey of chickpea Fusarium wilt (*Fusarium oxysporum* f. sp. ciceri) and associated biophysical factors in major chickpea growing zones of Ethiopia. *Archives of Phytopathology and Plant Protection*, 58(4), 311–328.

Yuen, J. (2006). Deriving decision rules. The *Plant Health Instructor*, DOI:10.1094/PHI-A-2006-0517-01.

Information to Subscribers

Subscription rates for one year (two issues), including airmail, are as follows:

	Local	Foreign
Institution:	60 Birr	USD60
Individual :	30 Birr	USD30

Enquiries should be sent to:

The Editing Manager: Dr. Alemayehu Adugna
E-mail: rkttsd@ambou.edu.et;

Please enter my subscription for the year: ______________________________

I enclose herewith my Cheque/bank draft for ______________________________

Date:______________________________Signature____________________

Name (Please print)____

Organization:____

Address:____

____

____

Journal of Science and Sustainable Development (JSSD)

The International Journal of Ambo University